AN EXPERIMENTAL AND ANALYTICAL STUDY OF WATE[R] HEAT PIPES FOR MODERATE TEMPERATURE RANGES

Billy Grant McKinney

George C. Marshall Space Flight Center
Marshall Space Flight Center, Alabama

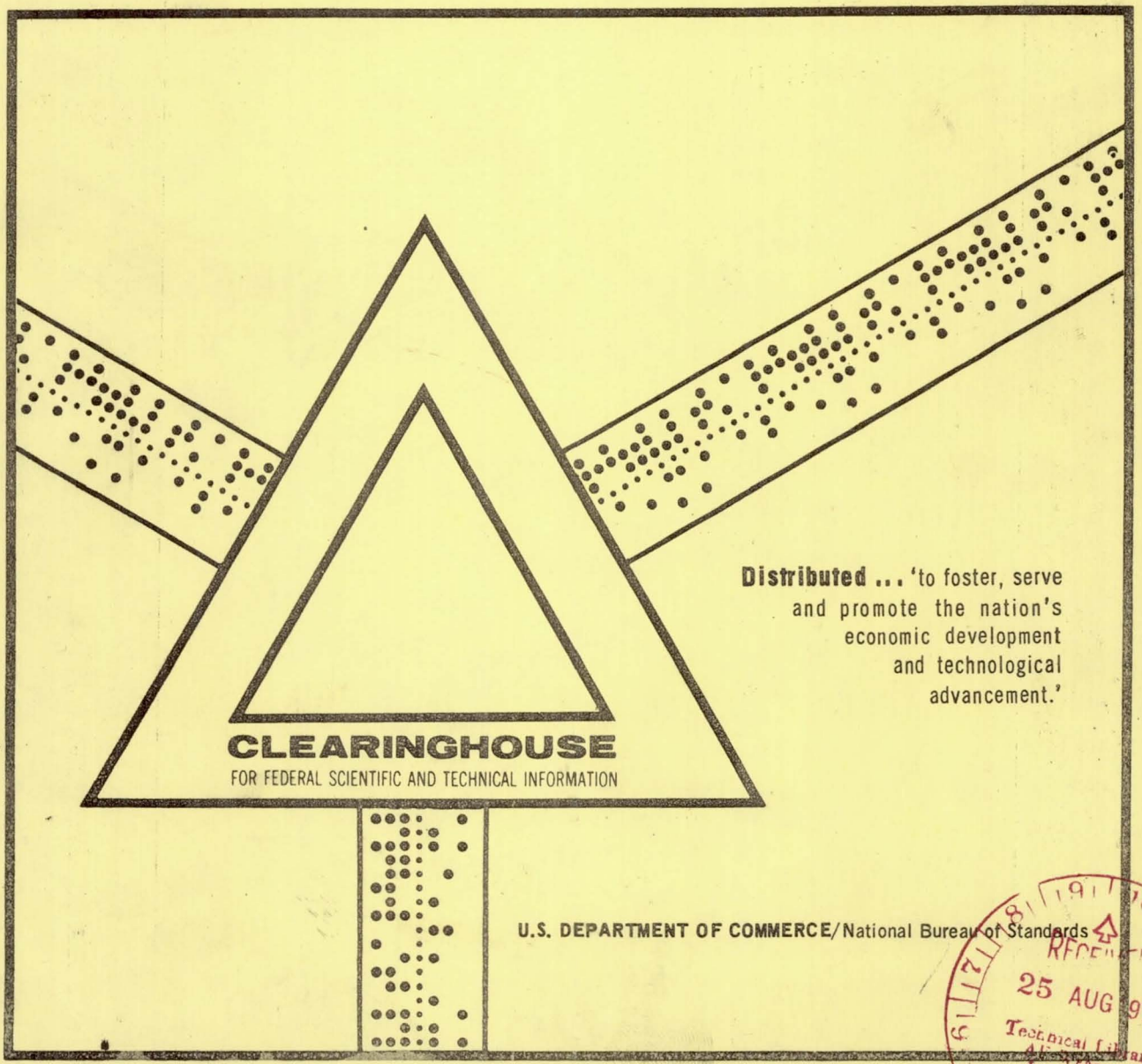

NASA TECHNICAL MEMORANDUM

1. NASA TM

Report No. X-53849

2. U/U

AN EXPERIMENTAL AND ANALYTICAL STUDY OF WATER HEAT PIPES FOR MODERATE TEMPERATURE RANGES

By Billy Grant McKinney
Astronautics Laboratory

5.

6. June 6, 1969

NASA

George C. Marshall Space Flight Center

Marshall Space Flight Center, Alabama

3. NATIONAL AERONAUTICS AND SPACE ADMIN.

TECHNICAL MEMORANDUM X-53849

AN EXPERIMENTAL AND ANALYTICAL STUDY OF WATER HEAT PIPES FOR MODERATE TEMPERATURE RANGES

By

Billy Grant McKinney

George C. Marshall Space Flight Center
Marshall Space Flight Center, Alabama 35812

ABSTRACT

Results of an experimental and analytical investigation of water heat pipes are presented. Eight water heat pipes used as radiating fins and eight water heat pipes having an adiabatic section and a condenser were investigated while in or near a vertical position. Different heat inputs were applied to maintain steady-state operation of the heat pipes at temperatures of approximately 200° F, 250° F, 300° F, and 350° F. A data acquisition system was used to record heat inputs, surface temperatures, interior temperatures, and pressures of the heat pipes.

Governing equations were developed for water heat pipes. These governing equations were programmed for a digital computer so that the effect of parameters contained in the equations could be studied. The parameters studied are permeability, apparent contact angle, and length of the adiabatic section. Solutions of the governing equations and the parametric studies are presented in graphical form.

The design and fabrication of the heat pipes is described. An assembly procedure designed to prevent contamination of the vapor space of a water heat pipe is presented. Experimental results are given for determining the permeability of 100- and 250-mesh stainless steel screens that were used as wicking material for the heat pipes.

A high altitude simulation system was used when testing the eight water heat pipes as radiating fins. From experimental data, comparisons were made for these water heat pipes. The comparisons, which are presented in the form of graphs, are as follows: Thermal conductivity of water heat pipes, temperature profile of a water heat pipe versus a solid rod of comparable material and dimensions, the effect of the length-to-diameter ratio on heat input, variation of heat input to wick thickness, heat input per pound of weight, and analytical results versus experimental results.

The eight water heat pipes having an adiabatic section were tested as a conductor between a heat source and a heat sink. Experimental data obtained were reduced and presented graphically as follows: Thermal conductivity of heat pipes, effect of length-to-diameter ratios on heat inputs, variation of heat input with wick thickness, heat input per pound of weight, and analytical results versus experimental results.

The results of this study show that, for water heat pipes used as radiating fins, the analytical analysis and the assumptions therein are justified by the agreement with the experimental data for a temperature range of 200° F - 350° F. Also shown by this study is that, for water heat pipes having

an adiabatic section, the analysis and the assumptions therein are most applicable for a temperature of approximately 250° F. Other results are that heat pipes increase the heat transfer rate when used as radiating fins or conductors, heat pipes are weight-saving devices, the magnitude of the radial Reynolds number has little or no effect on heat pipe design, and the study of the heat addition and rejection profile of a heat pipe should be extended so that heat pipes could be more efficiently designed.

NASA-GEORGE C. MARSHALL SPACE FLIGHT CENTER

TECHNICAL MEMORANDUM X-53849

AN EXPERIMENTAL AND ANALYTICAL STUDY* OF WATER HEAT PIPES FOR MODERATE TEMPERATURE RANGES

By

Billy Grant McKinney

*Submitted in partial fulfillment of the requirements for the degree of Doctor of Philosophy with Major in Mechanical Engineering in the Graduate School of the University of Alabama

UNIVERSITY, ALABAMA

1969

ASTRONAUTICS LABORATORY
SCIENCE AND ENGINEERING DIRECTORATE

ACKNOWLEDGMENTS

The author wishes to extend his sincere appreciation and gratitude to the following individuals and organizations.

Dr. C. K. Liu, who served as major adviser and committee chairman; his interest, encouragement, and guidance were invaluable during the author's graduate study at the University of Alabama.

The graduate committee, composed of Dr. B. F. Barfield, Dr. W. J. Schaetzle, Dr. G. B. McKay, Dr. O. R. Ainsworth, and Prof. W. K. Rey, who rendered guidance and counsel.

National Aeronautics and Space Administration for providing a graduate co-op position that made his graduate study possible.

His associates at Marshall Space Flight Center, who rendered valuable discussion and assistance.

His wife, Barbara, and daughters, Helen Denise and DeAnna Evon, for their encouragement.

TABLE OF CONTENTS

TABLE OF CONTENTS (Continued)

TABLE OF CONTENTS (Concluded)

LIST OF ILLUSTRATIONS

LIST OF ILLUSTRATIONS (Continued)

LIST OF ILLUSTRATIONS (Continued)

LIST OF ILLUSTRATIONS (Continued)

LIST OF ILLUSTRATIONS (Concluded)

LIST OF TABLES

DEFINITION OF SYMBOLS

Symbol	Definition
A	Area, ft^2
b	Constant
D	Diameter, ft
e	Emissivity
g	Gravitational acceleration, ft/hr^2
g_c	Constant, 4.175×10^8 lbm ft/lb_f hr^2
h	Film coefficient, Btu/ft^2-hr-°R
J	Mechanical equivalent of heat, 778 ft-lb_f/Btu
K	Permeability, ft^2
k	Thermal conductivity, Btu/hr-ft-°R
L	Length, ft
$\dot{m}$	Mass flow rate, lbm/hr
P_w	Specific wetted perimeter, 1/ft
p	Pressure, lb_f/ft^2
Q	Volume flow rate, ft^3/sec
q	Heat transfer rate, Btu/hr
R_{e_r}	Radial Reynolds number

DEFINITION OF SYMBOLS (Continued)

Symbol	Definition
r	Radius, ft
r_c	Radius of curvature of the pores in the wick, ft
r_n	Radius of bubble nucleus, ft
s	Constant
T	Temperature, °R or °F
t	Thickness of wick, ft
V	Velocity, ft/hr
W	Average velocity, ft/hr
z	Axial coordinate
α	Constant
β	Pipe angle (see Figure 1), deg
ϵ	Porosity, ft/ft
θ	Apparent contact angle, deg
λ	Latent heat of vaporization, Btu/lbm
μ	Viscosity, lb_f-hr/ft^2
ρ	Density, lbm/ft^3
σ	Surface tension, lb_f/ft

DEFINITION OF SYMBOLS (Concluded)

Symbol	Definition
σ_1	Stefan-Boltzmann constant, 0.1714×10^{-8} Btu/ft^2-hr-°R^4
Subscripts	
a	Adiabatic section
c	Condenser
e	Evaporator
eff.	Effective
ℓ	Liquid
max.	Maximum
o	Inter surface of heat pipe
s	Surface or surrounding
sat.	Saturation
v	Vapor phase or vapor space
w	Average

CHAPTER I

INTRODUCTION

A. Definition of a Heat Pipe

Heat pipe technology has advanced rapidly to its present state since it was "reinvented" in the early 1960's. A heat pipe is a self-contained device that achieves very high thermal conductance by means of two-phase fluid flow with capillary circulation. It is a device that depends upon the evaporation of a fluid at one end and the condensation of the fluid at the other end to transfer heat. The transportation of matter from the evaporator to the condenser is accomplished by vapor flow. The flow from the condenser to the evaporator is by capillary flow of a liquid through porous material. The space through which the vapor flows is referred to as the vapor space and the porous material is referred to as the wick.

Heat transfer by a heat pipe is accomplished by changing the states of a material from its liquid phase to a vapor and then from a vapor to its original state. The two modes of heat transfer most often considered for heat pipes are conduction and radiation. When radiation is the mode of heat transfer, the pipe is heated at one end while the remainder of the heat pipe is exposed so that heat may be radiated from the exposed surface to the

surrounding space. If conduction is the mode of heat transfer, heat is applied at one end of the pipe and a condenser is connected at the opposite end to remove the heat.

The heat pipe was first introduced with a configuration very similar to the one used at the present. A typical configuration is depicted in Figure 1.

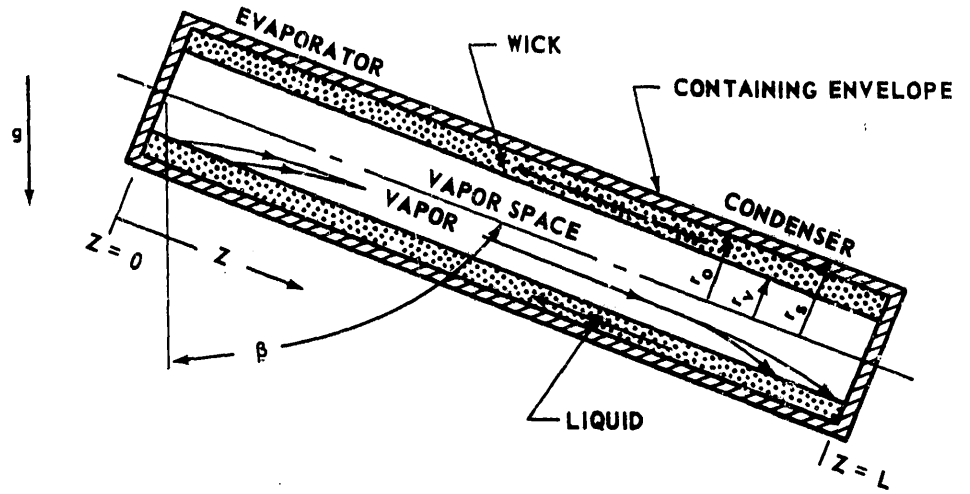

FIGURE 1. CONFIGURATION OF A HEAT PIPE

B. Survey of Literature

A patent by Gaugler [1] was entitled "Heat Transfer Device," and the device described therein is now known as a heat pipe. This patent was filed December 21, 1942 and granted June 6, 1944. The principle of the device was to evaporate a liquid at a point above where it was being condensed, without doing additional work to lift the liquid to where it was being evaporated.

From this patent arose the concept of a closed container with a wicking material using capillary action as the driving force when a volatile liquid was being evaporated and condensed. In this patent an example is

described using anhydrous ammonia as the working fluid and sintered powdered iron as the capillary structure. The author depicted several configurations of the capillary structure. The primary application advocated by Gaugler was transferring heat in refrigeration systems.

Gifford [2] described a device similar to a heat pipe. The device was a thermal check valve for use in helium or hydrogen liquifiers, refrigerators for various electronic devices, cryopumping, and storage dewars. For these applications it was desirable for the device to provide heat flow in one direction only. The device described consisted of a small stainless steel tube and was capable of transferring larger quantities of heat than a copper rod of comparable size.

After the heat pipe was "reinvented" the first work reported was to determine experimentally the heat transfer capability of heat pipes [3]. A water heat pipe (30 centimeters long) and two liquid sodium heat pipes (30 centimeters and 90 centimeters long, respectively) were subjected to tests to determine the maximum heat input. Wicking material used was either stainless steel screen or porous Alundum tubes. Heat transfer was by radiation and temperature profiles were obtained for the 90-centimeter-long heat pipe. In obtaining these temperature profiles, Grover, et al. accounted for the sharp drops at the unheated end of the heat pipe as being due to hydrogen generation. The conclusion arrived at by them was that 30 watts/centimeters^2 was the maximum heat input rate. It was concluded that this maximum rate was restricted by the deformation or drying of the wick.

A report by Cotter [4] was the first attempt to develop a quantitative engineering theory for the design and performance analysis of heat pipes. Employing simple physical laws, formulas and data developed in References 5, 6, and 7, and engineering judgement, Cotter developed expressions for the vapor pressure, maximum height of capillary rise, pressure gradient in the axial direction, and the amount of heat transferred. Two of the assumptions made by Cotter [4] were that the viscous losses in the vapor space and the wick were equal and that no boiling occurred in the wick. This work and the experiments mentioned above contributed much to the understanding of the mechanics involved in the operation of heat pipes.

In addition to Cotter [4], Marcus [8] did important theoretical work in heat pipe analysis. Marcus developed an expression for optimum wick thickness plus the other expressions essential in heat pipe analysis. This work was based on the assumption that viscous forces in the vapor are negligible and that boiling occurs in the wick. Through his efforts, knowledge of heat pipe analysis was extended, and an alternate method was developed for determining important parameters in heat pipe design.

With the basic theory of heat pipes established, Deverall [9] was one of the first to apply the heat pipe to a specific use. A heat pipe, 29 5/8 inches long and 3/4 inches O.D., was constructed and experimentally qualified to transfer heat isothermally from an externally mounted radioscope to the electronic component section of a satellite. This heat pipe consisted of a stainless steel tube, a 100-mesh stainless steel screen wick, and distilled

water as the working fluid. Some of the procedures important to heat pipe assembly and operations are discussed in this report [9]. Results of one of the tests showed that the heat pipe was essentially isothermal at 199° F over its length with a heat input of 102.8 watts; 95 watts were transferred to the cooling water.

In 1965, Ranken and Kemme [10] summarized the Los Alamos and Euratom heat pipe investigations for the preceding period. They presented and discussed the theory and types of heat pipes constructed prior to 1965. Available test data were also discussed.

Clayton, [11], and Kemme, [12, 13], experimentally determined operating characteristics of heat pipes. Clayton experimented with water heat pipes of two different lengths, 24 inches and 48 inches. In the water heat pipes, the following parameters were varied:

(1) Applied heat load

(2) Wick thickness

(3) Liquid sump (liquid in excess of the quantity required to fill the capillary structure)

(4) Effect of negative gravity

(5) Heater area.

Kemme experimented with heat pipes, 3/4 inch O.D. and 12 inches long, and varied the following parameters:

(1) Applied heat load

(2) Operating fluid (potassium and sodium)

(3) Wick configuration (channels, loose-fitting screen, tight-fitting screen, and a combination of screen and channels).

Clayton [11] and Kemme [12, 13] agreed that maximum performance of heat pipes could be predicted with some confidence using existing heat pipe equations. Clayton [11] concluded that contaminants in the pipe degrade performance and that a liquid sump is necessary for a satisfactory performance. Kemme concluded that heat transfer characteristics of heat pipes could be changed significantly by varying wick structure and that heat transfer capability of heat pipes could be substantially improved by the use of a two-component wick.

References 14, 15, and 16 present data useful in designing heat pipes. The data presented are properties or combinations of properties of fluids and wicking material used in heat pipes.

In References 14 and 15, two similar approaches to designing heat pipes are presented. Both are modifications of designs previously described. In these designs, there is a grouping of properties that optimize heat transfer in heat pipes. The data are exhibited in the form of graphs.

One of the first investigations for applying the heat pipe concept to spacecraft thermal control problems was conducted by Katzoff [17]. This report reviewed the theory of heat pipes, some possible applications, design computations, wick characteristics, multifluid operation, and other areas in which research and development are needed.

Three possible applications subjected to mathematical analysis by Katzoff [17] are:

(1) Maintenance of an evacuated cylinder at a uniform temperature by lining the inside surface with a saturated capillary structure

(2) Transfer of heat isothermally between parallel plates

(3) Improving temperature uniformity of an irradiated cylinder by wrapping heat pipes around the circumference at equal intervals.

An orbital experiment was conducted [18] to demonstrate that a heat pipe will operate, as predicted, in the absence of gravitational forces. The heat pipe was 12 inches long, 0.75 inch O.D., and constructed of a stainless steel tube lined along its full length with a 100-mesh stainless steel screen wick. Water was used as the working fluid. The heat pipe was operated in an earth orbit, and its performance was monitored by telemetry of several tracking stations during 14 revolutions. Heat was supplied to the heat pipe by a 10-watt electric heater.

The results of the orbital experiment indicated that the absence of gravitational forces does not affect the performance of a heat pipe. The start-up and equilibrium operations were similar to tests in a gravity field.

Reference 18 contains a useful assembly and cleaning procedure for heat pipes.

Haskin [19] made the first investigation for a heat pipe operating below room temperature. The heat pipe was 33 1/4 inches long, 3/4 inch O.D., and constructed of a stainless steel tube line along its full length with an Avril rayon cloth wick. Nitrogen was used as the working fluid. Heat loads of up to 130 watts were transferred axially in the heat pipe.

Results of this effort show that a heat pipe using nitrogen can transfer heat loads of 100 watts with about half the temperature drop of a solid copper rod of comparable size. The heat pipe was sensitive to inclinations from the horizontal position because of the weak capillary action that is due to the low surface tension of liquid nitrogen. A severe problem was encountered when the evaporator surface operating temperatures were near the critical temperature of nitrogen owing to the formation of a vapor film.

Anand and Hester [20] did analytical and experimental work with heat pipes and areas associated with heat pipes. The experimental program was to determine a suitable method of control for the heat pipe and to establish suitable wick/fluid configurations for certain temperature ranges. Sufficient understanding of heat pipe operation and fabrication methods was acquired to allow the design of a heat pipe for thermal control in a spacecraft application.

Neal [21] reported the results of a number of heat pipe experiments using various wick structures. Also, included in his report was a development of heat pipe design equations and a discussion of various working fluids for heat pipes.

Two heat pipe systems were designed, operated, and evaluated using wicks of refrasil, stainless steel screen, and sintered copper fiber. The first was 16 inches long, 1 1/2 inches O.D., and constructed of a copper tube lined along its full length with a 1/8-inch thick sintered copper fiber wick. Water was used as the working fluid. The second heat pipe was 24 inches long, 3/4 inch O.D., and constructed of a stainless steel tube with wicks of

refrasil and stainless steel screen. Either water or ethyl alcohol were used as the working fluid in this pipe.

In general, the condenser was cooled with water from the building supply at about 68° F for both heat pipes; however, some experiments were made with refrigerated coolant in order to observe the heat pipe operation as the working fluid froze in the wick. The startup of an initially frozen heat pipe was also conducted.

Results from this report [21] are as follows:

(1) The thermal conductivity of nonmetal wicks is too low for their use in heat pipes designed to transfer large heat loads.

(2) Wicks of refrasil should be bonded to the pipe wall to decrease the resistance to energy transfer.

(3) The relative limits for water and ethyl alcohol were predictable from the hydrodynamic theory.

(4) Liquid with large intermolecular forces are good heat pipe working fluids, because they exhibit high surface tensions and possess latent heats of vaporization.

(5) The power limitations of heat pipes studied were due to limitations on capillary pumping.

(6) The stainless steel screen wicks, formed by rolling the wire on a mandril, resulted in heat pipes that were not reproducible in detail.

(7) The startup of a frozen heat pipe, even at very low power levels, may lead to a burnout.

(8) The sintered copper fiber wick possessed a large capacity for transferring power, but the wick was not bonded to the heat pipe wall, and the contact resistance to heat transfer resulted in a very large overall temperature drop.

C. Role of the Heat Pipe in Modern Technology

Heat pipes can be used as a heat transfer device while acting as a structural member. Therefore, where the heat pipe is applicable it is a weight-saving device also. Space applications are favorable for the heat pipe since weight saving is of prime importance in space vehicles.

Recently, considerable work has been devoted to developing the heat pipe for application to nuclear power supplies. Heat pipes are used to transfer heat isothermally from the reactor core to a thermionic converter some distance away and to improve the efficiency and reduce the weight of the radiator. The use of the heat pipe in connection with a nuclear power supply could be considered for either space or earth installations.

A potentially attractive application of the heat pipe concept [22] is to utilize a closed heat pipe loop to absorb and reject excess of heat leaking through cryogenic tank walls during extended storage in space. A schematic of such a concept is illustrated in Figure 2. The working fluid used in this type of heat pipe is a cryogen with a boiling temperature slightly lower than that of the stored cryogen.

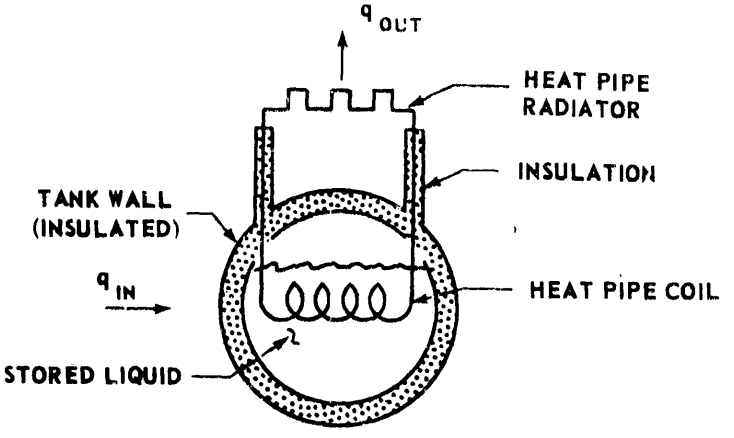

FIGURE 2. HEAT PIPE CONCEPT TO CONTROL BOILOFF RATE

As heat leaks through the normal insulation and is transmitted to the heat pipe in contact with the tank walls or stored cryogen, the heat pipe absorbs and transfers this heat to the outer loop which in turn radiates the heat to deep space. Since only part of the heat leak is absorbed by the heat pipe, the reduction of boiloff will depend on the percentage of stored cryogen in contact with the heat pipe. Application of this concept could result in a large weight savings if the duration of cryogen storage is a long period.

Heat pipes may have an application in improving the temperature uniformity of the outer surface of an object, such as a spacecraft, that is subjected to nonumiform heating from an external source. Consider a long metal cylinder which is subjected to radiation. The skin temperature of this cylinder would obviously be nonuniform because of nonuniform heating. The addition of heat pipes around the circumference at regular axial intervals will cause almost immediate transfer of heat received by the heat pipes from irradiated areas around to the shaded areas, with

practically no temperature drop. The heat pipes create a series of narrow isothermal bands around the vehicle, and the only variation in temperature is between each heat pipe and the adjacent metal. Therefore, heat conduction around the cylinder may be neglected, and the only appreciable heat flow in the metal skin will be axially between the heat pipe and the adjacent metal.

One important application of the heat pipe is to transport heat between a concentrated source, such as an electronic component, and a sink, such as a heat exchanger or radiator. The heat pipe would be of greater importance in the case where it could serve a two-fold purpose, such as where a structural member was required between the sink and the source.

Utilization of the heat pipe as a means of improving the performance of space radiators has been considered. Since the heat pipe is essentially an isothermal device, it can be used to eliminate the temperature differential between the tube and the solid fin of the radiator. The required surface area of the radiator will be reduced, since the radiator will be radiating at a higher temperature. When heat pipes are used in conjunction with vapor chambers as radiators, instead of the conventional central tube and fin design, substantial weight savings are realized.

The major role for the heat pipe is probably in space vehicles where weight saving is so important. After subsystems of space vehicles are more clearly defined, the applications cited here are only a few that can be expected to be discovered. It is important that the heat pipe be thought of as being in its infancy and its role in modern technology is not really completely defined at this time.

D. Basic Principles

The heat pipe, as previously defined and illustrated in Figure 1, consists of a sealed container lined with a wick that is saturated with a liquid at and near the saturation pressure corresponding to its liquid temperature. As heat is added to one end of the pipe, termed the evaporator, the liquid in the adjacent wick evaporates and absorbs its latent heat. Because of the resulting difference in vapor pressure, the generated vapor flows from the evaporator to the cooler, condenser end where the vapor condenses onto the wick and gives up its latent heat.

The evaporation of liquid at the vapor-liquid interface causes the residual liquid to retreat into the capillary structure, giving a meniscus radius of curvature and a contact angle that are smaller in the evaporator than in the condenser section, where the condensate is being deposited. This difference causes a pressure gradient in the liquid that pumps it through the wick from the condenser section back to the evaporator section, thus completing the cycle.

The heat pipe, an efficient heat transfer device, must operate within certain design limitations. The maximum total power that can be transferred in a heat pipe of given size and with a given fluid is determined by the ultimate pumping capacity of the capillary structure and by the onset of film boiling between the pipe wall and the wick. It has been found that the capillary pumping limitation is more prevalent than the film boiling limitation if metal wick structures are used.

The pumping capacity of the capillary structure depends on the size and geometry of the wick, as well as on the properties of the working fluid, such as its latent heat of vaporization, surface tension, density, and viscosity. The functional relationship between the ultimate pumping capacity of the wick and its geometrical factors, as well as the properties of the working fluid, can be obtained by applying general conservation equations to the system.

CHAPTER II

DEVELOPMENT OF THEORY

A. Static Condition

Suppose no heat is added to or removed from the heat pipe (Fig. 1), and the pipe is in static equilibrium. Then, the pressure distribution in the liquid phase, $P_\ell(z)$, obeys the hydrostatic law for an incompressible fluid;

$$P_\ell(z) = P_\ell(o) + \rho_\ell \frac{g}{g_c} z \cos\beta \tag{1}$$

The pressure in the vapor phase, $P_v(z)$, (assumed an ideal gas) has a Boltzmann distribution, but the variation in pressure may be neglected so that the pressure, P_v, may be assumed constant. At the interface between the liquid in the wick and the vapor in the vapor space, the radius of the pores, r_c, and the apparent contact angle, θ, must be such that the surface tension, σ, supports the pressure difference. Thus,

$$P_v(z) - P_\ell(z) = \frac{2\sigma\cos\theta}{r_c} \quad . \tag{2}$$

B. Steady-State Heat Pipe Regime

Consider a cylindrical heat pipe in a steady-state operation. Basic working relations will be derived by taking averages over the cross section of the pipe and by invoking simplifying assumptions.

The conservation of mass for a fluid with density, $\rho(z, r)$, and velocity, $\vec{V}(z, r)$, can be expressed as

$$\nabla \cdot \rho \vec{V} = 0 \quad . \tag{3}$$

Since there is no flow normal to the outer boundaries of the liquid region, the velocity components, V_z and V_r, satisfy the boundary conditions,

$$V_z(o, r) = V_z(L, r) = V_r(z, r_o) = 0 \quad . \tag{4}$$

The total axial flow of vapor, $\dot{m}_v$, and of liquid, $\dot{m}_\ell$, at the axial position, Z, are

$$\begin{aligned} \dot{m}_v(z) &= \int_o^{r_v} \rho_v(z, r)\ V_z(z, r)\ 2\pi r\ dr \\ \dot{m}_\ell(z) &= \int_{r_v}^{r_o} \rho_\ell(z, r)\ V_z(z, r)\ 2\pi r\ dr \quad . \end{aligned} \tag{5}$$

Applying Gauss' theorem to equation (3) in the cylindrical region between o and z and inside r_o, and using equations (4) and (5)

$$\dot{m}_v(z) + \dot{m}_\ell(z) = 0 \quad . \tag{6}$$

The average radial and axial pressure gradients will be inversely proportional to the flow areas in the radial and axial directions, respectively. For pipes in which $r_v\ L > r_o^2$, the radial pressure gradient, will be neglected, and it will be assumed that both the flow velocity and pressure in the liquid depend only on z.

The momentum equation for steady viscous incompressible flow with a velocity component in the Z direction only may be written as

$$\frac{dP_\ell}{dz} = \mu_\ell \frac{\partial^2 V_z}{\partial z^2} - \rho_\ell V_z \frac{\partial V_z}{\partial z} + \rho_\ell \frac{g}{g_c} \cos\beta \ . \tag{7}$$

Reference 4 shows that the second term on the right side of equation (7) is negligible relative to the first and third terms. Then equation (7) may be written in the following manner.

$$\frac{dP_\ell}{dz} = -\frac{\mu_\ell}{K} W + \rho_\ell \frac{g}{g_c} \cos\beta \tag{8}$$

where W is the average velocity of the liquid and K is the permeability of the wick. Equation (8) is a version of Darcy's law. Since

$$\dot{m} = \rho V A \ , \tag{9}$$

where A is the area perpendicular to the flow direction, equation (8) may be written as

$$\frac{dP_\ell}{dz} = -\frac{\mu_\ell}{K} \frac{\dot{m}_\ell}{\pi(r_o^2 - r_v^2)\rho_\ell} + \frac{g}{g_c} \rho_\ell \cos\beta \ . \tag{10}$$

The dynamics of the vapor flow is different since, in general, an equation like equation (10) relating the local pressure gradient with the local mass flow does not exist, and the initial term in equation (7) is often not negligible.

Vapor flow in the evaporator and the condenser is similar to pipe flow with injection and suction through a porous wall. The results from

Reference 5, which is concerned with flow through a cylindrical pipe with suction and injection, will be used for the condenser and the evaporator.

Using the results from Reference 5 and assuming incompressible laminar flow with uniform injection or suction, regimes may be established that depend on the magnitude of the Radial Reynolds number, R_{e_r}, where

$$R_{e_r} = + \frac{\rho_v r_v V_r}{\mu_v} = \frac{1}{2\pi\mu_v} \frac{d\dot{m}_v}{dz} \quad . \tag{11}$$

Note that R_{e_r} is positive for evaporation (injection) and negative for condensation (suction). For $|R_{e_r}| << 1$ viscous effects dominate, and the axial velocity profile is similar to the parabolic shape for Poiseville flow. Neglecting gravity, the resulting pressure gradient is approximately

$$\frac{dP_v}{dz} = - \frac{8\mu_v \dot{m}_v}{\pi \rho_v r_v^4} \left(1 + \frac{3}{4} R_{e_r} - \frac{11}{270} R_{e_r}^2 + \ldots\right) \tag{12}$$

with $|R_{e_r}| << 1$; therefore, terms of $R_{e_r}^2$ may be neglected. Equation (12) is derived with R_{e_r} assumed a constant and independent of z. These limitations on R_{e_r} are appropriate for the evaporator and the condenser of a heat pipe.

When $|R_{e_r}| >> 1$, high evaporation and condensation rates exist and the cases of evaporation and condensation differ. For high evaporation rates, the radial dependence of velocity is not parabolic but is proportional to $\cos \frac{\pi}{2} \left(\frac{r}{r_v}\right)^2$ and the pressure decreases in the direction of flow. When condensation rates are high, the flow is of the boundary layer type and the pressure increases in the direction of flow due to partial dynamic recovery of the decelerating flow. For flow of the boundary layer type, the

axial velocity is constant across most of the section, with the transition to zero velocity occurring in a thin layer near the wall. From Reference 4 for either evaporation or condensation, with the limit $R_{e_r} \to \infty$ leads to

$$\frac{dP_v}{dz} = -\frac{s\dot{m}_v}{4\rho_v r_v^4 g_c}\frac{d\dot{m}_v}{dz} \tag{13}$$

where $s = 1$ for evaporation and $s = \frac{4}{\pi^2}$ for condensation.

The Reynolds number,

$$R_{e_z} = \frac{\rho_v r_v V_z}{\mu_v} = \frac{\dot{m}_v}{\pi r_v \mu_v} \quad , \tag{14}$$

may be used to describe the vapor flow in the axial direction. If an adiabatic section connects the evaporator and condenser of a heat pipe, with $R_{e_r} \approx 0$ in the adiabatic section, then the Poiseuille formula,

$$\frac{dP_v}{dz} = -\frac{8\mu_v \dot{m}_v}{\pi \rho_v r_v^4} \quad , \tag{15}$$

may be used for laminar vapor flow in the adiabatic section.

Flow dynamics are also concerned with the relations between the vapor and liquid pressures and the vapor and liquid mass flows. In the static and steady-state cases, equation (2) is appropriate. In the steady-state case, P_v depends on z. The vapor and liquid mass flows are coupled with the liquid temperature at the interface, $T(z, r_v)$, which also determines the vapor pressure of the liquid, P. The local condensation rate, $\frac{d\dot{m}_\ell}{dz}$ is given by Reference 4 as

$$\frac{d\dot{m}_\ell}{dz} = -\frac{d\dot{m}_v}{dz} = \frac{\alpha\, r_v\, (P_v - P)}{\sqrt{RT/2\pi M}} \quad . \tag{16}$$

The numerical factor, $\alpha \approx 1$, includes both the probability of condensation of an impinging vapor molecule and the roughness of the meniscus interface formed by the capillary structure. Equation (16) may also be used for surface evaporation except when bubbles are forming, due to boiling, in the capillary structure.

For a heat pipe, though the amount of heat transfer may be very large, the axial and radial temperature gradients are very small and axial conduction terms are small compared to other terms. Using the preceding, Cotter [4] showed that the axial transport of energy is approximately

$$q = \lambda\, \dot{m}_v(z) \ , \tag{17}$$

where λ is the heat of vaporization of the fluid.

The basic equations presented in this section were taken from Reference 4, except changes were made in some of these equations. The major change was made in equation (10). The substitution of $\frac{\mu_\ell}{K}$ for $\frac{b\mu_\ell}{\epsilon r_c^2}$ was made so that the properties concerned could be determined experimentally or found in the literature.

C. Heat Pipe as a Radiating Fin

A heat pipe as a radiating fin may be defined as a heat pipe with a heat input, q, added to the evaporator and this heat input is radiated from the remaining section, the condenser, of the heat pipe. The addition and

rejection of heat is assumed to be at a constant rate. With the basic equations from the previous section, the relationship between q and other properties may be established.

From equations (6) and (17), the vapor and liquid mass flows may be obtained.

$$\dot{m}_v(z) = \dot{m}_\ell(z) = \frac{q}{\lambda} \tag{18}$$

Consider equation (10) and assume that heat is added and rejected as depicted in Figure 3.

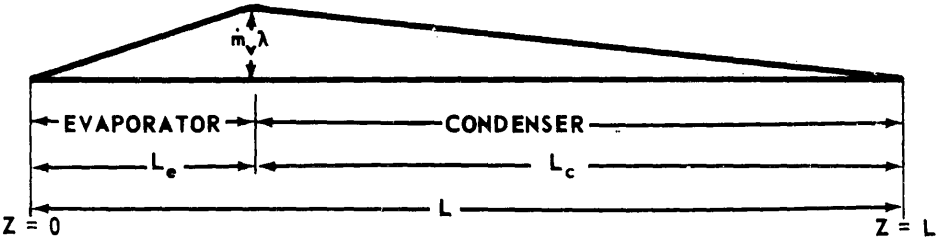

FIGURE 3. HEAT ADDITION AND REJECTION (RADIATING FIN)

The rate of heat transfer in the axial direction is assumed to be

$$q = \lambda \dot{m}_v = \begin{cases} \dfrac{q_e z}{L_e} & , \quad 0 \le z \le L_e \\ \dfrac{q_e (L - z)}{L_c} & , \quad L_e \le z \le L \end{cases} \tag{19}$$

and

$$\dot{m}_v = -\dot{m}_\ell = \begin{cases} \dfrac{q_e z}{\lambda L_e} , & 0 \le z \le L_e \\ \dfrac{q_e (L - z)}{\lambda L_c} , & L_e \le z \le L \end{cases} , \qquad (20)$$

where q_e is the total rate of heat transfer to the evaporator.

Using the above for $\dot{m}_\ell$, equation (10) can be integrated to obtain the pressure variation in the liquid.

$$\int_{P_\ell(o)}^{P_\ell(L)} dP_\ell = -\left[\frac{\mu_\ell q_e}{\lambda \pi (r_o^2 - r_v^2) K \rho_\ell}\right] \left[-\int_o^{L_e} \frac{z\, dz}{L_e} - \int_{L_e}^{L} \frac{(L - z)\, dz}{L_c} + \rho_\ell \frac{g}{g_c} \cos\beta \int_o^L dz\right]$$

then

$$\Delta P_\ell = P_\ell(o) - P_\ell(L) = -\frac{\mu_\ell q_e L}{2 K \rho_\ell \lambda \pi (r_o^2 - r_v^2)} - \rho_\ell \frac{g}{g_c} L \cos\beta . \qquad (21)$$

With $\dot{m}_v$ given by equation (20) and using equations (11), (12), and (13), the pressure variations in the vapor can be found. Two conditions, $|R_{e_r}| \ll 1$ and $|R_{e_r}| \gg 1$, may be considered.

1. $|R_{e_r}| \ll 1$

Neglecting $R_{e_r}^2$ terms, equation (12) becomes

$$\frac{dP_v}{dz} = -\frac{8 \mu_v \dot{m}_v}{\pi \rho_v r_v^4} \left(1 + \frac{3}{4} R_{e_r}\right) . \qquad (22)$$

Substituting equation (11) into equation (22) yields

$$\frac{dP_v}{dz} = -\frac{8\mu_v \dot{m}_v}{\pi \rho_v r_v^4}\left(1 + \frac{3}{8\pi\mu_v}\frac{d\dot{m}_v}{dz}\right) . \tag{23}$$

Substituting equation (20) into equation (23) and integrating

$$\int_{P_v(o)}^{P_v(L)} dP_v = -\frac{8\mu_v}{\pi\rho_v r_v^4}\left\{\int_o^{L_e}\left[\frac{q_e z}{\lambda L_e} + \frac{3}{8\pi\mu_v}\left(\frac{q_e z}{\lambda L_e}\right)\left(\frac{q_e}{\lambda L_e}\right)\right] dz + \int_{L_e}^{L}\left[\frac{q_e(L-z)}{\lambda L_c} + \frac{3}{8\pi\mu_v}\left(\frac{q_e(L-z)}{\lambda L_c}\right)\left(-\frac{q_e}{\lambda L_c}\right)\right]dz\right\}$$

then

$$\Delta P_v = P_v(o) - P_v(L) = \frac{4\mu_v q_e L}{\pi\rho_v r_v^4 \lambda} . \tag{24}$$

2. $|R_{e_r}| \gg 1$

Substituting equation (20) and $s = 1$, evaporator, and $s = 4/\pi^2$, condenser, into equation (13), and then integrating gives

$$\int_{P_v(o)}^{P_v(L)} dP_v = -\frac{1}{4\rho_v r_v^4 g_c}\int_o^{L_e}\left(\frac{q_e z}{\lambda L_e}\right)\left(\frac{q_e}{\lambda L_e}\right) dz - \frac{\frac{4}{\pi^2}}{4\rho_v r_v^4 g_c}\int_{L_e}^{L}\left[\frac{q_e(L-z)}{\lambda L_c}\right]\left(-\frac{q_e}{\lambda L_c}\right) dz ,$$

then

$$\Delta P_v = P_v(o) - P_v(L) = \frac{\left(1 - \frac{4}{\pi^2}\right) q_e^2}{8\rho_v r_v^4 \lambda^2 g_c} \tag{25}$$

The axial heat transfer depends on the capillary forces being able to sustain the required circulation of fluid. The maximum pressure differential between vapor and liquid that can be supported by surface tension in the capillary structure is defined by equation (2). Then for the particular case of uniform heat addition and removal for the heat pipe as a radiating fin, equations (2), (21), (24), and (25) may be used to define the limiting condition for the total axial heat transfer.

1. $|R_{e_r}| \ll 1$

$$\frac{4 \mu_v q_e L}{\pi \rho_v r_v^4 \lambda} + \frac{\mu_\ell q_e L}{2 K \rho_\ell \lambda \pi (r_o^2 - r_v^2)} + \rho_\ell \frac{g}{g_c} L \cos \beta = \frac{2 \sigma \cos \theta}{r_c} \quad . \tag{26}$$

2. $|R_{e_r}| \gg 1$

$$\frac{\left(1 - \frac{4}{\pi^2}\right) q_e^2}{8 \rho_v r_v^4 \lambda^2 g_c} + \frac{\mu_\ell q_e L}{2 K \rho_\ell \lambda \pi (r_o^2 - r_v^2)} + \rho_\ell \frac{g}{g_c} L \cos \beta = \frac{2 \sigma \cos \theta}{r_c} \tag{27}$$

D. Heat Pipe Having an Adiabatic Section

A heat pipe having an adiabatic section consists of an evaporator, condenser, and an adiabatic section connecting the other two sections. It is assumed that heat is added to the evaporator at a constant rate and removed at the condenser at a constant rate with flow through the connecting section being adiabatic.

Equation (18) is applicable in this case and can be used. Consider equation (10) and assume that heat is added and removed as depicted in Figure 4.

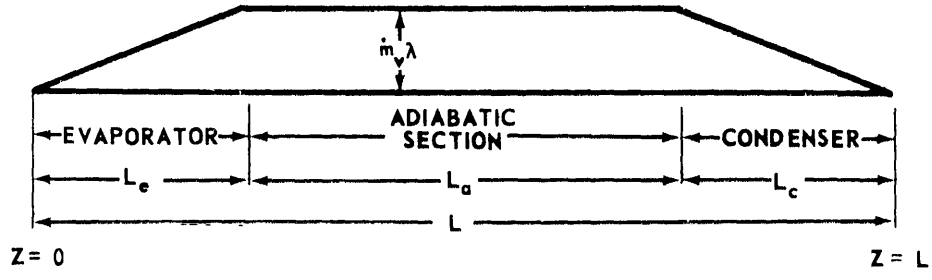

FIGURE 4. HEAT ADDITION AND REJECTION (ADIABATIC SECTION)

The rate of heat transfer in the axial direction is

$$q = \lambda \dot{m}_v \begin{cases} \dfrac{q_e z}{L_e} & , \quad 0 \le z \le L_e \\ q_e & , \quad L_e \le z \le L_e + L_a \\ \dfrac{q_e (L - z)}{L_c} & , \quad L_e + L_a \le z \le L \end{cases} \tag{28}$$

and

$$\dot{m}_v = - \dot{m}_\ell \begin{cases} \dfrac{q_e z}{\lambda L_e} & , \quad 0 \le z \le L_e \\ q_e/\lambda & , \quad L_e \le z \le L_e + L_a \\ \dfrac{q_e (L - z)}{\lambda L_c} & , \quad L_e + L_a \le z \le L \end{cases} , \tag{29}$$

where q_e is the total rate of heat transfer to the evaporator.

Using equation (29) for $\dot{m}_\ell$, equation (10) can be integrated to yield the pressure distribution in the liquid.

$$\int_{P_\ell(o)}^{P_\ell(L)} dP_\ell = -\left[\frac{\mu_\ell q_e}{\pi \lambda K \rho_\ell (r_o^2 - r_v^2)}\right]\left[-\int_o^{L_e} \frac{z\,dz}{L_e} - \int_{L_e}^{L_e + L_a} dz - \int_{L_e + L_a}^{L} \frac{(L-z)}{L_c} dz\right]$$

$$+ \rho_\ell \frac{g}{g_c} \cos\beta \int_o^L dz$$

$$\Delta P_\ell = P_\ell(o) - P_\ell(L) = -\frac{\mu_\ell q_e (L + L_a)}{2\pi \lambda K \rho_\ell (r_o^2 - r_v^2)} - \rho_\ell \frac{g}{g_c} L \cos\beta \qquad (30)$$

Two conditions, $|R_{e_r}| << 1$ and $|R_{e_r}| >> 1$, must be considered for the pressure variation in the vapor.

1. $|R_{e_r}| << 1$

To find the pressure variation for the condenser and the evaporator, substitute equation (29) into equation (23) and integrate. For the adiabatic section, substitute equation (23) into the equation (31) and integrate.

$$\frac{dP_v}{dz} = -\frac{8\mu_v \dot{m}_v}{\pi \rho_v r_v^4} \qquad (31)$$

then

$$\int_{P_v(o)}^{P_v(L)} dP_v = -\frac{8\mu_v}{\pi \rho_v r_v^4}\left\{\int_o^{L_e}\left[\frac{q_e z}{\lambda L_e} + \frac{3}{8\pi\mu_v}\left(\frac{q_e z}{\lambda L_e}\right)\left(\frac{q_e}{\lambda L_e}\right)\right] dz\right.$$

$$+ \int_{L_e}^{L_e + L_a} \frac{q_e}{\lambda} dz + \int_{L_e + L_a}^{L}\left[\frac{q_e(L-z)}{\lambda L_c}\right.$$

$$\left.\left. + \frac{3}{8\pi\mu_v}\left(\frac{q_e(L-z)}{\lambda L_e}\right)\left(-\frac{q_e}{\lambda L_e}\right)\right] dz\right\}$$

$$\Delta P_v = P_v(o) - P_v(L) = \frac{4 \mu_v q_e (L + L_a)}{\pi \lambda \rho_v r_v^4} \quad . \tag{32}$$

2. $|R_{e_r}| >> 1$

To find the pressure variation in the vapor for this case, substitute equation (29) into equations (13) and (31), then integrate over the appropriate interval.

$$\int_{P_v(o)}^{P_v(L)} dP_v = -\frac{1}{4 \rho_v r_v^4 g_c} \int_o^{L_e} \left(\frac{q_e z}{\lambda L_e}\right) \left(\frac{q_e}{\lambda L_e}\right) dz - \frac{8 \mu_v}{\pi \rho_v r_v^4} \int_{L_e}^{L_e + L_a} \frac{q_e}{\lambda} dz$$

$$- \frac{\frac{4}{\pi^2}}{4 \rho_v r_v^4 g_c} \int_{L_e + L_a}^{L} \frac{q_e (L - z)}{\lambda L_c} \left(-\frac{q_e}{\lambda L_c}\right) dz \ ,$$

$$\Delta P_v = P_v(o) - P_v(L) = \frac{\left(1 - \frac{4}{\pi^2}\right) q_e^2}{8 \rho_v r_v^4 \lambda^2 g_c} + \frac{8 \mu_v q_e L_a}{\pi \rho_v r_v^4 \lambda} \tag{33}$$

For this case, using equations (2), (30), (32), and (33), the limiting condition on the total axial heat transfer is as follows:

1. $|R_{e_r}| << 1$

$$\frac{4 \mu_v q_e (L + L_a)}{\pi \lambda \rho_v r_v^4} + \frac{\mu_\ell q_e (L + L_a)}{2 \pi \lambda K \rho_\ell (r_o^2 - r_v^2)} + \rho_\ell \frac{g}{g_c} L \cos \beta$$

$$= \frac{2 \sigma \cos \theta}{r_c} \quad . \tag{34}$$

2. $|R_{e_r}| >> 1$

$$\frac{\left(1 - \frac{4}{\pi^2}\right) q_e^2}{8 \rho_v r_v^4 \lambda^2 g_c} + \frac{8 \mu_v q_e L_a}{\pi \rho_v r_v^4 \lambda} + \frac{\mu_\ell q_e (L + L_a)}{2 \pi \lambda K \rho_\ell (r_o^2 - r_v^2)}$$

$$+ \rho_\ell \frac{g}{g_c} L \cos \beta = \frac{2 \sigma \cos \theta}{r_c} \quad . \tag{35}$$

E. Considering Boiling in the Wick

Marcus [8] derived an equation for the maximum heat transfer for a heat pipe if boiling in the wick is considered. In this derivation it was assumed that viscous forces in the vapor are negligible and the heat pipe has an adiabatic section. The maximum heat transfer is

$$q_{max.} \quad 2\pi \bar{r}_w \left[\frac{T_{sat.} \sigma \rho_\ell K L_e k_{eff.} \left(\frac{2}{r_n} - \frac{P_w}{\epsilon}\right) \left\{\frac{P_w \sigma}{\epsilon} - \left(P_{v_e} - P_{v_c}\right) - \rho_\ell \frac{g}{g_c} L \cos \beta\right\}}{\mu_\ell L \rho_v J} \right]^{\frac{1}{2}} \tag{36}$$

where an approximation for $k_{eff.}$ is $k_{eff.} = \epsilon k_\ell + (1 - \epsilon) k_{wick}$, r_n = radius of bubble nucleus, and $\bar{r}_w = \frac{r_v + r_o}{2}$, then neglecting $P_{v_e} - P_{v_c}$

$$q_{max.} \quad \pi r_o \left(1 + \frac{r_v}{r_o}\right) \left[\frac{T_{sat.} \sigma \rho_\ell K L_e k_{eff.} \left(\frac{2}{r_n} - \frac{P_w}{\epsilon}\right) \left\{\frac{P_w \sigma}{\epsilon} - \rho_\ell \frac{g}{g_c} L \cos \beta\right\}}{\mu_\ell L \rho_v J} \right]^{\frac{1}{2}} . \tag{37}$$

F. Governing Equations Summarized

Equations (26), (27), (34), (35), and (37) are the governing equations for a heat pipe. After solving for $q_{max.}$ for each case, and considering that $\frac{r_v}{r_o}$ for a specific temperature is the primary variable, these equations are as follows:

1. Heat Pipe as a Radiating Fin

a. $|R_{e_r}| \ll 1$

$$q_{max.} = \left(\frac{2\,\sigma \cos\theta}{r_c} - \rho_\ell \frac{g}{g_c} L \cos\beta \right) \left[\frac{r_o^6 \left(\frac{r_v^4}{r_o^4} - \frac{r_v^6}{r_o^6} \right)}{\overline{\overline{A}}\, r_o^2 \left(1 - \frac{r_v^2}{r_o^2} \right) + \overline{B} r_o^4 \left(\frac{r_v^4}{r_o^4} \right)} \right] \tag{38}$$

where

$$\overline{\overline{A}} = \frac{4\,\mu_v L}{\pi\,\rho_v \lambda} \quad , \quad \overline{B} = \frac{\mu_\ell L}{2\,K\,\rho_\ell \lambda\,\pi} \quad . \tag{39}$$

b. $|R_{e_r}| \gg 1$

$$q_{max.} = \left(\frac{1}{2\overline{A}} \right) \left[r_o^4 \left(\frac{r_v^4}{r_o^4} \right) \left(- \frac{\overline{B}}{r_o^2 \left(1 - \frac{r_v^2}{r_o^2} \right)} \right) + \left\{ \frac{\overline{B}^2}{\left[r_o^2 \left(1 - \frac{r_v^2}{r_o^2} \right) \right]^2} - \frac{4\overline{A}}{r_o^4 \left(\frac{r_v^4}{r_o^4} \right)} \left(\overline{C} - \frac{2\,\sigma \cos\theta}{r_c} \right) \right\}^{\frac{1}{2}} \right] , \tag{40}$$

where

$$\overline{A} = \frac{\left(1 - \frac{4}{\pi^2} \right)}{8\,\rho_v \lambda^2 g_c} \quad , \quad \overline{B} \quad \frac{\mu_\ell L}{2\,K\,\rho_\ell \lambda\,\pi} \quad , \quad \overline{C} = \rho_\ell \frac{g}{g_c} L \cos\beta \, . \tag{41}$$

2. Heat Pipe Having an Adiabatic Section

a. $|R_{e_r}| \ll 1$

$$q_{max.} = \left(\frac{2\sigma \cos\theta}{r_c} - \rho_\ell \frac{g}{g_c} L \cos\beta \right) \left[\frac{r_o^6 \left(\frac{r_v^4}{r_o^4} - \frac{r_v^6}{r_o^6} \right)}{\bar{\bar{A}} r_o^2 \left(1 - \frac{r_v^2}{r_o^2} \right) + \bar{\bar{B}} r_o^4 \left(\frac{r_v^4}{r_o^4} \right)} \right] \tag{42}$$

where

$$\bar{\bar{A}} = \frac{4 \mu_v (L + L_a)}{\pi \rho_v \lambda} \quad , \quad \bar{\bar{B}} = \frac{\mu_\ell (L + L_a)}{2 K \rho_\ell \lambda \pi} \quad . \tag{43}$$

b. $|R_{e_r}| \gg 1$

$$q_{max.} = \frac{-E + \left[E^2 - 4D \left(\rho_\ell \frac{g}{g_c} L \cos\beta - \frac{2\sigma \cos\theta}{r_c} \right) \right]^{\frac{1}{2}}}{2D} \quad , \tag{44}$$

where

$$D = \frac{\left(1 - \frac{4}{\pi^2} \right)}{8 \rho_v \lambda^2 r_o^4 \left(\frac{r_v^4}{r_o^4} \right) g_c} \tag{45}$$

$$E = \frac{8 \mu_v L_a}{\pi \rho_v r_o^4 \left(\frac{r_v^4}{r_o^4} \right) \lambda} + \frac{\mu_\ell (L + L_a)}{2 K \rho_\ell \lambda \pi r_o^2 \left(1 - \frac{r_v^2}{r_o^2} \right)} \quad .$$

c. Marcus' equation

$$q_{max.} = \pi r_o \left(1 + \frac{r_v}{r_o}\right) \left[\overline{\overline{D}} k_{eff} \left(\frac{2}{r_n} - \frac{P_w}{\epsilon}\right) \left(\frac{P_w \sigma}{\epsilon} - \rho_\ell \frac{g}{g_c} L \cos\beta\right)\right]^{\frac{1}{2}} , \quad (46)$$

where

$$\overline{\overline{D}} = \frac{T_{sat.} \sigma \rho_\ell K L_e}{\mu_\ell L \rho_v J} . \quad (47)$$

G. Solution of the Governing Equations

Equations (38), (40), (42), (44), and (46) were programmed for the digital computer to permit rapid evaluation of the heat input to a heat pipe. These equations were solved for specific cases. The temperatures considered were 200° F, 250° F, 300° F, and 350° F. Each equation was solved with varying $\frac{r_v}{r_o}$ and the above temperatures for heat pipes with r_o equal to 0.0208, 0.0312, 0.0625, and 0.1250 foot. The wicking material used was 250 mesh screen made of 316 stainless steel wire with a diameter of 0.0016 inch. The input data to the computer, given in Appendix A, were from the references or calculated.

The solution of equations (38) and (40) was accomplished by using input data from Appendix A and a digital computer. These solutions are shown in Figures 5 through 8. Equations (38) and (40) were derived by considering the heat pipe as a radiating fin with small evaporation and condensation rates considered in equation (38) and large evaporation and condensation rates considered in equation (40). Considering the calculated data,

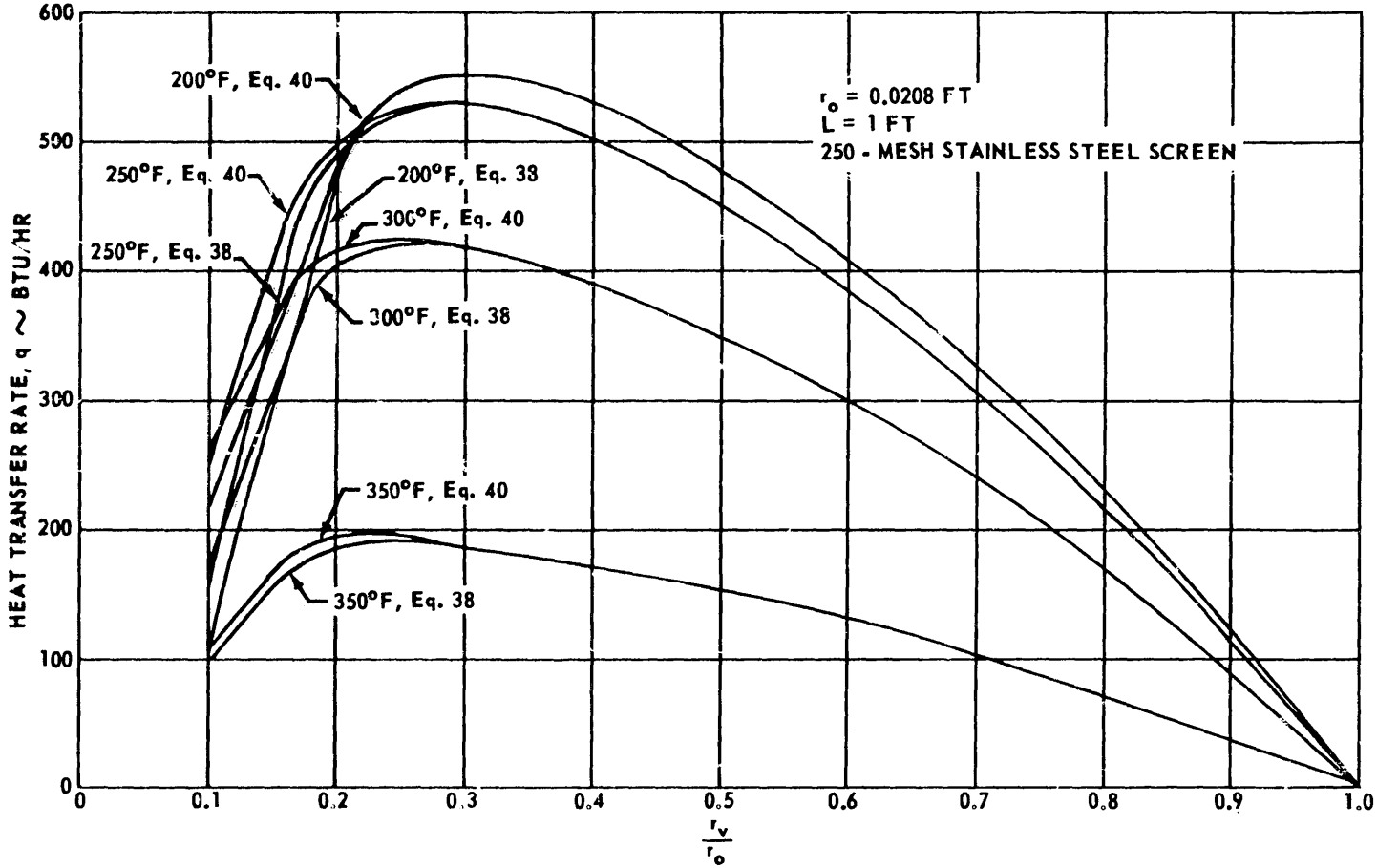

FIGURE 5. HEAT TRANSFER RATE VERSUS r_v/r_o (RADIATING FIN)

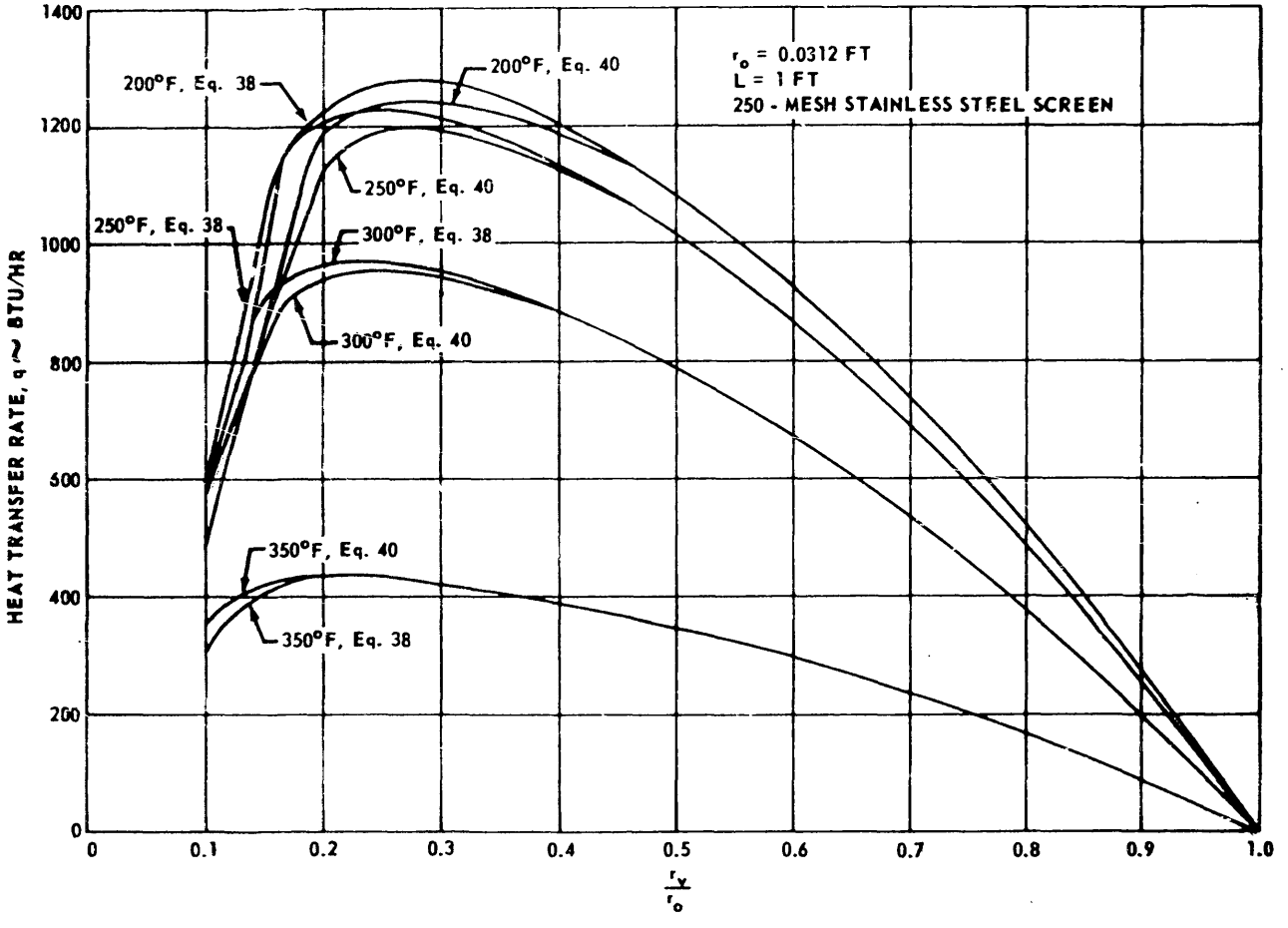

FIGURE 6. HEAT TRANSFER RATE VERSUS r_v/r_o (RADIATING FIN)

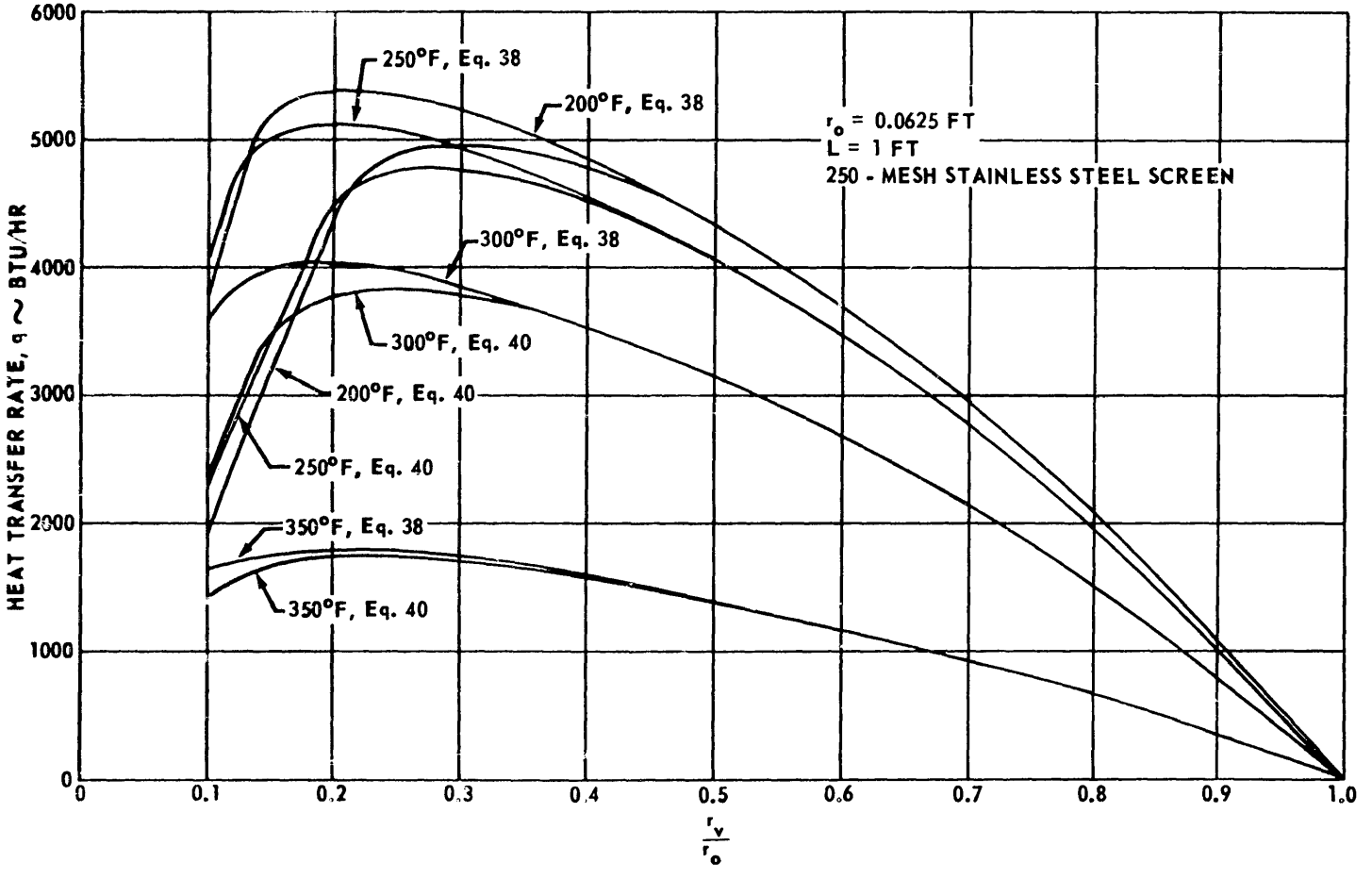

FIGURE 7. HEAT TRANSFER RATE VERSUS r_v/r_o (RADIATING FIN)

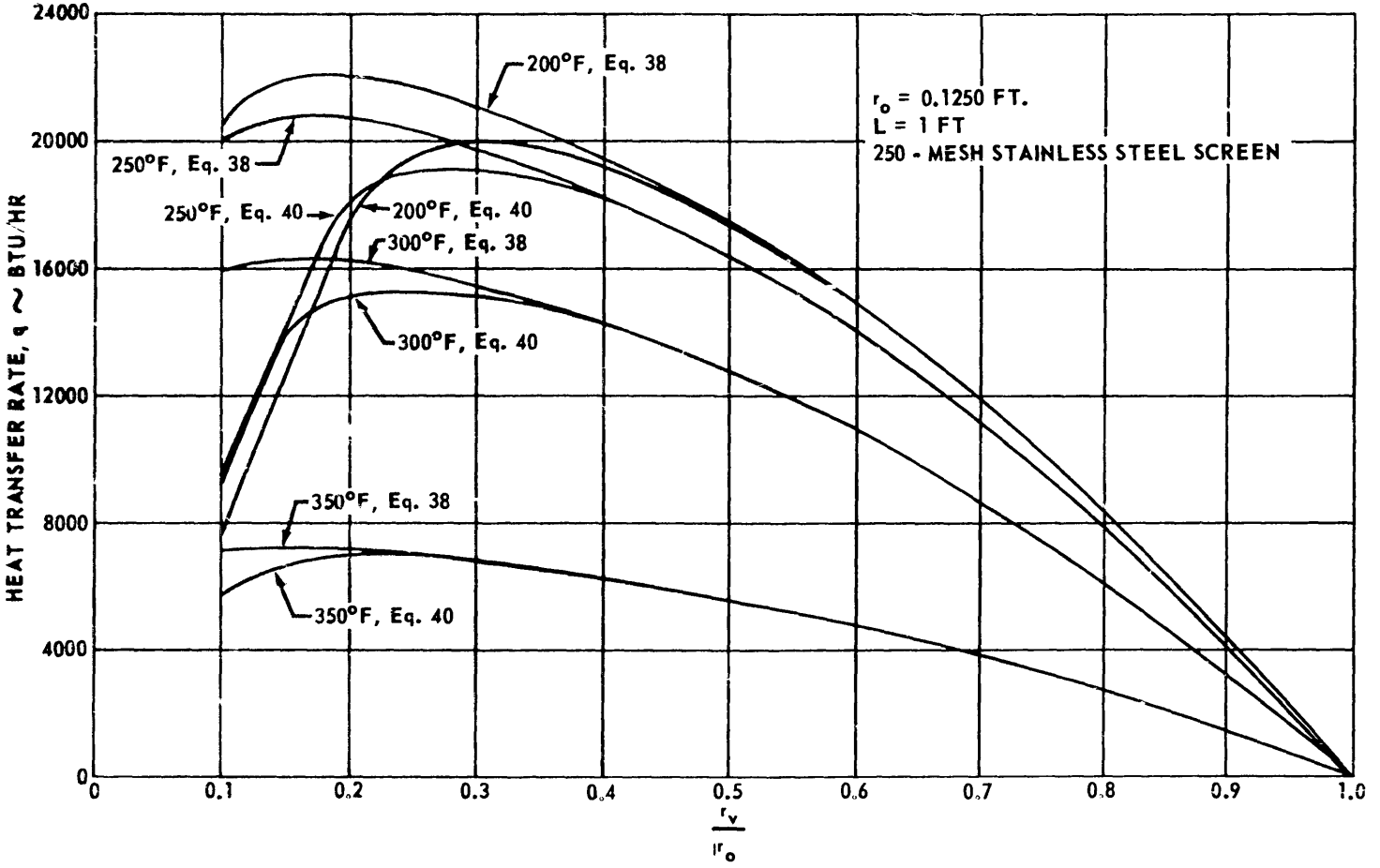

FIGURE 8. HEAT TRANSFER RATE VERSUS r_v/r_o (RADIATING FIN)

as shown by the curves, it is concluded that evaporation and condensation rates have no effect on the heat transfer rate for heat pipes with $\frac{r_v}{r_o} > 0.5$.

The solution of equations (42), (44), and (46) was obtained by use of a digital computer and input data as given in Appendix A. The solution to these equations is shown in Figures 9 through 12. Equations (42) and (44) were derived by considering a heat pipe with an adiabatic section having slow evaporation and condensation rates for equation (42) and rapid evaporation and condensation rates for equation (44). Equation (46) was derived by Marcus in Reference 8. As in the previous case, evaporation and condensation rates have no effect on the heat transfer rate for heat pipes with $\frac{r_v}{r_o} > 0.5$.

H. Parametric Studies

The governing equations were solved by a digital computer for different permeabilities, apparent contact angles, and lengths of adiabatic section to determine the effect these parameters had on the heat transfer rates.

1. Permeability

Three values different from the value shown in Appendix A were used for the permeability. The values of permeability used were 6.5×10^{-10}, 3.25×10^{-9}, and 3.25×10^{-2} ft^2. When these values were used (all other inputs as given in Appendix A) the optimum, r_v/r_o, becomes larger as the value for the permeability was increased. The optimum, r_v/r_o, is considered the value of r_v/r_o at which the maximum heat transfer rate occurs. The equations were solved for each value of permeability, temperature, and

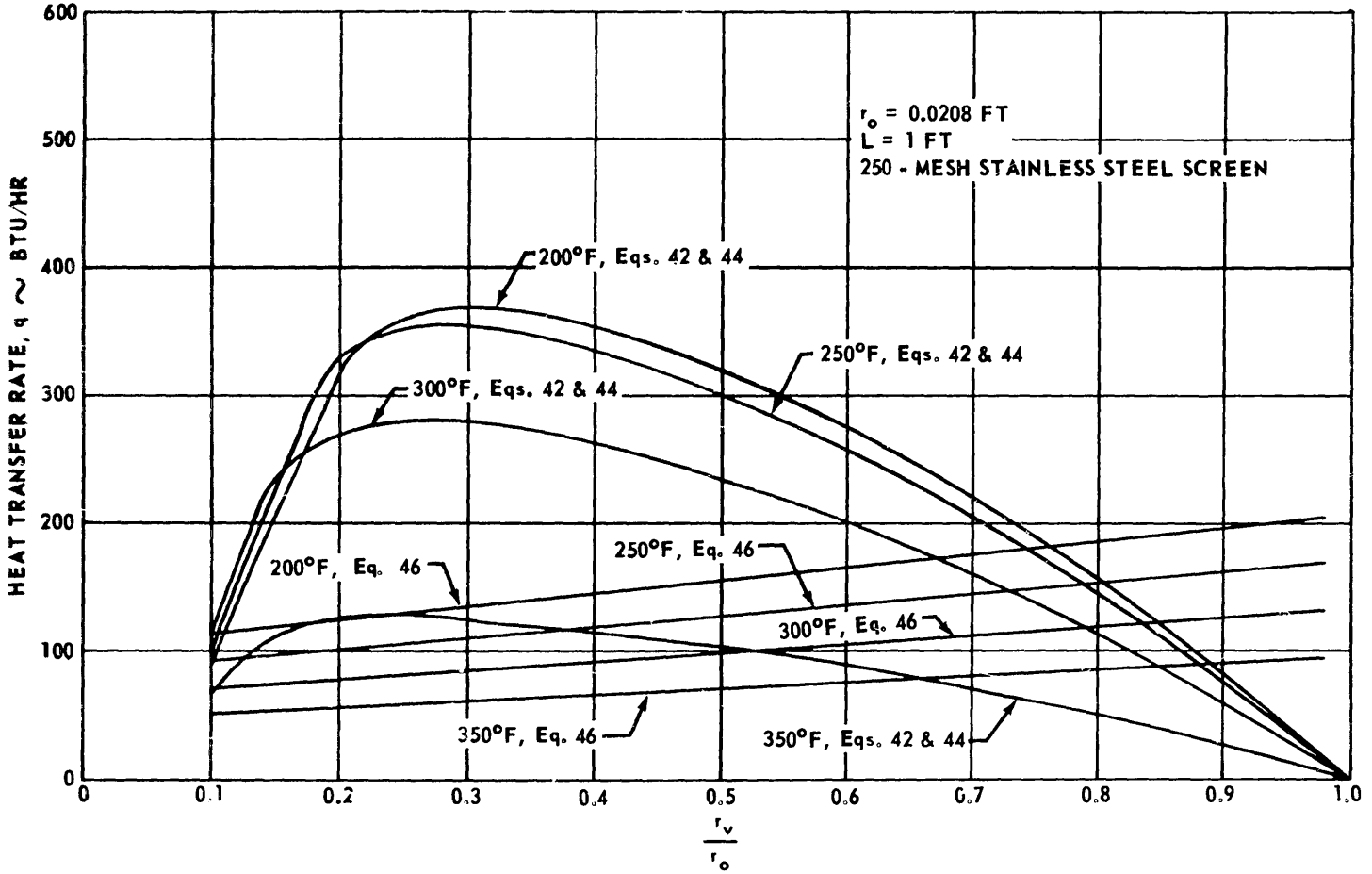

FIGURE 9. HEAT TRANSFER RATE VERSUS r_v/r_o (ADIABATIC SECTION)

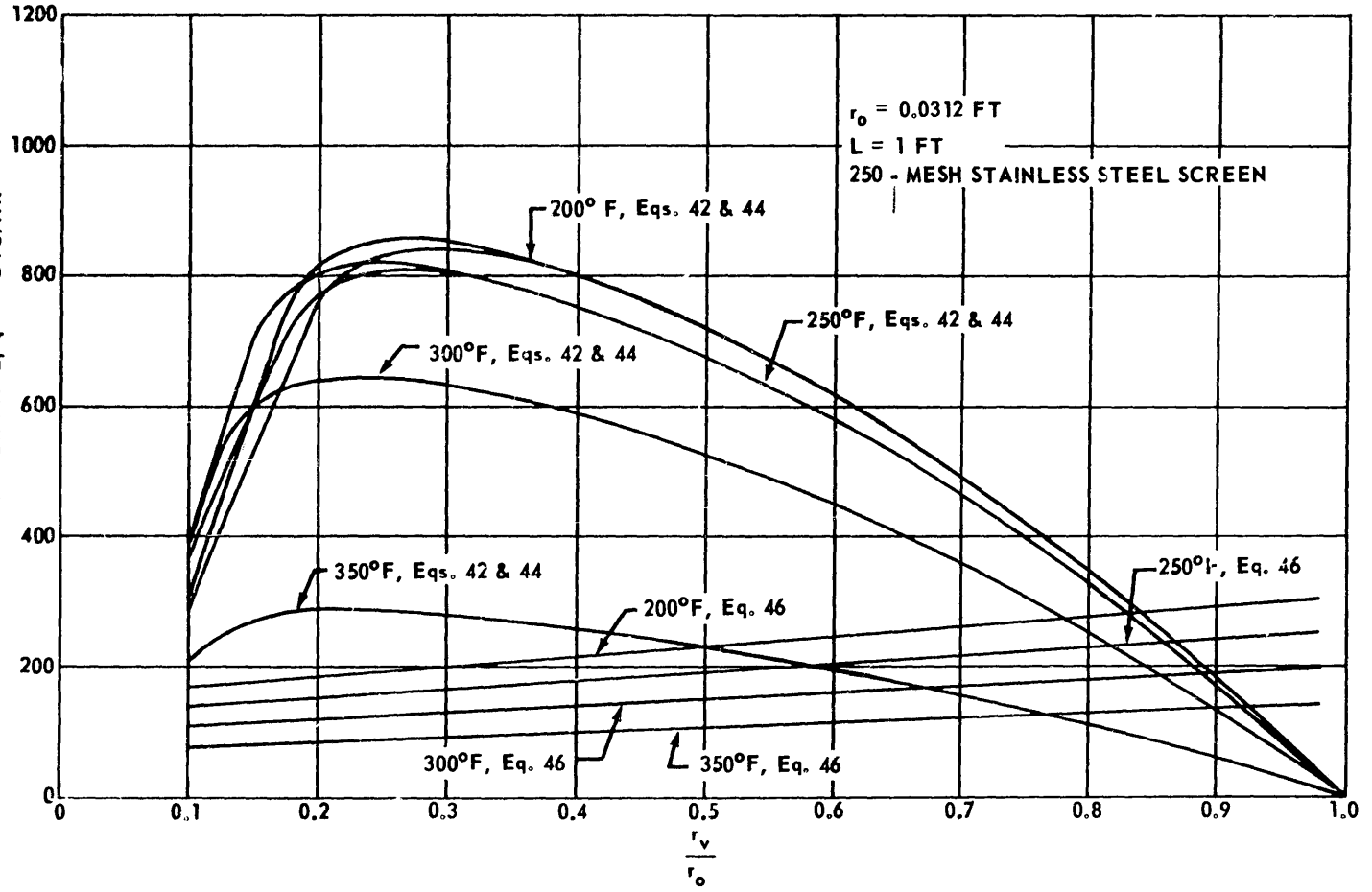

FIGURE 10. HEAT TRANSFER RATE VERSUS r_v/r_o (ADIABATIC SECTION)

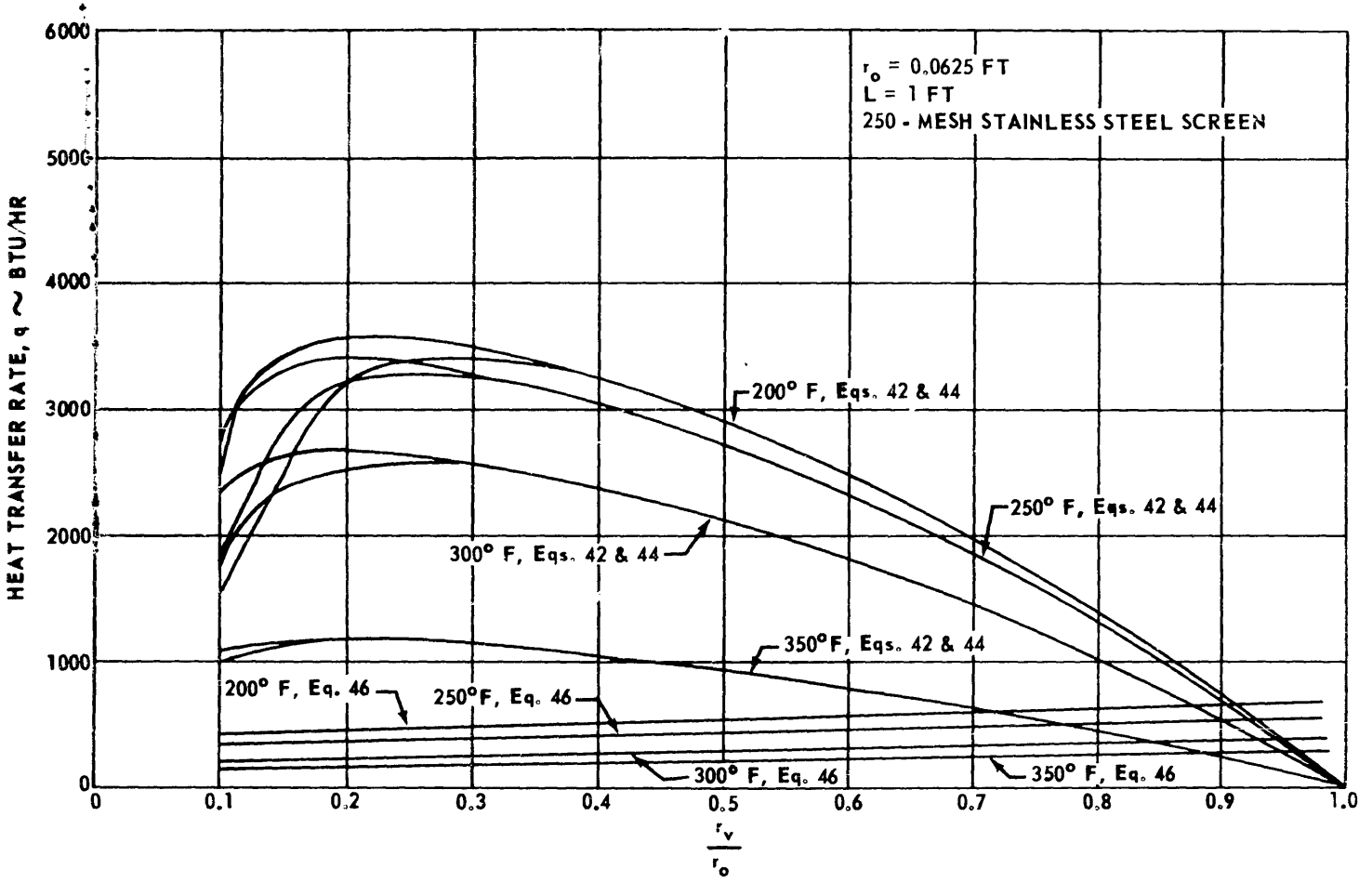

FIGURE 11. HEAT TRANSFER RATE VERSUS r_v/r_o (ADIABATIC SECTION)

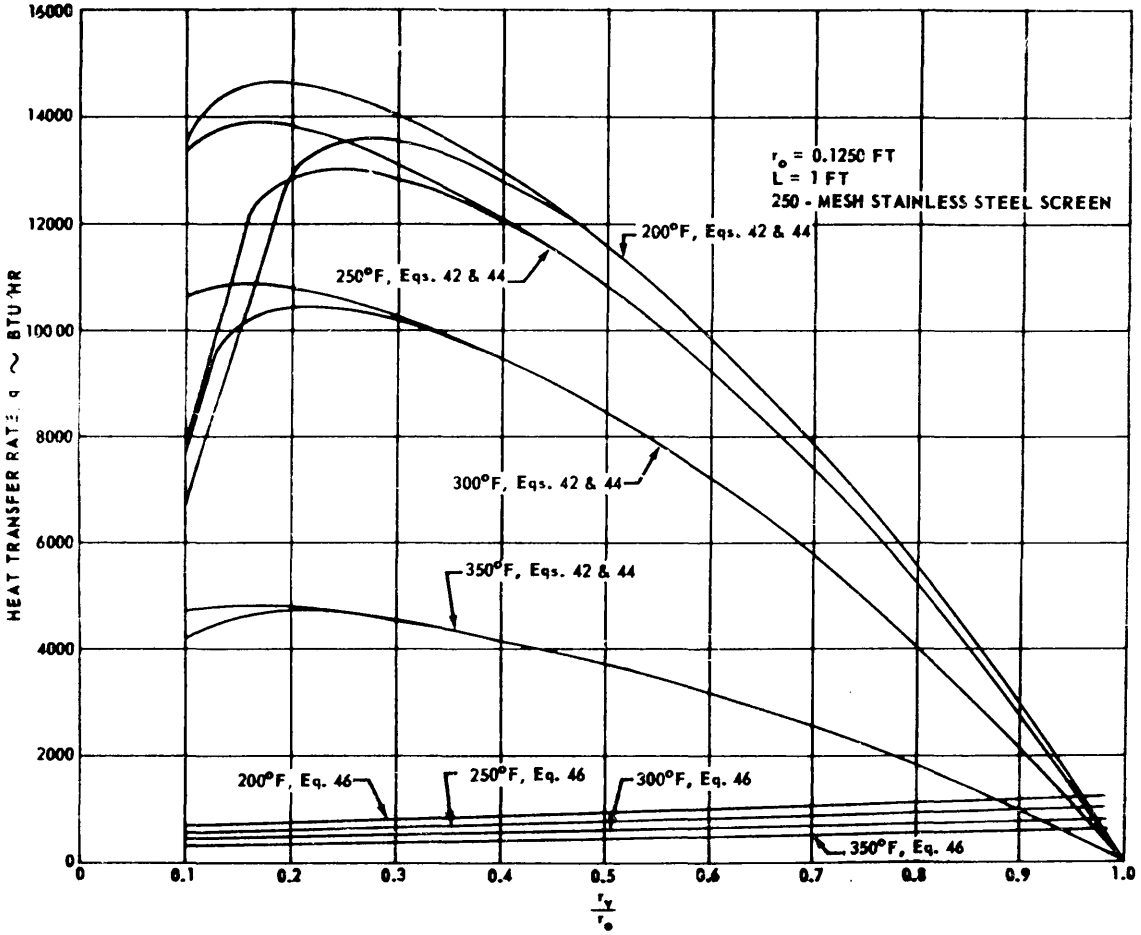

FIGURE 12. HEAT TRANSFER RATE VERSUS r_v/r_o (ADIABATIC SECTION)

The variation of the heat transfer rate with permeability for a heat pipe as a radiating fin is shown in Figure 13. To make the comparison depicted in Figure 13, the following were used: Equation (38), r_o equal to 0.0312 foot, and temperature equal to 250° F. Using equation (42), with r_o equal to 0.0312 foot and a temperature of 250° F, the variation of the heat transfer rate with permeability for a heat pipe having an adiabatic section is shown in Figure 14.

For the larger values of permeability, the effects of the evaporation and condensation rates become more pronounced. As the value of permeability increases, the range of r_v/r_o effected increases, for example:

Permeability, K	Not effected by evaporation and condensation rates
3.25×10^{-10} ft^2	$\frac{r_v}{r_o} > 0.5$
6.50×10^{-10} ft^2	$\frac{r_v}{r_o} > 0.7$
3.25×10^{-9} ft^2	$\frac{r_v}{r_o} > 0.8$
3.25×10^{-8} ft^2	$\frac{r_v}{r_o} > 0.95$

To investigate the effect of the apparent contact angle, five values other than zero degree (as given in Appendix A) were used for the apparent contact angle. The values used for the angle were 10, 20, 30, 35, and 40 degrees. When these values were used (all other inputs were as given in Appendix A), the heat transfer rate decreased as the apparent contact angle increased. Equations (38) and (42) were solved for each of the values of the angles, temperature, and r_o. These equations were chosen because, for a

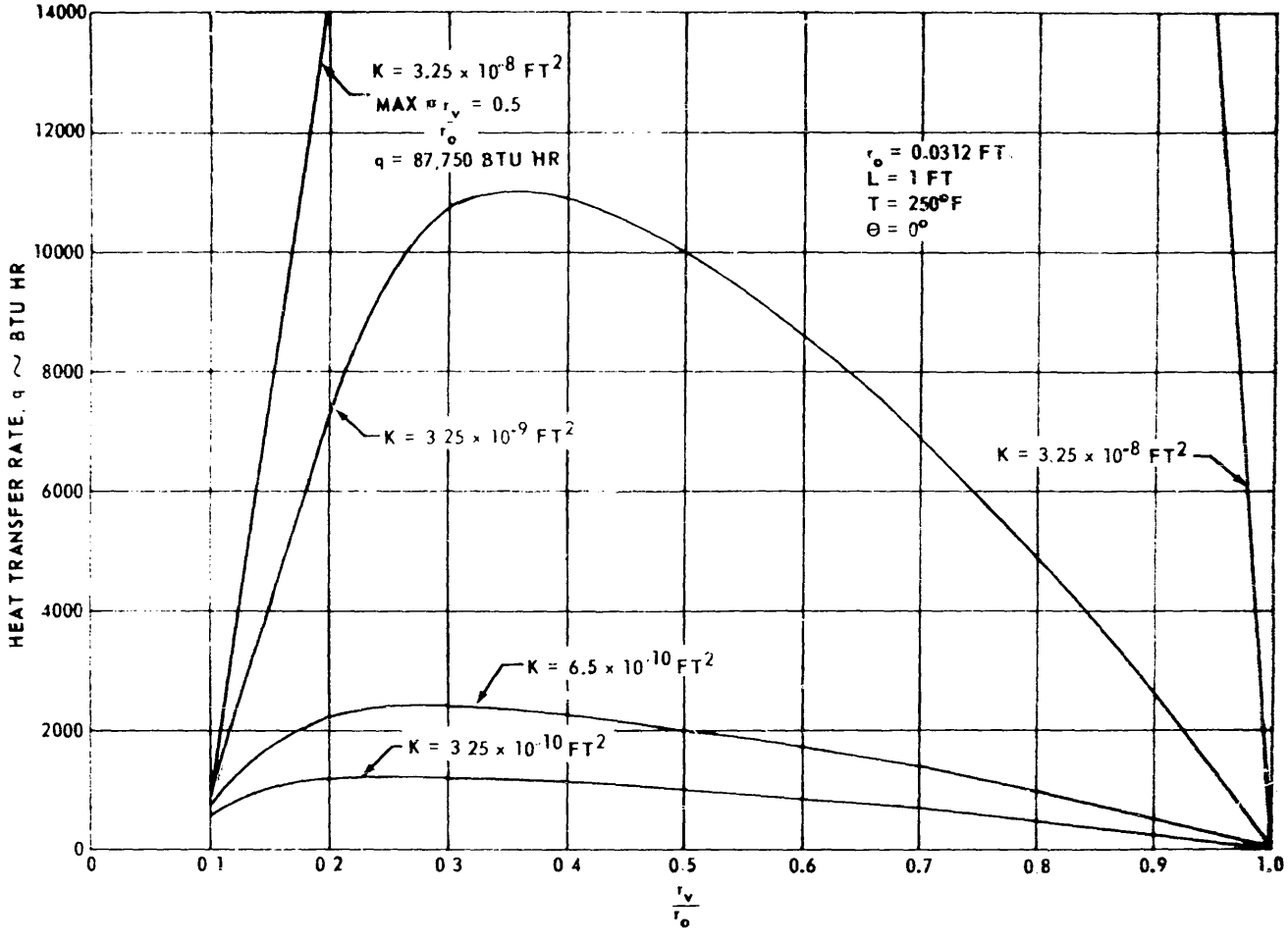

FIGURE 13. HEAT TRANSFER RATE VERSUS r_v/r_o (RADIATING FIN)

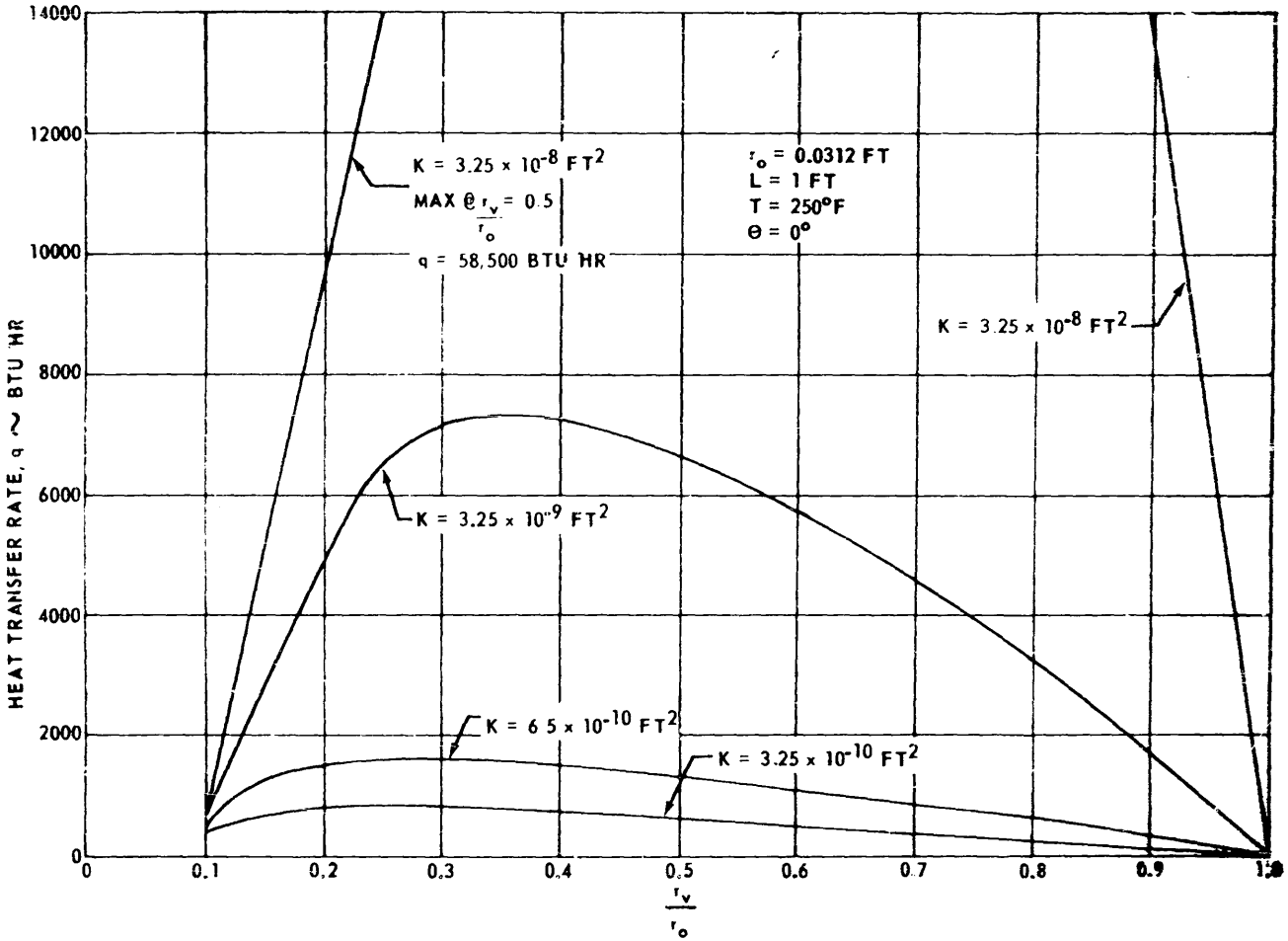

FIGURE 14. HEAT TRANSFER RATE VERSUS r_v/r_o (ADIABATIC SECTION)

change in angle, the optimum, $\frac{r_v}{r_o}$, did not change. Also, neither of the equations are effected by evaporation and condensation rates for $\frac{r_v}{r_o} > 0.5$.

2. Apparent Contact Angle

The variation of the heat transfer rate with apparent contact angle for a heat pipe as a radiating fin is shown in Figure 15. To make the comparison depicted in Figure 15, equation (38), $r_o = 0.0312$ foot, and a temperature of 200° F were used. Using equation (42), $r_o = 0.0312$ foot and a temperature of 200° F, the variation of the heat transfer rate with apparent contact angle for a heat pipe having an adiabatic section is shown in Figure 16.

By varying the apparent contact angle, it can be shown that heat pipes cease to operate as the angle enlarges at a specific temperature. In effect, for any given temperature, there is a maximum apparent contact angle. With other parameters, as defined in Appendix A, the maximum apparent contact angles for heat pipes are as follows:

Temperature	Maximum Apparent Contact Angle - Approximate
200° F	43 deg
250° F	38.5 deg
300° F	32.5 deg
350° F	22 deg

3. Length of Adiabatic Section

To determine the effect which the adiabatic section had on the heat transfer rate, the governing equations were solved with different lengths for the adiabatic section. The values of the other parameters remained constant,

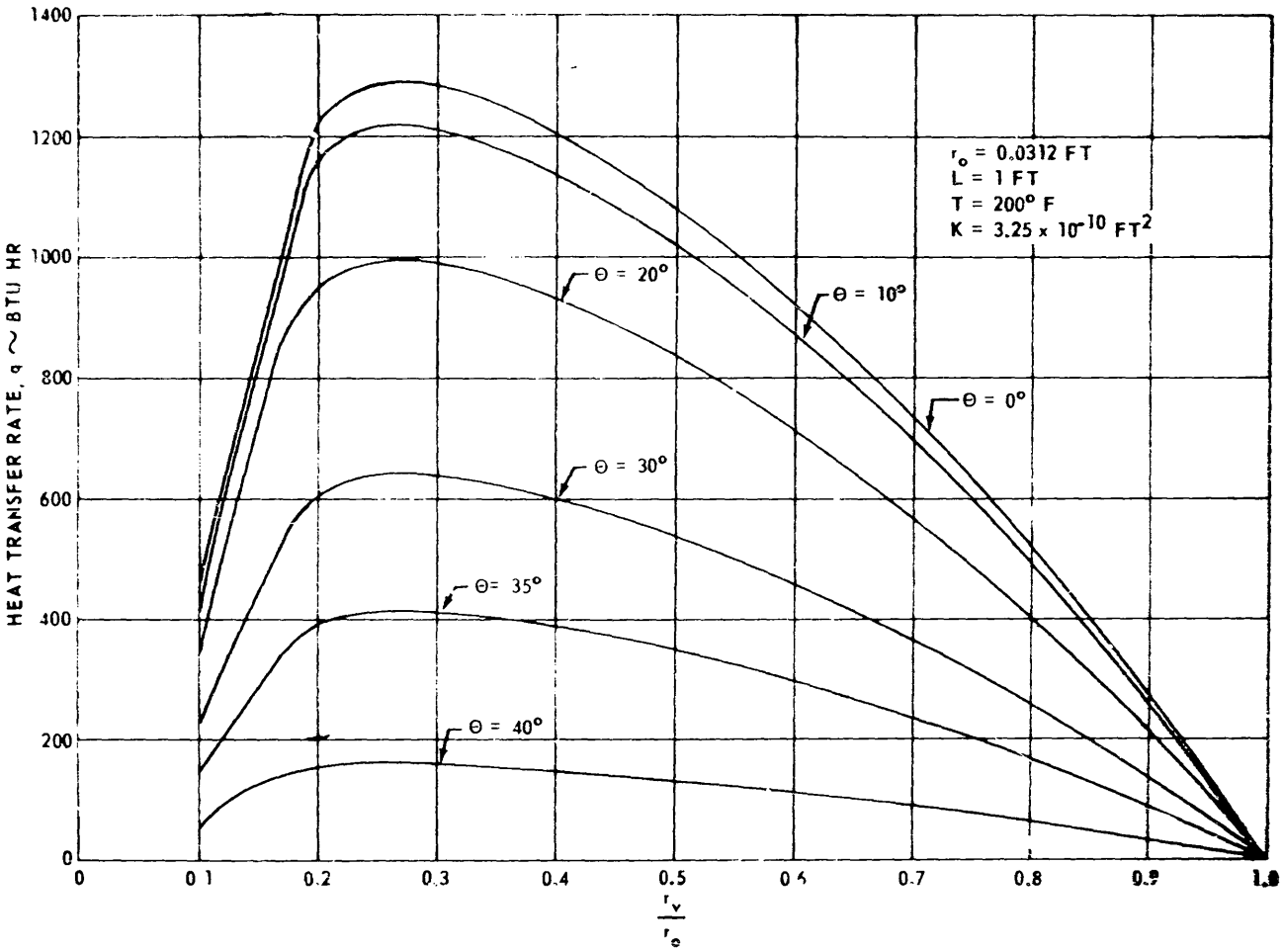

FIGURE 15. HEAT TRANSFER RATE VERSUS r_v/r_o (RADIATING FIN)

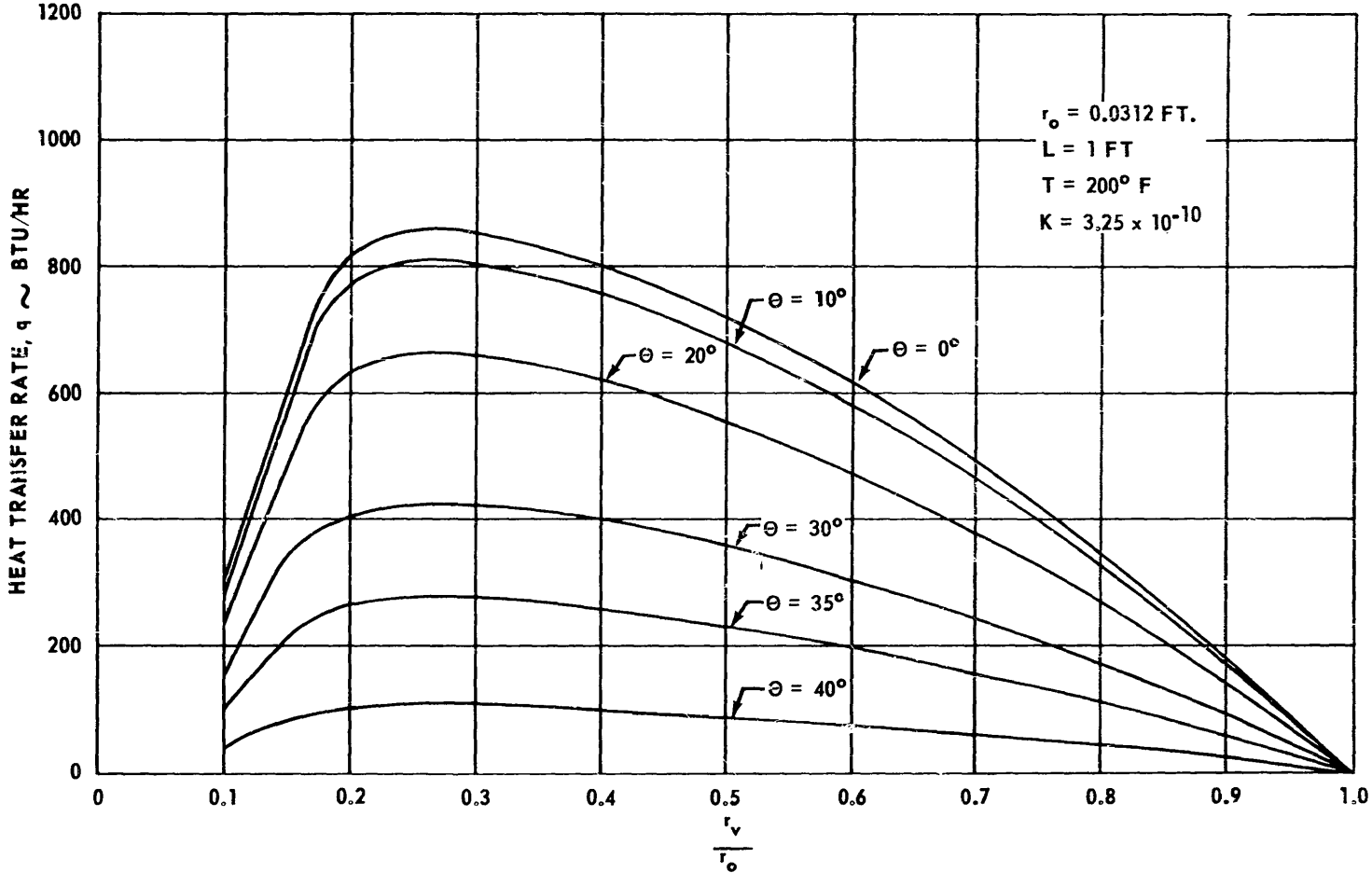

FIGURE 16. HEAT TRANSFER RATE VERSUS r_v/r_o (ADIABATIC SECTION)

as given in Appendix A. The values used for the length of the adiabatic section were 0, 0.125, 0.20, 0.25, 0.333, and 0.50 foot. When the length of the adiabatic section is zero, the heat transfer rate (Figs. 3 and 4) is the same as that for a heat pipe used as a radiating fin. To show the variation of the heat transfer rate, equation (42), an r_o of 0.0312 foot and a temperature of 250° F were used. The variation of the heat transfer rate for a particular heat pipe is depicted in Figure 17.

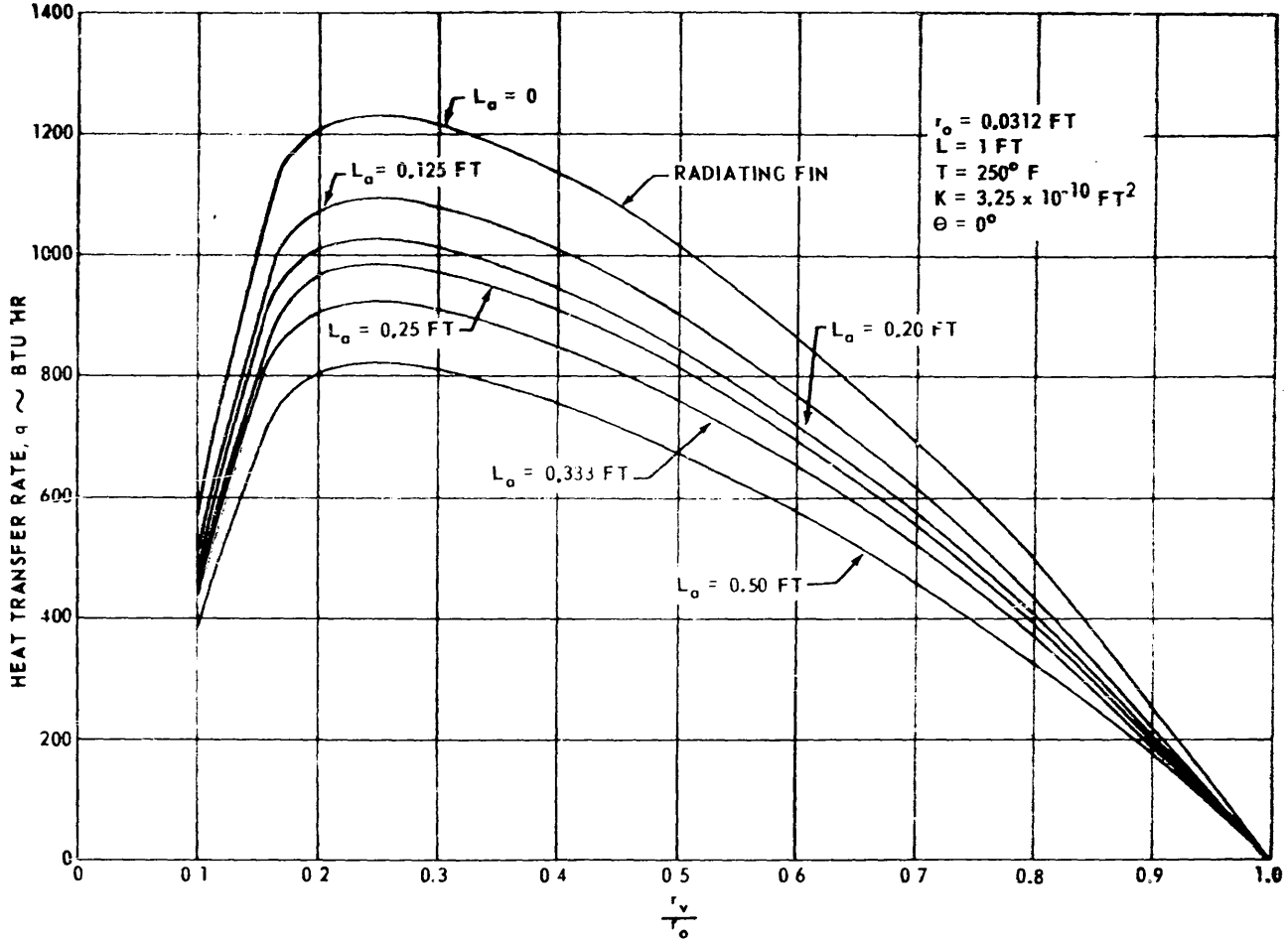

FIGURE 17. HEAT TRANSFER RATE VERSUS r_v/r_o (ADIABATIC SECTION)

CHAPTER III

DESCRIPTION AND DESIGN OF EXPERIMENTS

A. Properties of Fluid and Wicking Material for Heat Pipe Design

Properties of the fluid that must be considered when designing heat pipes are surface tension, latent heat of vaporization, viscosity, etc. Due to the availability of distilled water and also for the temperature range considered in these experiments, it was advisable to use distilled water. A figure in Reference 14 shows the optimum temperature for heat pipes with water as the working fluid is approximately 300° F.

A property of wicking material that is most important when testing heat pipes in the vertical position is capillary rise. The radius of the pores and the permeability are important when heat pipes are tested in either the horizontal or vertical position. Since in these experiments the heat pipes are oriented vertically, the capillary rise capability of the wicking material must be determined. For these experiments the capillary rise required is 1 foot. Data were taken from References 14 and 17 to obtain Figure 18. By observation of Figure 18, to obtain a capillary rise of 1 foot, the screen should be 250-mesh. Therefore, a 250-mesh stainless steel screen was chosen for these experiments, except for one heat pipe in which 100-mesh stainless

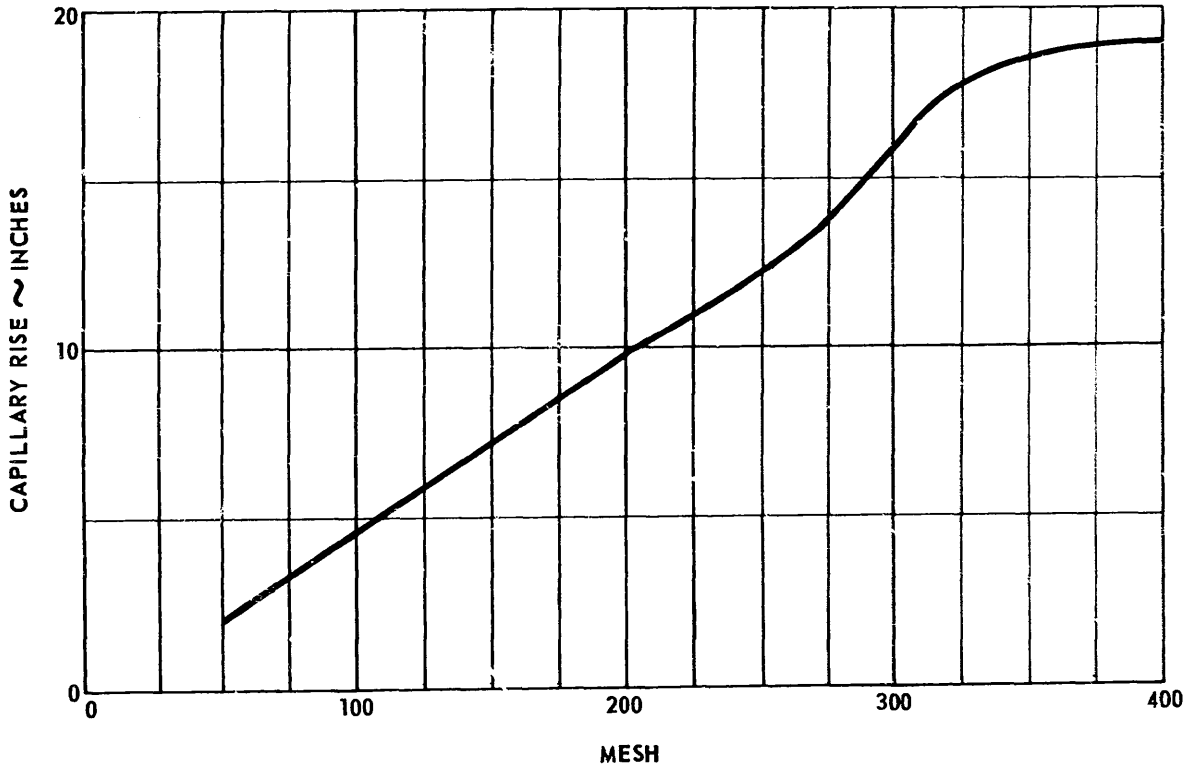

FIGURE 18. CAPILLARY RISE VERSUS SCREEN MESH

steel screen was used. The 100-mesh screen was used to establish whether the data used for capillary rise were correct for designing heat pipe wicks.

The radius of the pores of the screen were determined by considering that the diameter of the pores would be the same dimension as one side of the square openings in the screen. The dimension of the square openings was equal to 1 inch minus the mesh size (250) times the diameter of the wire (0.0016) divided by the mesh size. For the 250 mesh screen, the radius of the pores, r_c, equals 1.0×10^{-4} feet [$(1 - 250 \times 0.0016)/250 \times 12 = 1.0 \times 10^{-4}$ feet].

The permeability, K, was determined experimentally for 100- and 250-mesh screens. The procedure and experimental apparatus for determining the permeability of screens are described in Appendix B. Values of permeability determined for the two screens are as follows:

Screen	K
100-mesh stainless steel wire diameter = 0.0045 inch, Type 316	2.67×10^{-9} ft^2
250-mesh stainless steel wire diameter = 0.0016 inch, Type 316	3.25×10^{-10} ft^2

B. Determination of Wick Thickness for Experimental Heat Pipes

In References 4, 8, and 19, methods for determining the wick thickness required for heat pipes are presented. References 4 and 19 use the same method; first $q_{max.}$ is optimized with respect to the radius of curvature, r_c, and then it is optimized with respect to r_v/r_o. If this procedure is followed,

the optimum ratio of r_v/r_o is approximately $\sqrt{\frac{2}{3}}$. An equation for determining the optimum wick thickness is presented in Reference 8. This equation is only for a thin wick. If the equation from Reference 8 were used to determine the wick thickness for a heat pipe operating at a specific temperature, the thickness of the wick is independent of the radius of the heat pipe. Also, when determining wick thicknesses by using Reference 8, it is necessary to determine several parameters experimentally. If this equation were used, with the unknown parameters estimated, for determining the wick thicknesses required in this experiment then the approximate value of r_v/r_o, for a heat pipe at 300° F, is 0.9.

From the study presented in Chapter II of this dissertation, the optimum value of wick thicknesses should be such that r_v/r_o is approximately 0.3. This value of r_v/r_o would exist only for heat pipes operating under the conditions as established in Chapter II and Appendix A.

For the experiments included here, it was necessary to limit wick thicknesses so that r_v/r_o would be $0.8 < \frac{r_v}{r_o} < 0.98$. The factors which determined this range for r_v/r_o were the available power supplies and quantity of wicking material.

C. Assembly of Heat Pipes

Previous experiments indicate that one of the most important procedures for consideration is the assembly of the heat pipe. The heat pipe should be sealed so that pressure may be built up inside the heat pipe.

Precaution should be taken to prevent contamination of the inside of the heat pipe. Compatibility of materials and cleanliness should also be considered.

In this experiment, compatibility of materials was assured by use of a wick of stainless steel screen, a container of stainless steel, and water as a working fluid. Contamination and compatibility are important, because if foreign gases collect in the vapor space, the part of the heat pipe occupied by these gases will cease to operate as a heat pipe.

Since in this experiment two types of heat pipes are considered, assembly procedures differ. The steps in the assembly and the major parts of the heat pipes are given in Appendix C.

D. Experimental Investigation of Heat Pipes as Radiating Fins

The experimental setup consisted of two heat pipes, a test fixture, the high altitude simulation systems, and the data acquisition system, as illustrated in Figure 19. The test fixture with two heat pipes attached, just prior to placing in the vacuum chamber, are shown in Figure 20. A detailed description of the high altitude simulation system and the data acquisition system is presented in Appendix D.

The test fixture was designed to support two heat pipes. It consisted of plates and bars to furnish support only. The fixture had the capability of rotating the heat pipes through 360 degrees. Therefore, the heat pipe could be fixed in any position. Teflon was used as insulation where a junction existed between the heat pipe, or heater cover, and the test fixture (Fig. 20).

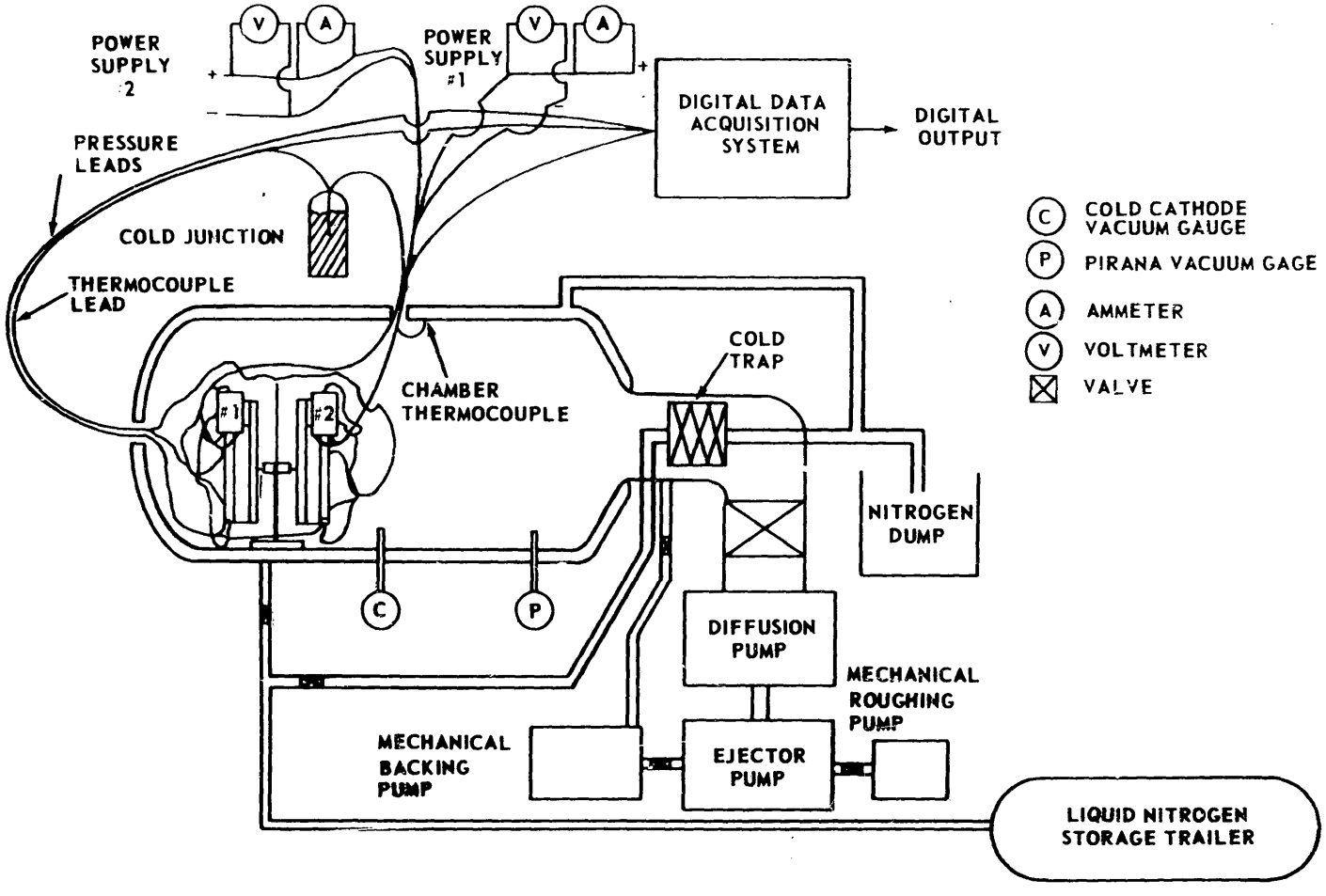

FIGURE 19. SCHEMATIC OF TEST SETUP (RADIATING FIN)

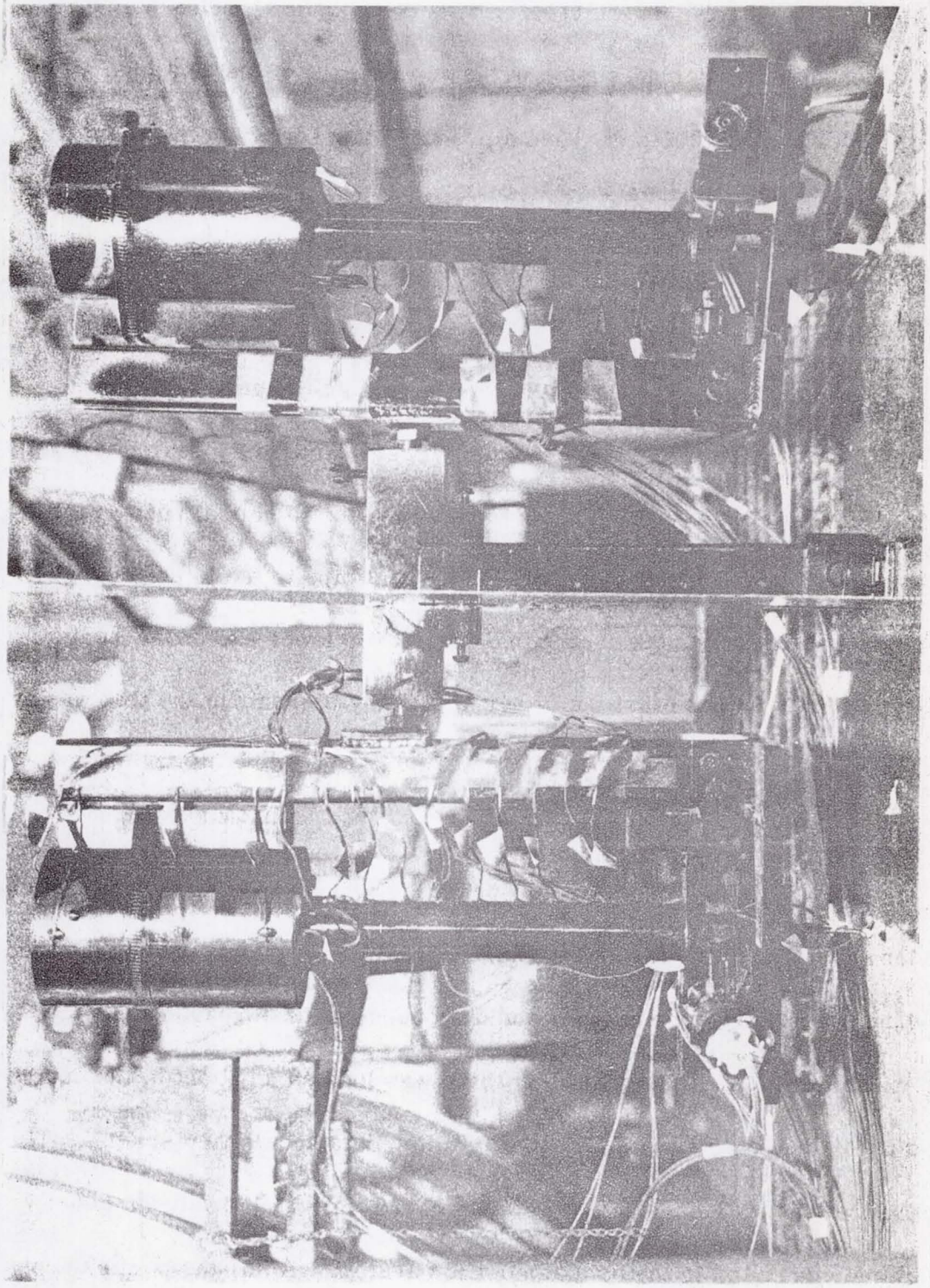

The test speciman consisted of a heat pipe, a heater element, 3 thermocouples attached to the heater, 9 thermocouples attached to the surface of the heat pipe, 2 thermocouples in the vapor space of the heat pipe (if r_o was greater than 0.0208 foot), and a pressure transducer. The approximate location of the above are shown in Figure 21. The heat pipes were approximately 14 inches long, of different radii, and constructed of stainless steel. The outer radii and other data for the heat pipes tested are shown in Table I.

The heater was constructed by winding a 26-gauge wire (Xactglo, Inconel, Claud S. Gordon Co., Cleveland, Ohio) around approximately 3 inches of the heat pipe. The heater wire was attached to a terminal post on the lower end of the heater, wound around the heat pipe to the top of the heater, and then returned to another terminal post at the lower end of the heater. The heaters were wound so that the power necessary to perform the test was available. The power inputs to the heater were determined by digital measurements.

The test apparatus was supported in the vacuum chamber by the test fixture. The thermocouple leads were taped to the test fixture and then fed through the chamber wall with a standard vacuum feedthrough connector. A thermocouple cold junction (an ice bath) was located adjacent to the chamber, and the thermocouples were connected to the data acquisition system. The pressure transducer leads were similarly fed through the vacuum chamber wall and connected to the data acquisition system. Also, the power supply leads were fed through the vacuum chamber wall and connected to the power

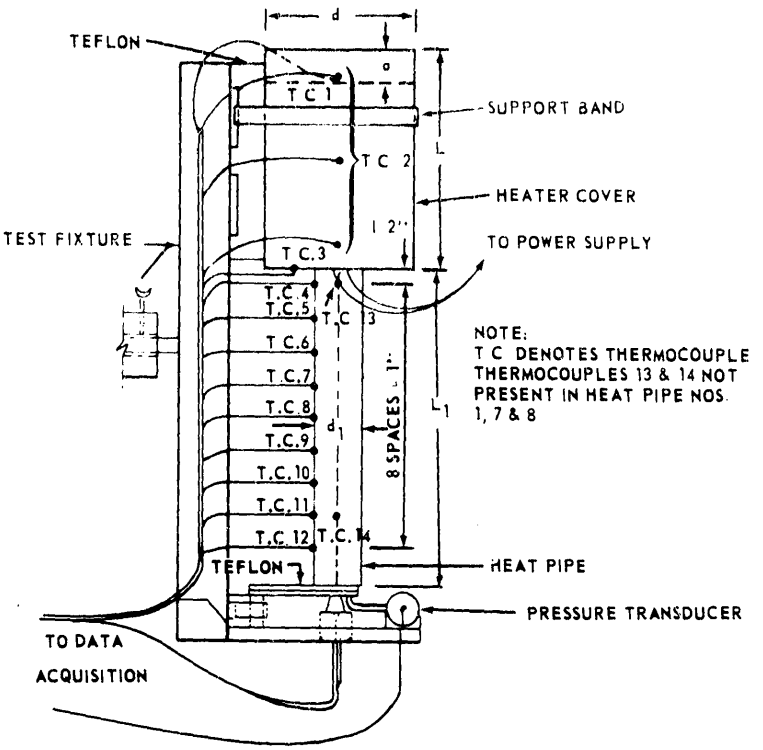

Heat Pipe Number	a inches	L inches	L inches	d inches	d_1 inches
1	$1\frac{1}{4}$	$6\frac{3}{4}$	10	$4\frac{1}{2}$	$1\frac{1}{4}$
2	1	$6\frac{1}{2}$	10	$4\frac{1}{2}$	$1\frac{1}{2}$
3	$1\frac{1}{4}$	$6\frac{3}{4}$	10	$4\frac{1}{2}$	$2\frac{1}{4}$
4	1	$6\frac{1}{4}$	10	6	$3\frac{3}{4}$
5	1	$6\frac{1}{2}$	$9\frac{1}{2}$	$4\frac{1}{2}$	$1\frac{1}{4}$
6	$1\frac{1}{4}$	$6\frac{3}{4}$	10	$4\frac{1}{2}$	$1\frac{1}{2}$
7	$1\frac{1}{4}$	$6\frac{3}{4}$	10	$4\frac{1}{2}$	$\frac{7}{8}$
*8	1	$6\frac{1}{2}$	10	$4\frac{1}{2}$	$1\frac{1}{4}$

*Heat Pipe No. 8 tested while at 45 degrees to the horizontal.

FIGURE 21. TEST SPECIMEN (RADIATING FIN)

TABLE I. DIMENSIONS AND DATA (RADIATING FIN)

Heat Pipe	1	2	3	4	5	6	7	8
Inside Diameter - inches	$\frac{1}{2}$	$\frac{3}{4}$	$1\frac{1}{2}$	3	$\frac{3}{4}$	$\frac{3}{4}$	$\frac{1}{2}$	$\frac{1}{2}$
Outside Diameter - inches	$1\frac{1}{4}$	$1\frac{1}{2}$	$2\frac{1}{4}$	$3\frac{3}{4}$	$1\frac{1}{4}$	$1\frac{1}{2}$	$\frac{7}{8}$	$1\frac{1}{4}$
Inside Radius, r_o - feet	0.0208	0.0312	0.0625	0.1250	0.0312	0.0312	0.0208	0.0208
Outside Radius, r_s - feet	0.0520	0.0625	0.0938	0.1562	0.0520	0.0625	0.0364	0.0520
Wick Thickness, t - feet	0.0024	0.0024	0.0024	0.0024	0.0028	0.0060	0.0024	0.0024
Radius of Vapor Space, r_v - feet	0.00184	0.0288	0.0601	0.1226	0.0284	0.0252	0.0184	0.0184
$\frac{r_v}{r_o}$	0.88	0.92	0.96	0.98	0.91	0.81	0.88	0.88
Mesh of Screen	250	250	250	250	100	250	250	250
Layers of Screen	8	8	8	8	3	20	8	8
Length of Screen - inches	$11\frac{3}{4}$	18	37	75	$6\frac{3}{4}$	$42\frac{1}{2}$	$11\frac{3}{4}$	$11\frac{3}{4}$
Distilled Water - Cubic Centimeters	15	20	35	85	15	25	25	25

source. Separate vacuum feedthrough connectors were used for the power leads and thermocouple leads to avoid interference. The test fixture, specimen, and vacuum chamber walls were painted black to minimize the reflected energy.

The tests were designed to explore the operation of eight water heat pipes at temperatures of approximately 200° F, 250° F, 300° F, and 350° F. One of the parameters that was studied was the power input to heat pipes with different ratios of r_v/r_o. From other studies it was known that approximately 6 hours were required to achieve steady-state heat transfer. The power input required to bring a heat pipe to a specific temperature could be approximately determined by referring to the analysis. To reach steady state at the four temperatures required approximately 1 week. To permit faster achievement of steady state, power supplies were left on at night. Steady state was considered to be established when all temperatures recorded varied less than 1 degree per hour. This assumption was well borne out by longer runs that established a steady-state condition where essentially no temperature variations were noticeable. No readings were recorded when the vacuum was greater than 1×10^{-5} mm of Hg. The pressure was monitored to check the temperature measurements.

The test runs are summarized in Table E-I and Figures E-1 through E-8 in Appendix E.

The test procedure was essentially the same for all test runs once the specimen was prepared for that particular test. The test runs were begun

by simultaneously turning on the data acquisition system, the power supplies to the specimen heaters, the backing pump, the heaters to the ejector pump, and diffusion pump, the cooling water to the pump condensers, and then pressurizing the liquid nitrogen storage trailer. After a test was started, the power supplies and other equipment that was safe were left on overnight. When the diffusion and ejector pump oil reached approximately 520° F, the roughing pump was turned on, and the liquid nitrogen flow to the pumping system cold trap was begun. Liquid nitrogen flow to the vacuum chamber cooling jacket was begun for tests 7f and 8f. The vacuum was then read on the Pirani gauge, and the system was switched to "hi-vacuum," or onto the diffusion and ejector pumps when the vacuum reached 150 microns.

After hi-vacuum operation was achieved, the procedure consisted of periodically checking the vacuum, the thermocouple ice bath, the heater power supply readings, the specimen temperature distribution, and the pressure. The power input was raised or lowered as necessary to reach a desired temperature. The specimen temperature was observed until steady state was achieved, and then a new test run was begun by changing the power inputs. Once a series of test runs was completed (or at the end of the work week), all of the test equipment was turned off. The cooling water to the ejector and diffusion pump oil condenser was left on for approximately 2 hours to protect solder joints.

E. Experimental Investigation of Heat Pipes Having an Adiabatic Section

The experimental setup consisted of two heat pipes, a test fixture, a water supply system, and the data acquisition system as illustrated in Figure 22. The test fixture with two heat pipes attached are depicted in Figure 23. The test fixture is the same one used in the previous tests. The data acquisition system used for the heat pipes with an adiabatic section is described in Appendix D.

The test specimen consisted of a heat pipe with a copper tube, a heater element, 2 thermocouples attached to the heater, 3 thermocouples attached to the metallic surface of the heat pipe, 2 thermocouples in the water supply, 2 thermocouples in the vapor space of the heat pipe (if r_o was greater than 0.0208 foot), insulation from the bottom of the heater to the end of the heat pipe, and a pressure transducer. The approximate location of the preceding are shown in Figure 24. The heat pipes were approximately 14 inches long, constructed from stainless steel, and with a copper tube wound around approximately 4 inches. The specimen heater is similar to those for heat pipes as radiating fins, as described in the preceding section. The dimensions and other data for the heat pipes tested are shown in Table II.

The test fixture with two heat pipes attached was placed on a table. Then the thermocouple, pressure transducer, and power supply leads were attached to a patch panel from which cables led to the recording system or the power supplies. All thermocouple leads were passed through an ice bath. The water supply and drain lines were connected to the copper tubes on the

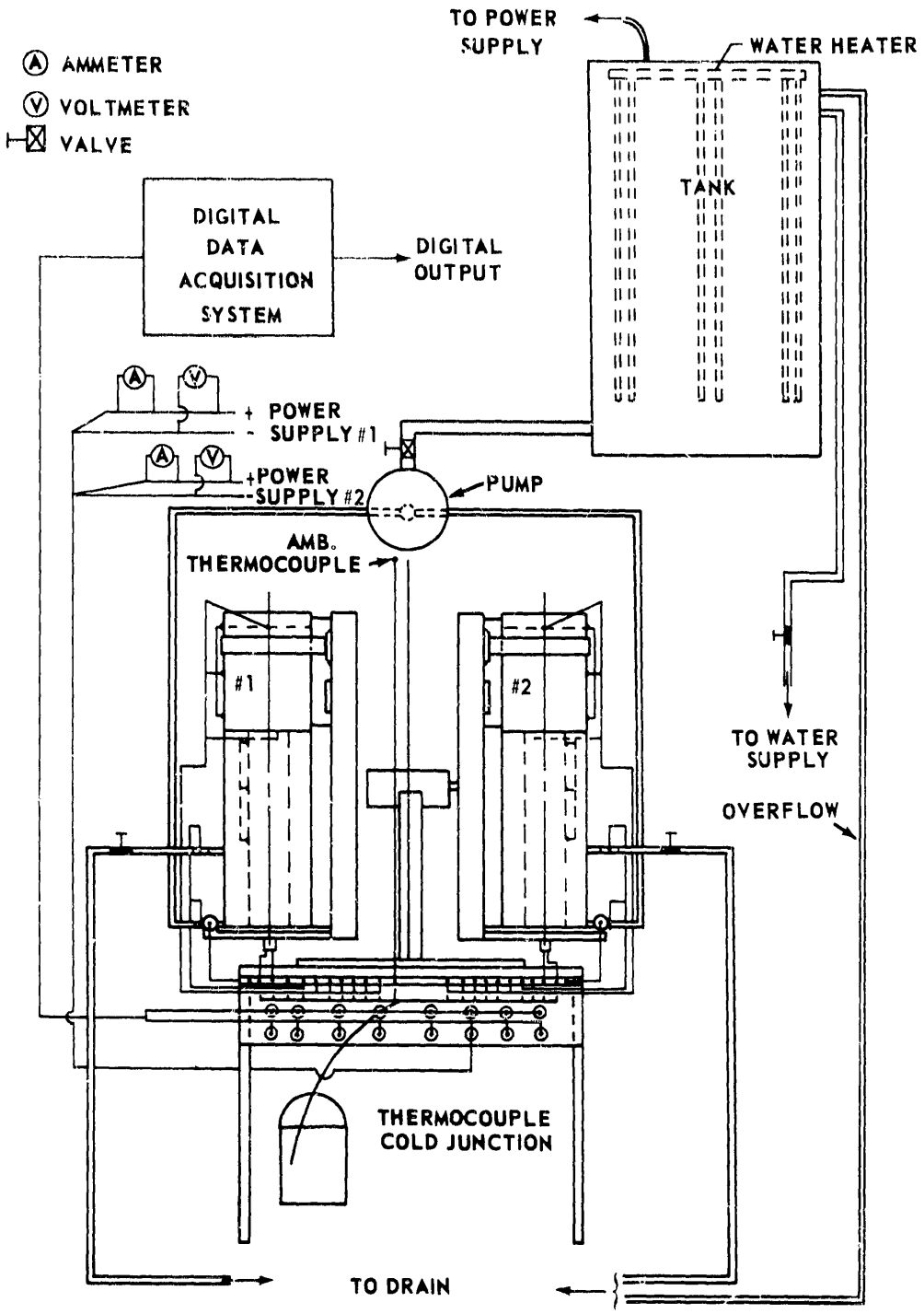

FIGURE 22. SCHEMATIC OF TEST SETUP (ADIABATIC SECTION)

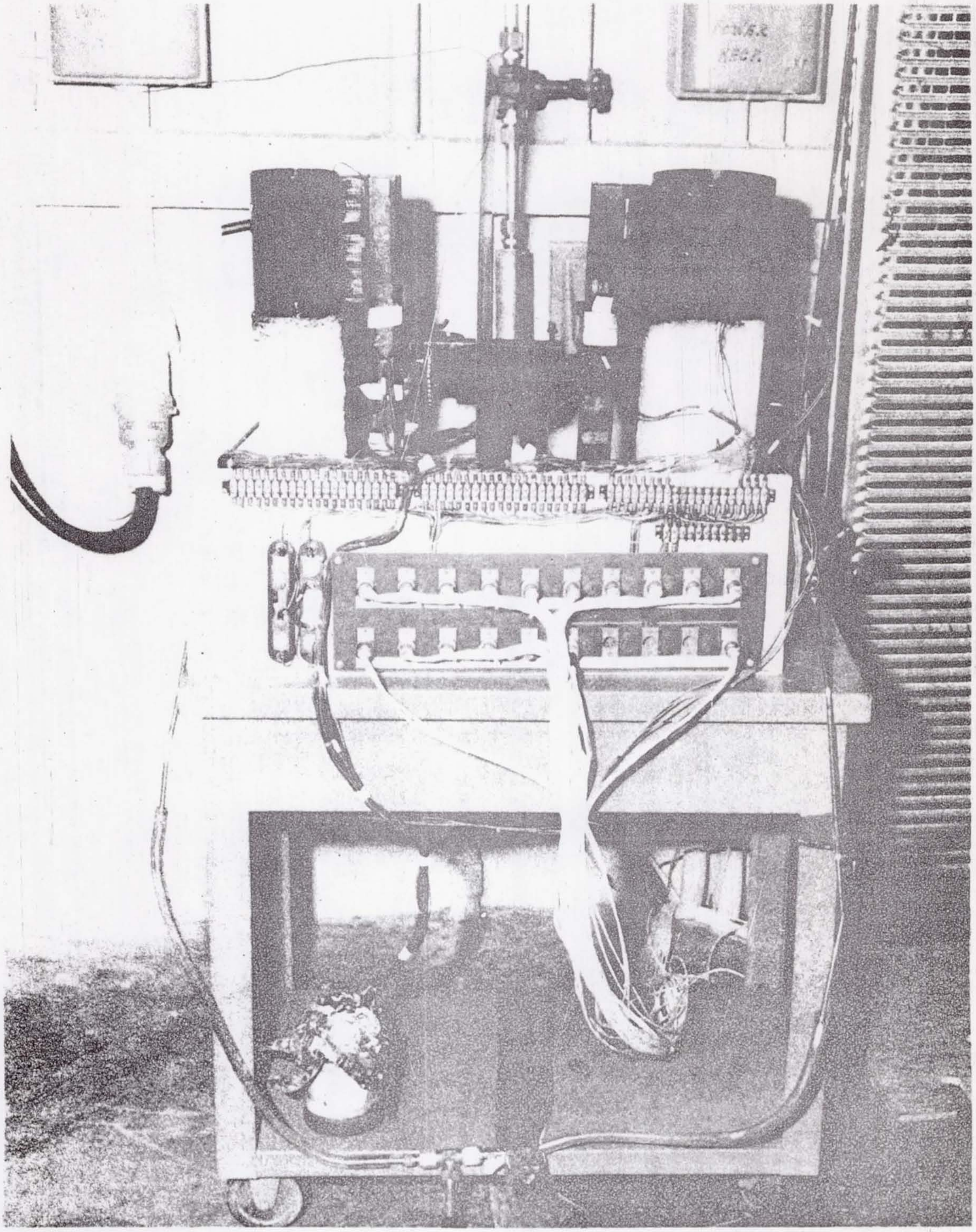

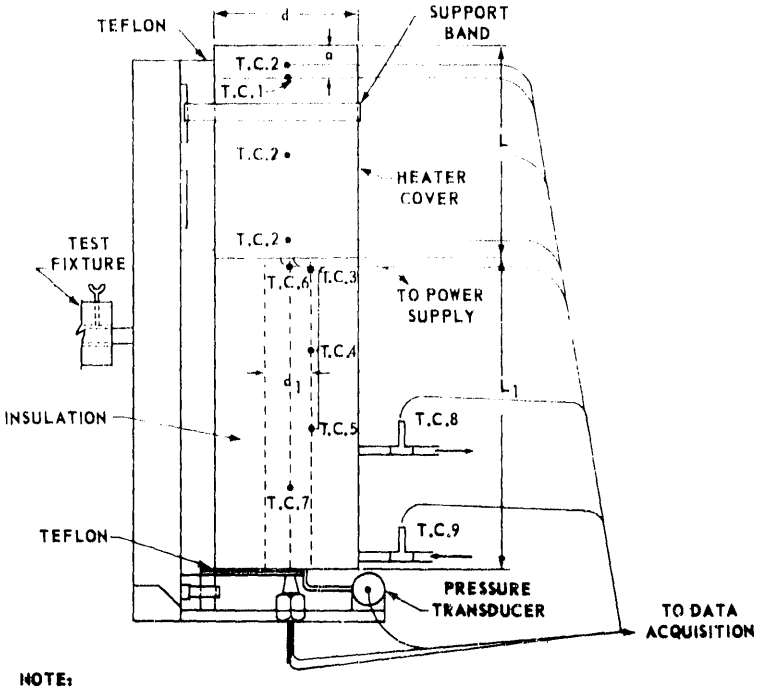

NOTE:
T.C. DENOTES THERMOCOUPLE T.C.'S 6 & 7 NOT PRESENT IN HEAT PIPE NOS. 9 & 16.

Heat Pipe Number	a inches	L inches	L_1 inches	d inches	d_j inches
*9	1	$6\frac{1}{2}$	10	$4\frac{1}{2}$	$1\frac{1}{4}$
*10	$1\frac{1}{4}$	$6\frac{3}{4}$	10	$4\frac{1}{2}$	$1\frac{1}{2}$
*11	$1\frac{1}{4}$	$6\frac{3}{4}$	10	$4\frac{1}{2}$	$2\frac{1}{4}$
12	1	$6\frac{1}{2}$	10	6	$3\frac{3}{4}$
13	$\frac{1}{2}$	$6\frac{1}{2}$	10	$4\frac{1}{2}$	$1\frac{1}{2}$
14	$\frac{1}{2}$	$6\frac{3}{4}$	10	$4\frac{1}{2}$	$2\frac{1}{4}$
15	$1\frac{1}{4}$	$6\frac{3}{4}$	10	$4\frac{1}{2}$	$1\frac{1}{4}$
16	$1\frac{1}{4}$	$6\frac{3}{4}$	10	$4\frac{1}{2}$	$2\frac{1}{4}$

* Condenser length approximately 4 inches; approximately 1 1/2 inches for 12-16.

FIGURE 24. TEST SPECIMEN (ADIABATIC SECTION)

TABLE II. DIMENSIONS AND DATA (ADIABATIC SECTION)

Heat Pipe	9	10	11	12	13	14	15	16
Inside Diameter - inches	$\frac{1}{2}$	$\frac{3}{4}$	$1\frac{1}{2}$	3	$\frac{3}{4}$	$1\frac{1}{2}$	$\frac{1}{2}$	$1\frac{1}{2}$
Outside Diameter - inches	$1\frac{1}{4}$	$1\frac{1}{2}$	$2\frac{1}{4}$	$3\frac{3}{4}$	$1\frac{1}{2}$	$2\frac{1}{4}$	$1\frac{1}{4}$	$2\frac{1}{4}$
Inside Radius, r_o - feet	0.0208	0.0312	0.0625	0.1250	0.0312	0.0625	0.0208	0.0625
Outside Radius, r_s - feet	0.0520	0.0625	0.0938	0.1562	0.0625	0.0938	0.0520	0.0938
Wick Thickness, t - feet	0.0024	0.0024	0.0024	0.0024	0.0060	0.0114	0.0036	0.0024
Radius of Vapor Space, r_v - feet	0.0184	0.0288	0.0601	0.1226	0.0252	0.0511	0.0172	0.0601
$\frac{r_v}{r_o}$	0.88	0.92	0.96	0.98	0.81	0.82	0.83	0.96
Mesh of Screen	250	250	250	250	250	250	250	250
Layers of Screen	8	8	8	8	20	38	12	8
Length of Screen - inches	$11\frac{3}{4}$	18	37	75	$42\frac{1}{2}$	$162\frac{1}{2}$	$17\frac{1}{4}$	37
Distilled Water - Cubic Centimeters	15	20	35	85	25	120	20	35

heat pipes. When the preceding was completed, the test setup was complete and testing could begin.

The tests were designed to explore the operation of eight water heat pipes at temperatures of approximately 200° F, 250° F, 300° F, and 350° F. One of the parameters that was studied was the heat input to heat pipes with an adiabatic section having different r_v/r_o ratios. From preliminary testing it was determined that approximately 5 hours was required to achieve steady-state heat transfer. The heat input required to raise a heat pipe to a specific temperature was approximately determined by referring to the analysis. To obtain steady-state operation at the four temperatures required approximately one week. To assure that steady state was reached each day, the power supplies were turned on each day at approximately 7 A.M. As in the previous tests, steady state was considered to be reached when all temperatures recorded varied less than 1° F per hour. The pressure in the vapor space was monitored to check the temperature measurements. The data from the tests are summarized in Appendix F.

The test procedure was essentially the same for all tests once the specimen was prepared. The test runs were begun by simultaneously turning on the data acquisition systems, the power supplies to the specimen heaters, and the water supply to the specimen. After the heat load had been applied for approximately an hour, the pump was turned on so that the water supplied to each heat pipe could be accurately controlled.

After steady state for the water supply was reached, the procedure consisted of periodically checking the thermocouple ice bath, the heater power supply readings, the specimen temperature distribution, the temperature of the water entering, and leaving the heat pipe and the pressure. The power input was raised or lowered as necessary to reach a desired temperature. The specimen temperature was observed until steady state was achieved; the temperatures and pressures were then recorded, and the flow rates of the water were measured. A new test was begun by changing the power inputs and adjusting the flow of the water. At the end of each day, all test equipment was turned off.

CHAPTER IV

ANALYSIS OF EXPERIMENTAL RESULTS

A. Determination of Apparent Contact Angle for Heat Pipes as Radiating Fins

Most of the parameters in the theoretical analysis were determined experimentally or taken from the references, but the apparent contact angle was not determined by these procedures. This angle could probably be determined experimentally, but due to the complex nature of the interfaces in the heat pipe, the angle for each temperature was determined by using experimental data accumulated in the testing of the heat pipes. The apparent contact angle for each test was determined by comparing calculated heat inputs and the heat inputs determined experimentally using data taken from six water heat pipes as radiating fins. The calculated heat inputs were determined by varying the apparent contact angle while holding the other parameters constant in the governing equations. In effect, this approach experimentally determined the apparent contact angle.

The apparent contact angle, θ, versus the temperature for the experimental data is plotted in Figure 25. The dotted line in Figure 25 depicts the maximum apparent contact angles that can exist in the analysis presented in Chapter II. The solid line is an approximate average of the experimental results. The values on this line were used in all calculations that follow.

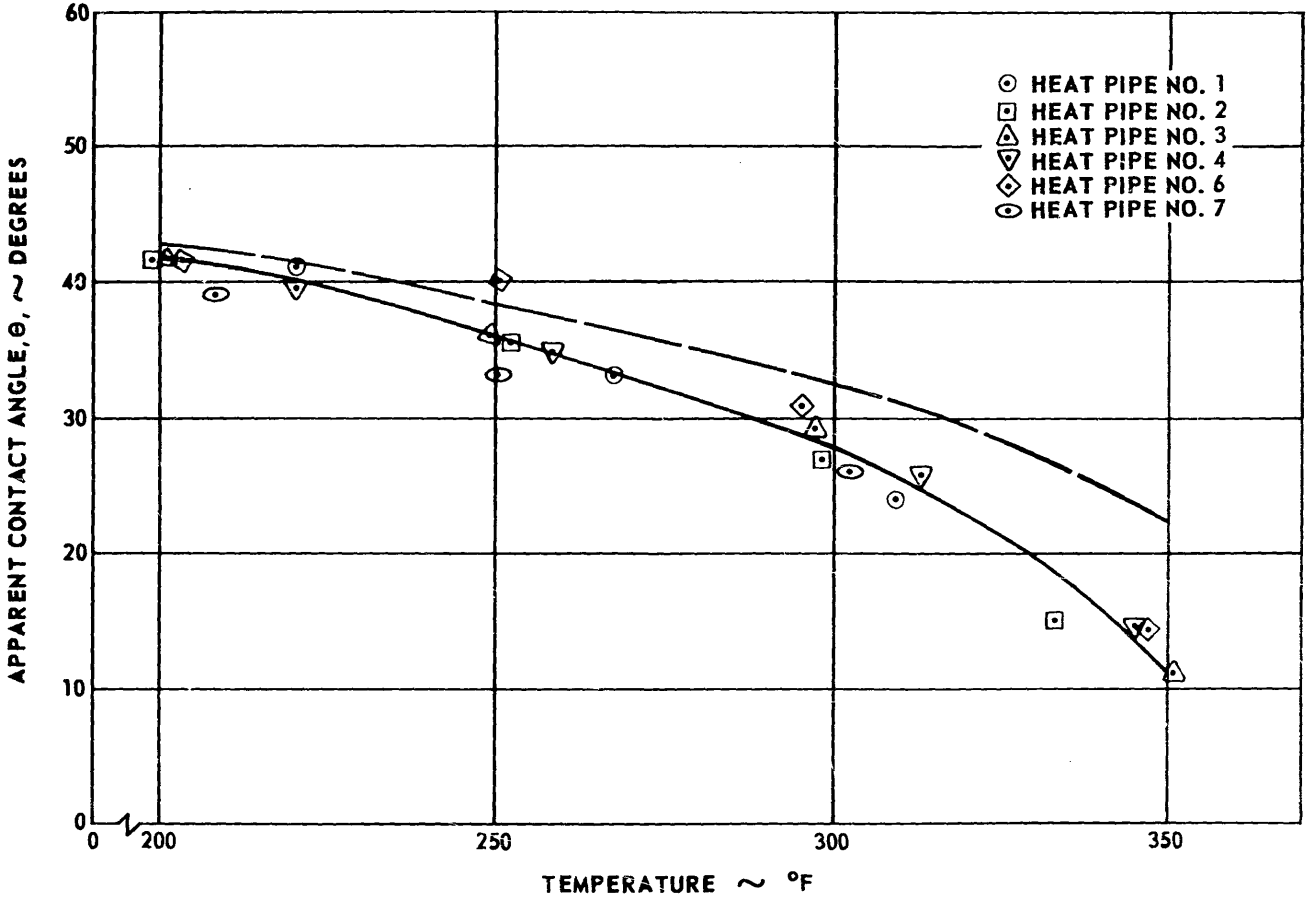

FIGURE 25. APPARENT CONTACT ANGLE VERSUS TEMPERATURE (RADIATING FIN)

The values of the apparent contact angle for use in the comparisons of heat pipes as radiating fins are as follows:

Temperature $T \sim °F$	Apparent Contact Angle $\theta \sim$ degrees
200	41.5
250	36
300	28
350	11

By observing Figure 25, it was apparent that a trend for the apparent contact angle was established by the experimental data, and therefore, the data on the solid line could be used. As the radius of the heat pipe increased, or as the ratio $\frac{r_v}{r_o}$ decreased, the apparent contact angle generally increased slightly. No data were plotted for Heat Pipes Nos. 5 and 8. Heat Pipe No. 5 contained wicking material of 100-mesh stainless steel screen and did not function as a heat pipe. Heat Pipe No. 8 was tested at 45 degrees to the horizontal, and for this case, analytical data for comparison purposes were not available.

B. Comparisons - Heat Pipes as Radiating Fins

To compare heat pipes to other radiating fins and to compare the effects that dimension changes had on heat pipes as radiating fins, it was necessary to develop the tables shown in Appendix E. One of the most important steps in developing these tables was using the computer program described in Reference 23. The procedure for developing these tables is described in detail in Appendix E.

1. Thermal Conductivity Versus Temperature (Radiating Fin)

The thermal conductivity of a stainless steel rod, as shown by the dotted line in Figure 26, was taken from page 22 of Reference 24. The thermal conductivity of the heat pipes at each temperature was determined by interpolating the results calculated for solid rods from the computer program and comparing them with the heat input in the experiments. These results are shown in Figure 26.

The data shown by Figure 26 indicate that the thermal conductivity is dependent on the wick thickness. Therefore, for the range of r_v/r_o in the experiments, three curves were drawn for three different r_v/r_o's. The r_v/r_o ratios chosen were approximately 0.8, 0.9, and 0.97. These curves indicate an increase in thermal conductivity with an increase in temperature and wick thickness.

2. Temperature Profile of a Heat Pipe and a Solid Rod of Comparable Size

To compare the change in temperature caused by a heat pipe occupying a portion of a solid rod and a solid rod of comparable size, a test case for a heat pipe and a run for a solid rod from the computer program of Reference 23 were chosen. The computer run was obtained by using a solid rod the same size as the heat pipe with a thermal conductivity of 10 Btu/hr-ft-°R, which is approximately the thermal conductivity of the heat pipe walls. For the computer run, the base and surrounding temperatures were assumed to be the same as the heat pipe operating temperature and the temperature of the inside of the vacuum chamber. The test case chosen was Test No. 4b and the

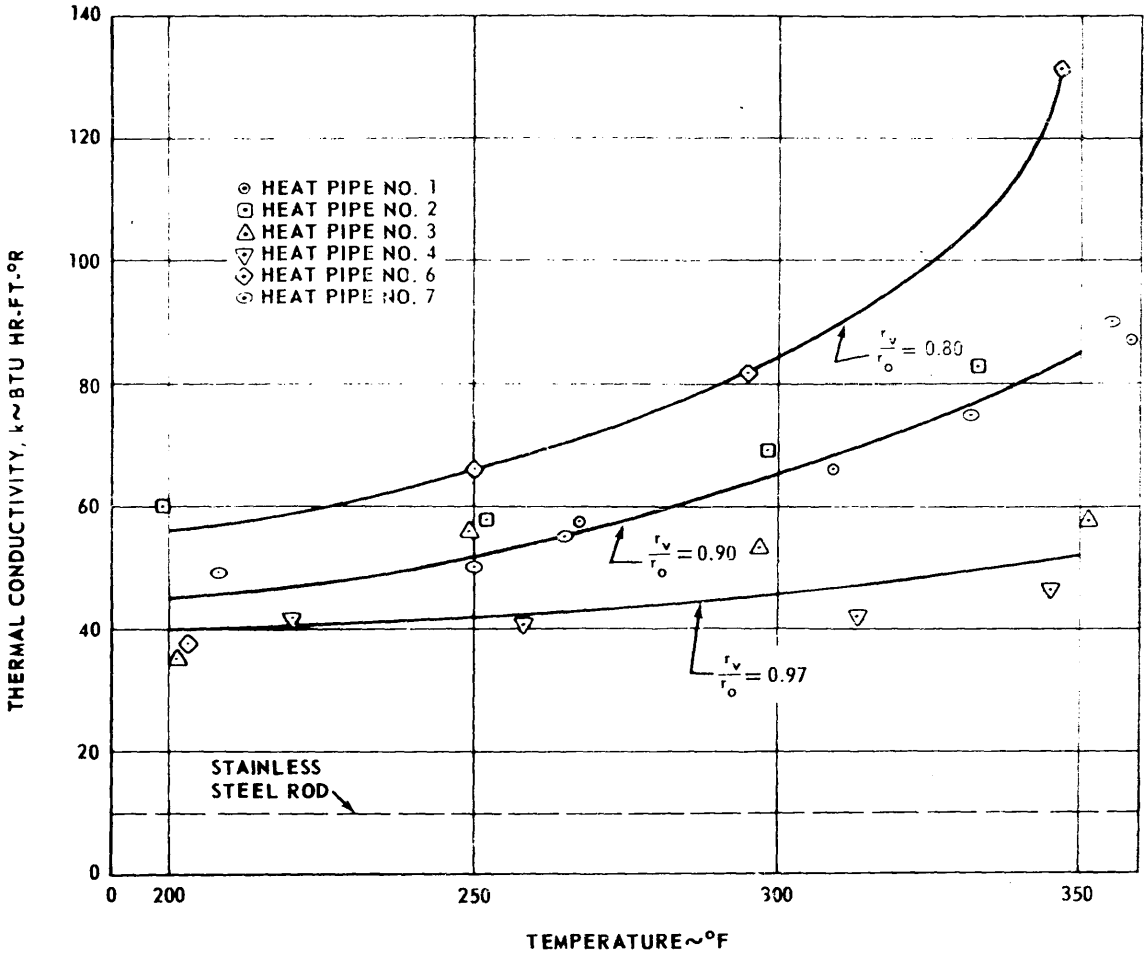

FIGURE 26. THERMAL CONDUCTIVITY VERSUS TEMPERATURE (RADIATING FIN)

temperatures, as shown in Figure E-4, were taken from the experimental data. The data from the computer run are shown in Table E-III of Appendix E. The comparison of the heat pipe and the solid rod is shown in Figure 27.

Observing Figure 27, it is apparent that by making a fin a heat pipe, the temperature at the end farthest from the source more nearly approaches the base temperature than if the fin was a solid rod of comparable material. Test No. 4b shows that a heat pipe will raise the temperature of this end approximately 45° F above the temperature of the end of a solid rod. Examining the test data for each heat pipe and comparing with data from the computer, the temperature differences between a heat pipe and a solid rod for the ends away from the source are shown in Table E-IV of Appendix E.

3. Length-To-Diameter Ratio Versus Heat Input (Radiating Fin)

L/D ratios for heat pipes have been discussed in previous investigations, but data for making a comparison for L/D ratios were unavailable. In this investigation, however, experiments were conducted using four heat pipes having a constant wick thickness and different L/D ratios. The L/D radios fell in the range of 4 to 24. To compare L/D ratios, the heat inputs through the containing cylinder were not considered. To arrive at the heat inputs, interpolations of the results of Table E-II in Appendix E were made. These results are plotted in Figure 28 and are compiled in Table E-V of Appendix E.

As the L/D ratio became small, the heat input varied approximately as the radius of the vapor space. This was especially true when going from

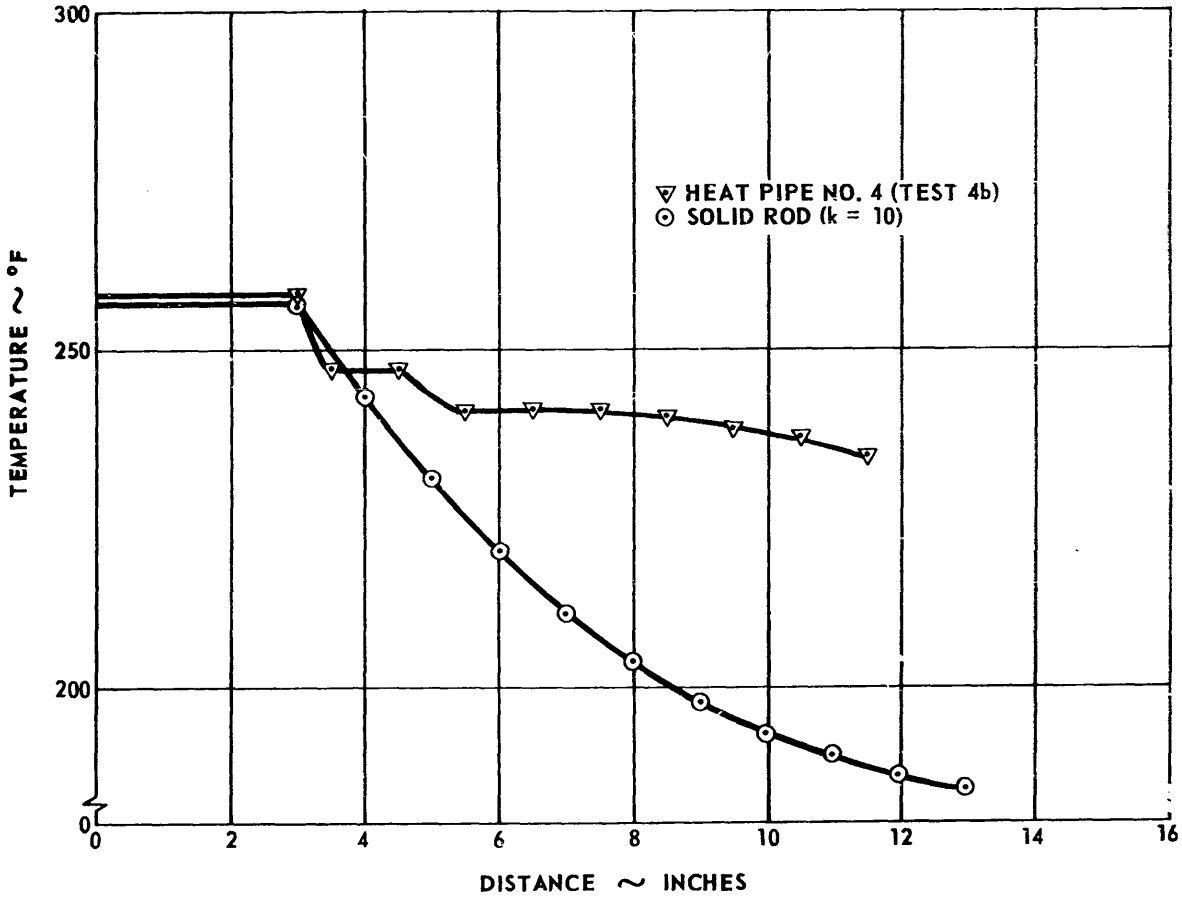

FIGURE 27. COMPARISON OF HEAT PIPE AND SOLID ROD (RADIATING FIN)

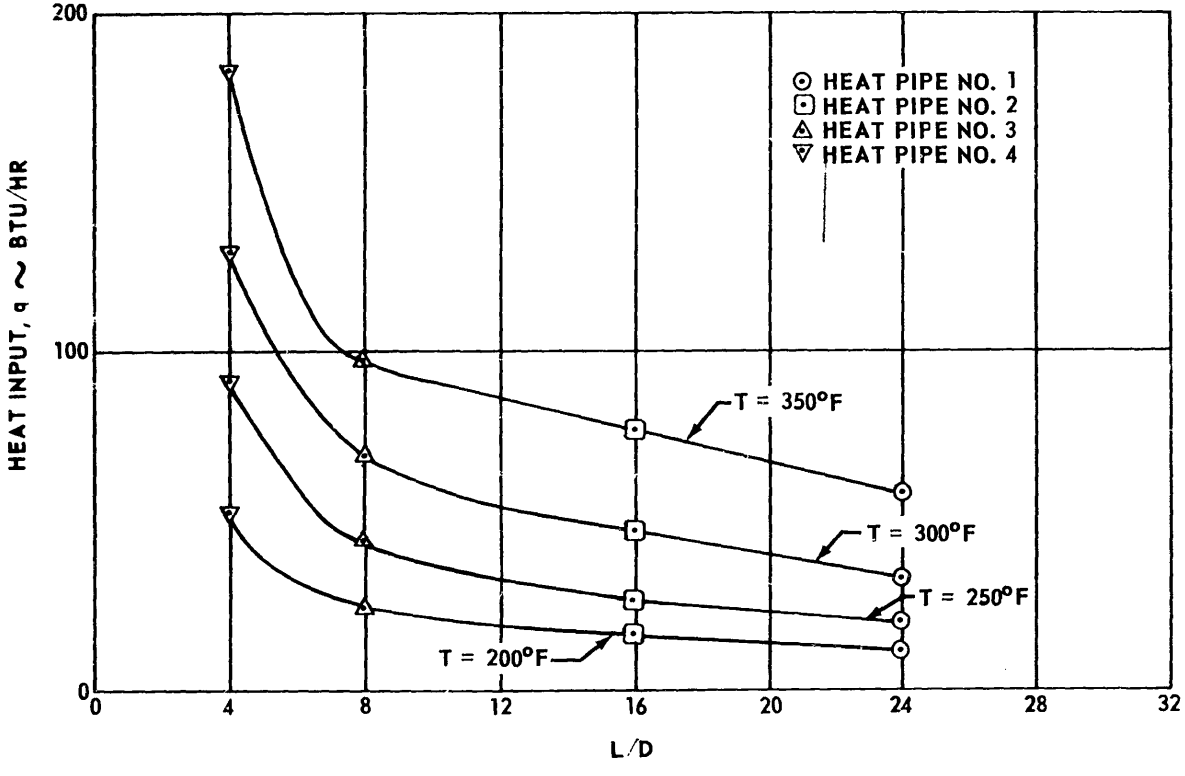

FIGURE 28. HEAT INPUT VERSUS L/D (RADIATING FIN)

an L/D of 8 to an L/D of 4, for in this case, the heat input and the radius of the vapor space approximately doubled. For values of L/D larger than 8, this relation did not hold, because the variation in the heat input was less than the variation in the radius of the vapor space.

4. Variation in Heat Input with Variation in r_v/r_o Ratio (Radiating Fin)

To define the variation in heat input with a variation in the r_v/r_o ratio, Heat Pipe Nos. 2 and 6 were chosen. The dimensions of these two heat pipes are the same except that for Heat Pipe No. 2, r_v/r_o equals 0.92, and for Heat Pipe No. 6, r_v/r_o equals 0.81. Also, the amount of distilled water required for each of these heat pipes was different, because the amount of working fluid required is dependent on the amount of wicking material present in the heat pipe. Results from Table E-II were used to plot Figure 29, which indicates the variation of heat input with the variation of r_v/r_o. The heat input through the stainless steel container of the heat pipe was not considered.

Figure 29 indicates that there is an increase in the heat input to a heat pipe as the ratio r_v/r_o decreases for the temperature range of 250° F to 350° F. To decrease r_v/r_o requires an increase in wick thickness if other dimensions remain constant. Actually, it appears that the curve for an r_v/r_o of 0.81 should follow the dotted line from 200° F to 250° F. Therefore, the increase of heat inputs would exist for the temperature range of 200° F to 300° F if the ratio r_v/r_o was decreased. Calculations indicate that an increase in heat input should exist for an increase in wick thickness.

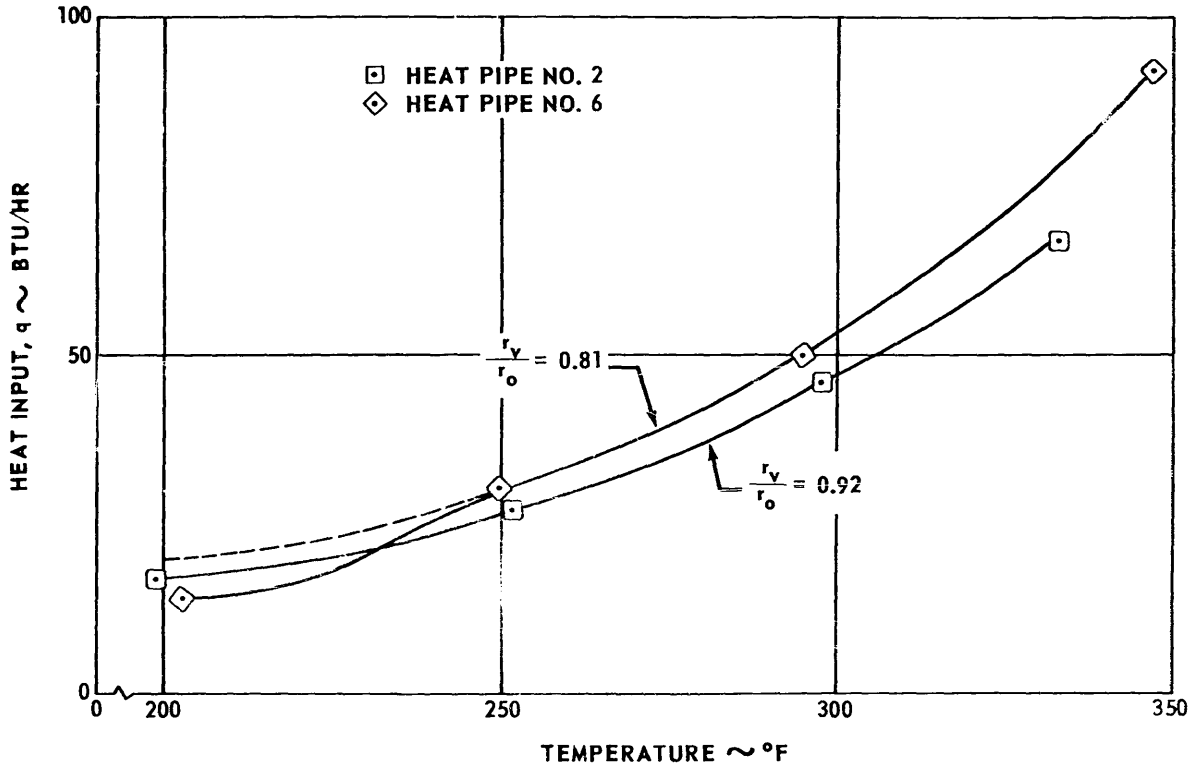

FIGURE 29. HEAT INPUT VERSUS TEMPERATURE FOR VARYING r_v/r_o (RADIATING FIN)

5. Heat Input Per Pound of Weight (Radiating Fin)

A comparison was made to determine the amount of heat input per unit of weight for heat pipes and solid rods. For this comparison, Heat Pipe No. 3 and a model heat pipe were compared with two stainless steel rods and a copper rod. The geometry of these heat pipes and rods are depicted in Figure E-9 of Appendix E. The data and a description of how the data were obtained are shown in Table E-VI and Appendix E. The comparison is made in Figure 30.

The model heat pipe was constructed because the experimental heat pipes had thick walls. The thick walls were used because of problems involved in fabricating heat pipes having thin walls. For a pressure safety factor at 2 and a yield strength of 90 000 psi, the wall thickness required was only 0.002 inch. Since it would be impossible to fabricate a heat pipe of this thickness, a wall thickness of 0.05 inch was chosen for the paper fabrication of the model heat pipe. It seems feasible to fabricate heat pipes with a wall thickness of 0.05 inch if proper precautions and the latest techniques are used. Where weight is critical, it may be necessary to fabricate thin-walled heat pipes.

6. Analytical Results Versus Experimental Results (Radiating Fin)

The analytical results were compared to experimental results by using data from Table E-II of Appendix E. The results were compared for four heat pipes. Heat Pipes Nos. 5 through 8 were not considered for this comparison. The comparison is shown in Figure 31 with the experimental

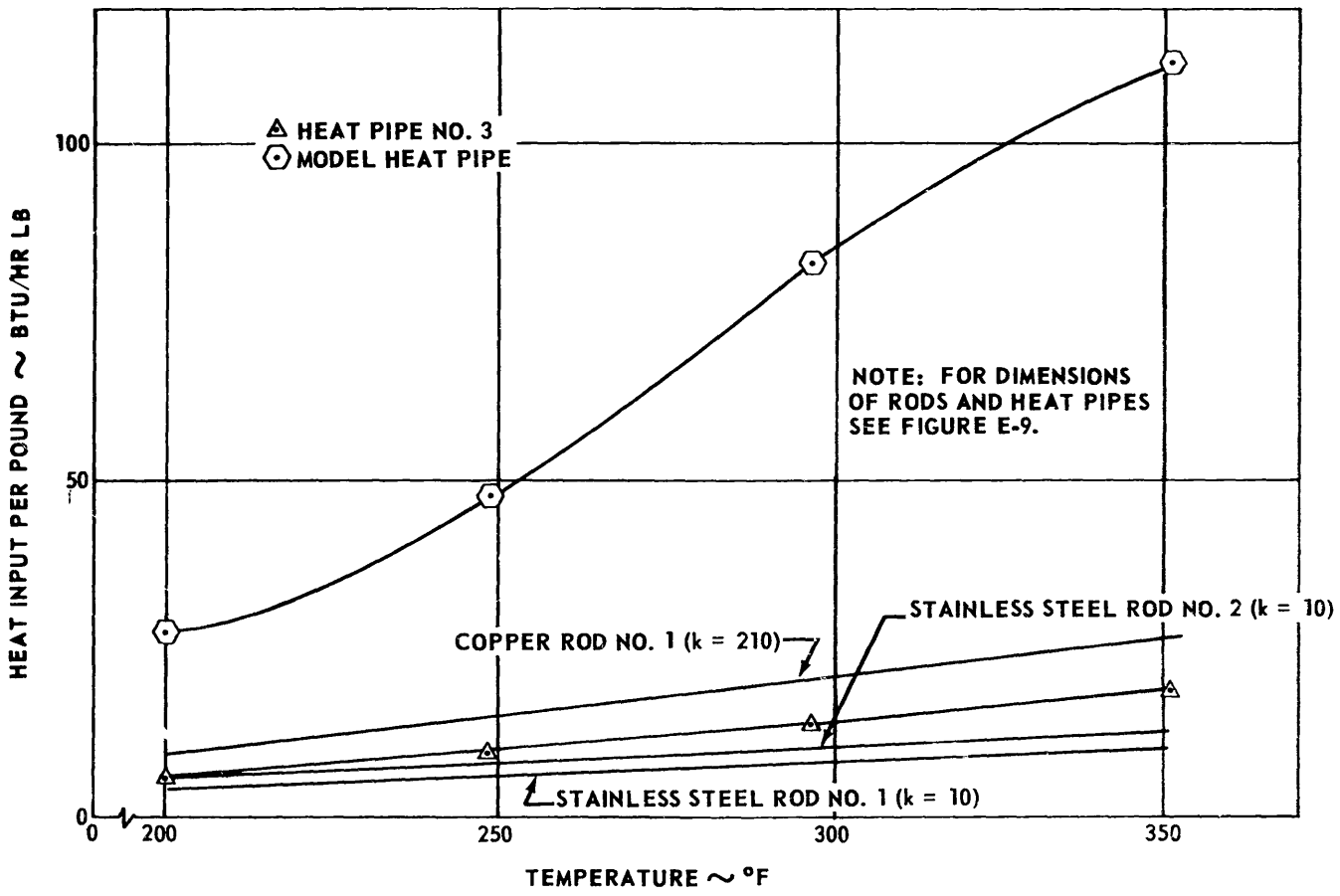

FIGURE 30. HEAT INPUT PER POUND FOR HEAT PIPES AND SOLID RODS (RADIATING FIN)

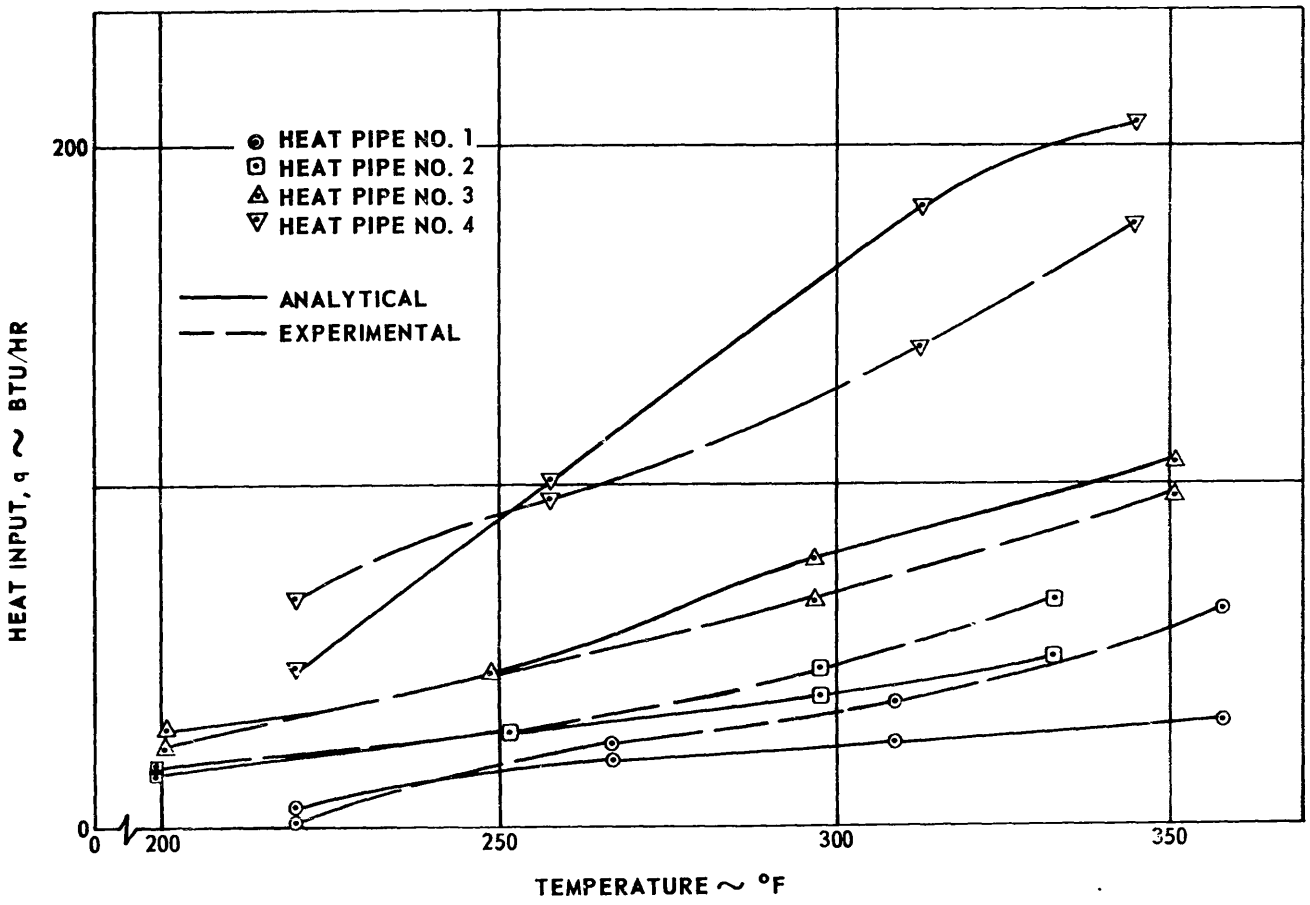

FIGURE 31. ANALYTICAL AND EXPERIMENTAL RESULTS COMPARED (RADIATING FIN)

results shown by the dashed lines and the calculated results from equation (38) by the solid lines.

The four heat pipes compared had a $r_v/r_o \geq 0.83$ or were of thin wick construction. Heat Pipe No. 7 had an r_v/r_o equal to 0.88, which approximately corresponds to the plots for Heat Pipe No. 1 in Figure 31. Calculated data were not available for Heat Pipe Nos. 5 and 8. For Heat Pipe No. 6, which had a r_v/r_o equal to 0.81, the calculated data fell well above the experimental data. The difference between experimental and calculated data was nearly constant for temperatures 200° F, 250° F, and 300° F, but this difference, as shown in Table E-II, decreased at 350° F.

C. Comparisons - Heat Pipes Having an Adiabatic Section

To compare heat pipes to other conductors and to compare the effect that dimension changes had on heat pipes having an adiabatic section, it was necessary to develop the tables in Appendix F. To formulate these tables, Reference 25 was used extensively. The procedure for developing these tables is described in detail in Appendix F.

1. Thermal Conductivity Versus Temperature (Adiabatic Section)

The thermal conductivity of a stainless steel rod, as shown by the dotted line in Figure 32, was taken from Reference 24. The thermal conductivity of the heat pipes at each temperature was determined by interpolating the results calculated for solid rods and comparing them with the heat input in the experiments. These results are shown in Figure 32.

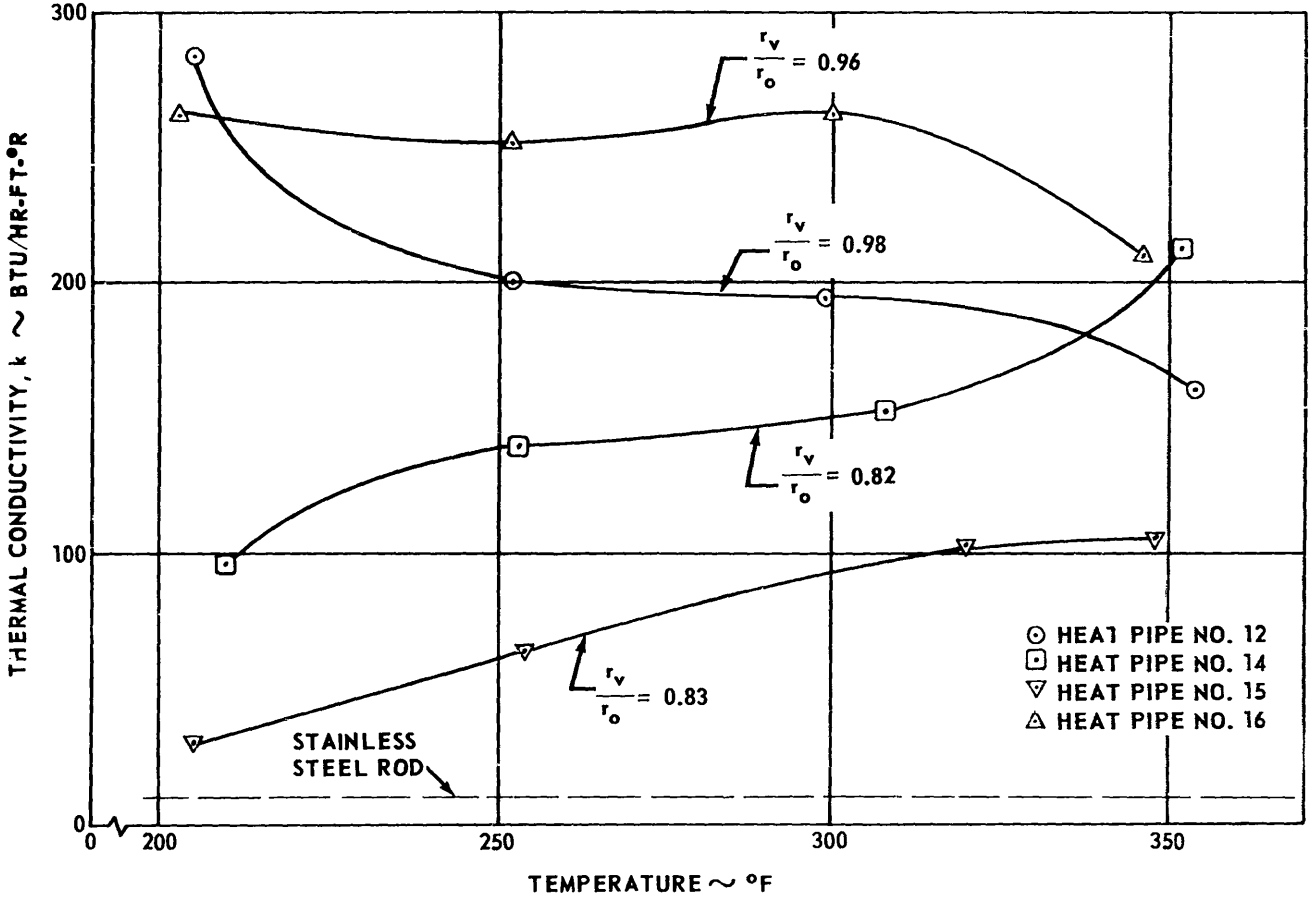

FIGURE 32. THERMAL CONDUCTIVITY VERSUS TEMPERATURE (ADIABATIC SECTION)

The data shown in Figure 32 indicate that the thermal conductivity of heat pipes having an adiabatic section is dependent on the wick thickness and the diameter of the heat pipe. The parameter wick thickness had an opposite effect on the two types of heat pipes studied. Heat Pipe Nos. 12 and 16 have r_v/r_o ratios of 0.96 and 0.98, respectively, and for these heat pipes, the thermal conductivity decreases as the temperature increases. For Heat Pipe Nos. 14 and 15, the r_v/r_o ratios are 0.82 and 0.83, respectively, and for these heat pipes, the thermal conductivity increases as the temperature increases. The diameters of Heat Pipe Nos. 14 and 15 are 0.1250 and 0.0416 foot, respectively, and could account for the difference in the thermal conductivity of these pipes. Since the diameter of Heat Pipe Nos. 14 and 16 is 0.1250 foot, it appears that a thin wick is more effective for lower temperatures and thick wicks more effective for higher temperatures.

2. Length-To-Diameter Ratio Versus Heat Input (Adiabatic Section)

In this section, four heat pipes with a constant wick thickness but different L/D ratios were compared by using experimental results. The heat pipes had L/D ratios of 4, 8, 16, and 24. The heat transported directly through the stainless steel cylinder was not considered in this comparison. To arrive at the heat inputs, interpolations of the results of Table F-II were made. These results are plotted in Figure 33 and are compiled in Table F-III of Appendix F.

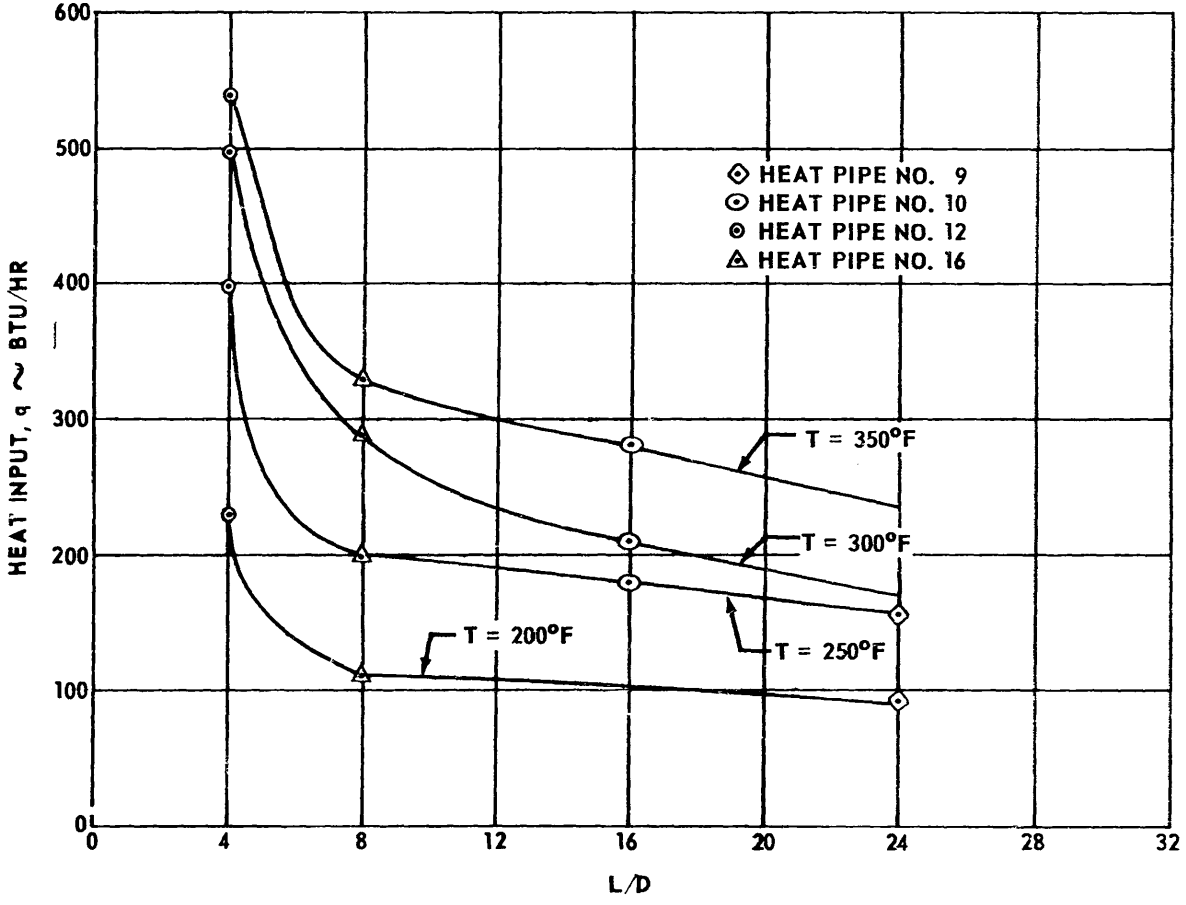

FIGURE 33. HEAT INPUT VERSUS L/D (ADIABATIC SECTION)

As the L/D ratio became small, the heat input varied approximately as the radius of the vapor space varied. This approximation was especially applicable for the values of L/D = 4 to 8. For values of L/D greater than 8, the variation in the heat input was less than the variation in the radius of the vapor space.

3. Heat Input Versus r_v/r_o Ratio (Adiabatic Section)

To define the variation in heat input with a variation in the r_v/r_o ratio, Heat Pipe Nos. 10, 13, 14, and 16 were chosen. These heat pipes make two pairs of heat pipes whose dimensions are identical except for their r_v/r_o ratios. The r_v/r_o ratios are as follows: Heat Pipe No. 10 is $r_v/r_o = 0.92$; Heat Pipe No. 13 is $r_v/r_o = 0.81$; Heat Pipe No. 16 is $r_v/r_o = 0.96$; and Heat Pipe No. 14 is $r_v/r_o = 0.82$. Since the quantity of distilled water depended on the wicking material in the heat pipe, the quantity present in the above four heat pipes was different. Results from Table F-II were used to plot Figure 34, which shows the variation of heat input with the variation of the r_v/r_o ratio. The heat input through the stainless steel container of the heat pipe was not considered.

4. Heat Input Per Pound of Weight (Adiabatic Section)

A comparison was made to determine the amount of heat input per unit of weight for heat pipes and solid rods. For this comparison, Heat Pipe No. 16 and a model heat pipe were compared with two copper rods. The heat pipes considered had an adiabatic section. The geometry of these heat pipes and rods is depicted in Figure F-9 of Appendix F. The data for this

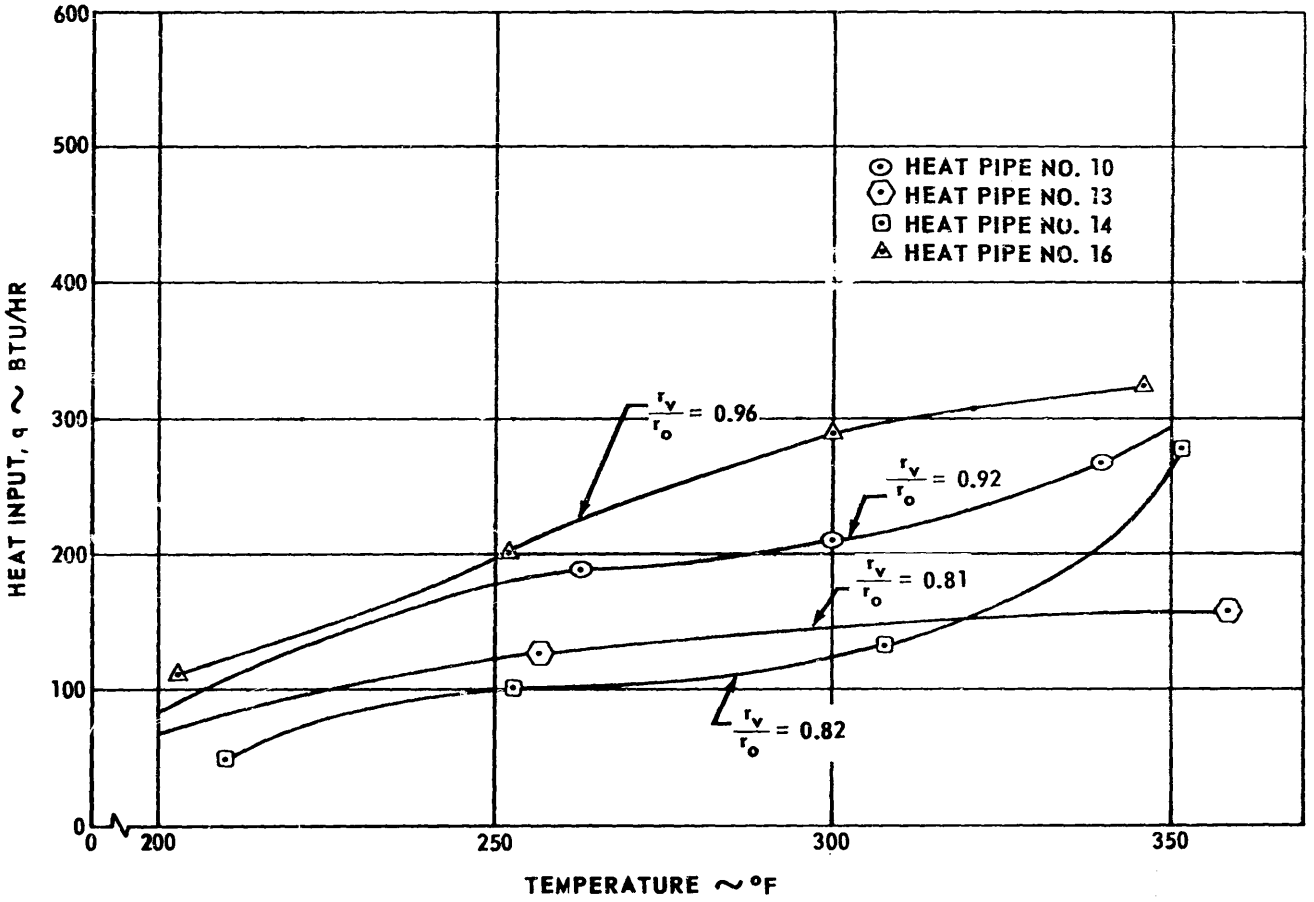

FIGURE 34. HEAT INPUT VERSUS TEMPERATURE FOR VARYING r_v/r_o (ADIABATIC SECTION)

comparison are shown in Table F-IV of Appendix F and a description of how the data were obtained is contained in Appendix F. A comparison for these heat pipes and the two copper rods is shown in Figure 35.

As for the case of the radiating fins, an analytical model of a heat pipe was formulated which did not contain the excessive weight of the heat pipes which were tested. The dimensions required for these heat pipes are identical to those for heat pipes as radiating fins and are discussed in a previous section.

5. Analytical Results Versus Experimental Results (Adiabatic Section)

The analytical results were compared to experimental results by using data from Table F-II and data interpolated from tables in Appendix F. The experimental and analytical data for Heat Pipe Nos. 12 and 16 were used. The comparison is shown in Figure 36 with the experimental results shown by the dashed line, the calculated results from equation 42 ($L_a = 8\frac{1}{2}$ inches) shown by the solid line, and the calculated results from Marcus' equation shown by the dash-dot line.

The two heat pipes had a r_v/r_o ratios of 0.96 and 0.98 and, therefore, were of thin wick construction. By observing Figures F-1 through F-8 in Appendix F, it was concluded that the length of the adiabatic section varied from approximately 2 inches to $8\frac{1}{2}$ inches. The length of the adiabatic section for Heat Pipe Nos. 12 and 16 was approximately $8\frac{1}{2}$ inches. For the heat pipes with thick wicks, the calculated heat inputs were much greater than the heat inputs determined by the experiments.

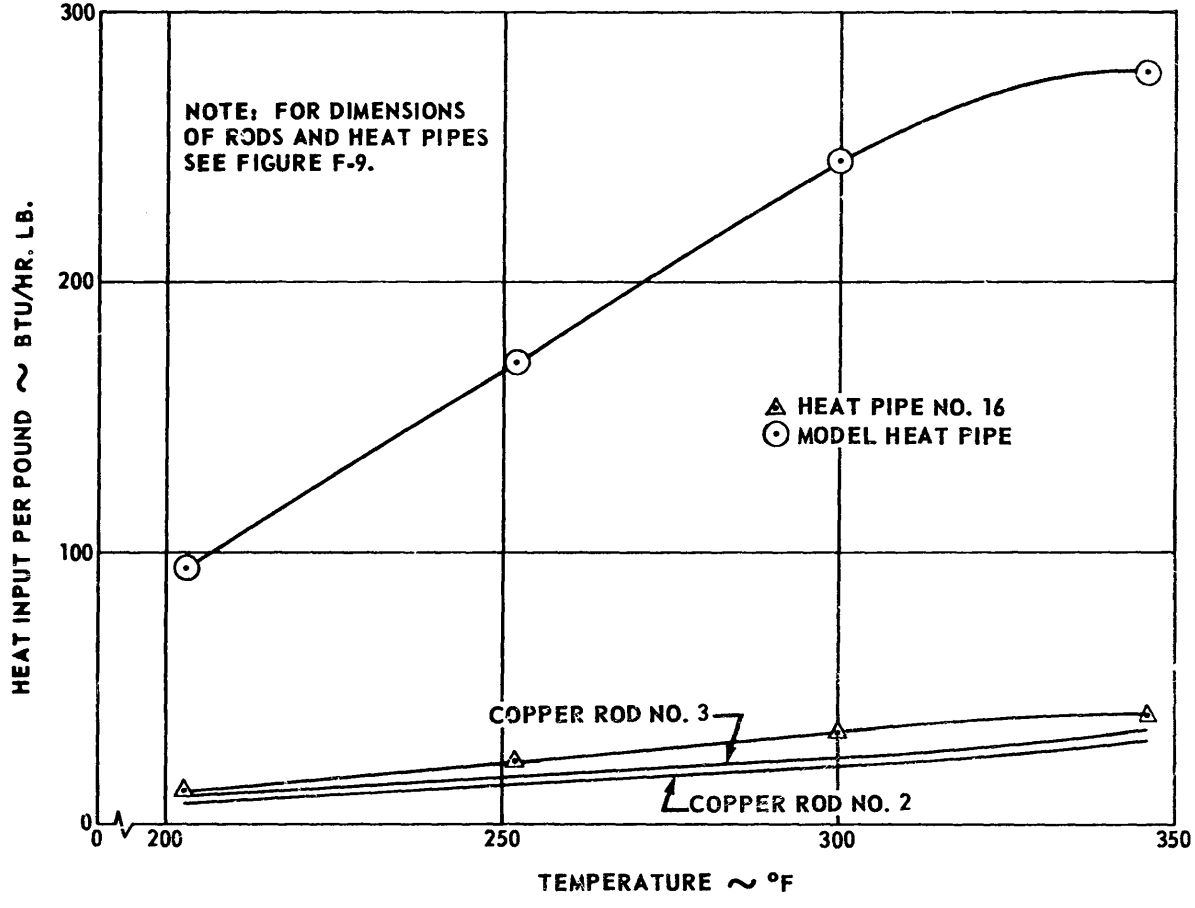

FIGURE 35. HEAT INPUT PER POUND FOR HEAT PIPES AND SOLID RODS (ADIABATIC SECTION)

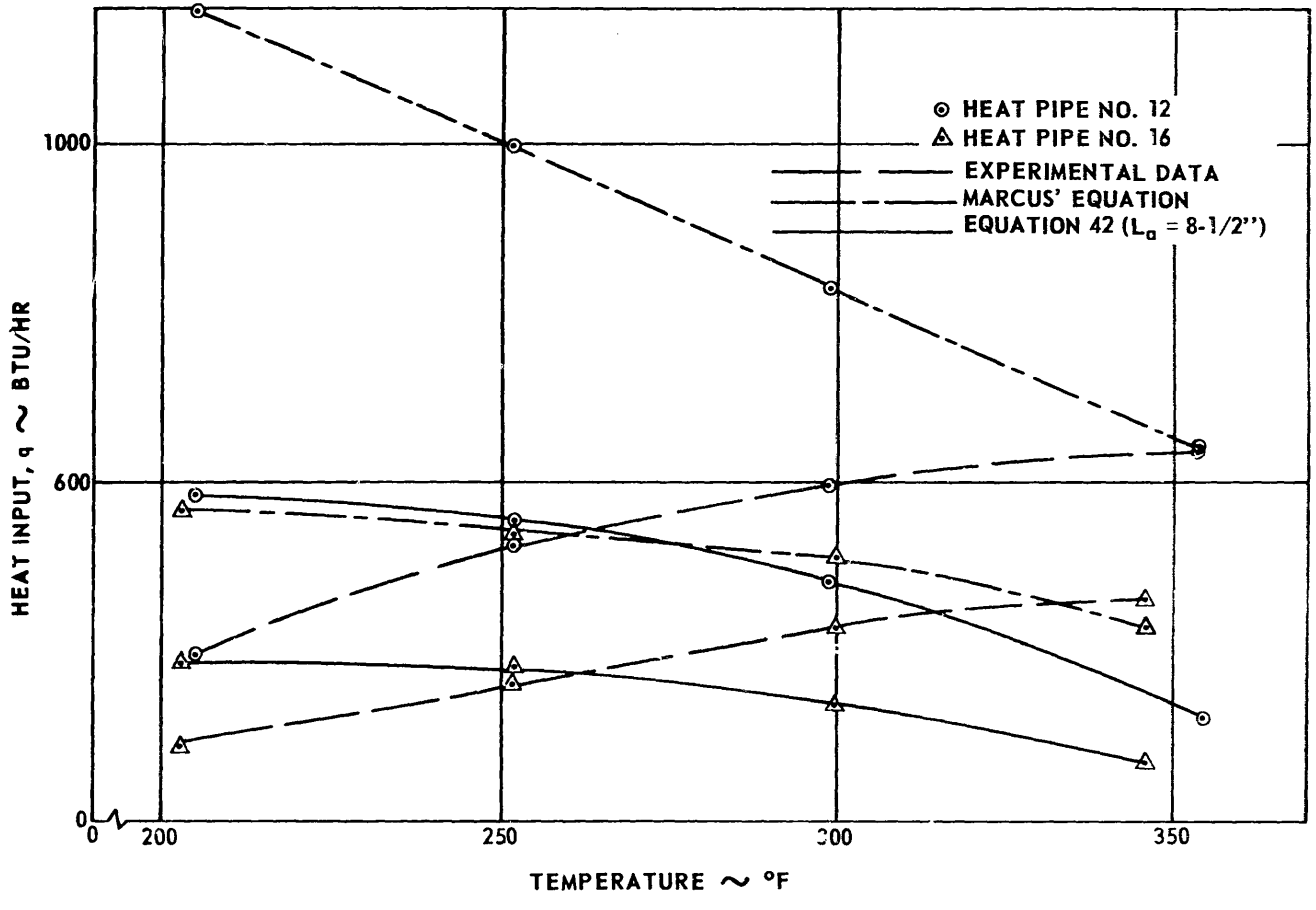

FIGURE 36. ANALYTICAL AND EXPERIMENTAL RESULTS COMPARED (ADIABATIC SECTION)

CHAPTER V

CONCLUSIONS AND RECOMMENDATIONS

An analysis was developed that predicts the maximum heat transfer rate ($q_{max.}$) for steady-state operation of water heat pipes. The analysis will be applicable to heat pipes that have similar geometries and are operating under approximately the same conditions. The $q_{max.}$ is corroborated by experimental data for a temperature range of 200° F to 350° F.

The analysis, for water heat pipes used as radiating fins, was corroborated by experimental data for the temperature range considered in this dissertation. Where analytical and experimental data differed, the percent difference would be acceptable in designing water heat pipes to be used as radiating fins. The trend of all experimental data, for water heat pipes used as radiating fins, was the same as the analysis indicated.

Specifically, the temperature range where the analysis is most applicable for water heat pipes having an adiabatic section is 250° F to 275° F. This range is probably determined by the assumed heat addition and rejection profile depicted in Figure 4. Maintaining an adiabatic section was almost

impossible when testing water heat pipes. Therefore, possibly a heat addition and rejection profile that resembles the profile depicted in Figure 3 should be assumed.

By solving the equations that define $q_{max.}$, it was determined that for $r_v/r_o > 0.5$ that $|R_{e_r}| << 1$ or $|R_{e_r}| >> 1$ had little or no effect on $q_{max.}$. Since in practice, r_v/r_o will generally be greater than 0.5, the magnitude of $|R_{e_r}|$ is not an important factor in water heat pipe design.

From the experimental data, it was concluded that heat pipes are capable of increasing the heat transferred for either type of heat pipe investigated. This increase was accompanied by an increase in thermal conductivity substantially above the thermal conductivity of the containing cylinders.

Heat pipes are weight-saving devices as shown in Figures 30 and 35. Figure 30 shows that a thin-walled heat pipe used as a radiating fin is approximately three times more efficient at 200° F and four times more efficient at 350° F than is a copper rod. In Figure 35, these values increase to 10 (formerly 3) and $7\frac{1}{2}$ (formerly 4) when a heat pipe with an adiabatic section is used.

Thin-walled heat pipes used as radiating fins should be investigated experimentally to further justify the heat transferred per pound of weight.

The heat addition and rejection profiles, as shown in Figures 3 and 4, should be determined experimentally for different temperature ranges. Using these experimental heat addition and rejection profiles, the analytical and experimental determination of $q_{max.}$ should agree for all temperatures where the profiles are available.

APPENDIX A

INPUT DATA FOR SOLVING GOVERNING EQUATIONS

To compute $q_{max.}$ from the governing equations by use of a digital computer, it was necessary to establish the properties of the distilled water and the wicking material. These properties are shown in Table A-1.

TABLE A-I. PROPERTIES FOR COMPUTER INPUT

Temperature, °F, °R	200° F 660° R	250° F 710° R	300° F 760° R	350° F 810° R
Screen Type	250 mesh	250 mesh	250 mesh	250 mesh
Radius, r_o - ft	*	*	*	*
Surface Tension, σ - lb_f/ft	4.1×10^{-3}	3.75×10^{-3}	3.4×10^{-3}	3.0×10^{-3}
Density of Liquid, ρ_ℓ - lbm/ft^3	60.1	58.8	57.3	55.6
Density of Vapor, ρ_v - lbm/ft^3	0.030	0.072	0.155	0.299
Viscosity of Liquid, μ_ℓ - lb_f hr/ft^2	1.77×10^{-9}	1.32×10^{-9}	1.05×10^{-9}	9.1×10^{-10}
Viscosity of Vapor, μ_v - lb_f hr/ft^2	7.3×10^{-11}	8.0×10^{-11}	8.6×10^{-11}	9.2×10^{-11}
Length of Evaporator, L_e - ft	0.25	0.25	0.25	0.25
Length of Adiabatic Sec., L_a - ft	0.50	0.50	0.50	0.50

TABLE A-I. PROPERTIES FOR COMPUTER INPUT (Concluded)

Temperature, °F, °R	200° F 660° R	250° F 710° R	300° F 760° R	350° F 810° R
Length of Heat Pipe, L - ft	1.0	1.0	1.0	1.0
Permeability, K - ft^2	3.25×10^{-10}	3.25×10^{-10}	3.25×10^{-10}	3.25×10^{-10}
Radius of Curvature, r_c - ft	1×10^{-4}	1×10^{-4}	1×10^{-4}	1×10^{-4}
Latent Heat of Vaporization, λ - Btu/lbm	978	945	910	871
$\cos \theta$	1	1	1	1
$\cos \beta$	1	1	1	1
Gravitational Acceleration, g - ft/hr^2	4.175×10^8	4.175×10^8	4.175×10^8	4.175×10^8
Constant, g_c - lbm/lb_f, ft/hr^2	4.175×10^8	4.175×10^8	4.175×10^8	4.175×10^8
Mechanical Equivalent of Heat, J - ft-lb/Btu	778	778	778	778
Thermal Conductivity, $k_{eff.}$ - Btu/hr-ft-°R	2.0	3.0	4.0	5.0
Radius of Bubble Nucleus, r_n - ft	2.08×10^{-5}	2.08×10^{-5}	2.08×10^{-5}	2.08×10^{-5}
Specific Wetted Perimeter, P_w - 1/ft	2.0×10^4	2.0×10^4	2.0×10^4	2.0×10^4
Porosity, ϵ	0.70	0.70	0.70	0.70

* r_o = 0.0208, 0.0312, 0.0625, and 0.1250 feet

APPENDIX B

EXPERIMENTAL DETERMINATION OF PERMEABILITY OF 100- AND 250-MESH STAINLESS STEEL SCREENS

1. Introduction

A common material used for heat pipe wicks is a stainless steel screen. The wick is an important factor in the operation of the heat pipe. A wick that is properly designed will ensure that sufficient liquid is always available in the evaporator of the heat pipe so that the heat transferred will be a maximum.

The flow rate of the liquid in the wick is limited by the maximum driving force from the capillary pressure and by the pressure losses from viscous dissipation. The capillary pressure depends on the surface tension of the liquid and the pore size of the wick. The viscous losses depend on the viscosity of the liquid and the permeability of the wick. This Appendix presents the measurement of permeability of two stainless steel screens that can be used to form wicks of heat pipes. The two screens were 100-mesh made of 0.0045 inch diameter, type 316 stainless steel wire and 250-mesh made of 0.0016 inch diameter, type 316 stainless steel wire.

2. Analysis of Experiment

Since the flow in most heat pipe wicks is usually laminar, Darcy's Law $Q = \frac{KA}{\mu} \frac{dP}{dz}$ describes the flow. This law is valid for one-dimensional flow in porous media that is dominated by viscous effects. The permeability, K, is the constant that must be experimentally determined.

The experiment consists of measuring the flow rate through the porous media (stainless steel screen) over a range of pressure drops. With the flow rate, Q, an area of porous media, A, the viscosity, μ, and dP/dz known, and by rearranging Darcy's Law, the permeability, K, may be calculated.

3. Experimental Apparatus

The system is composed of a supply of distilled water, the test section, and the instrumentation to measure the flow, pressure drop, and the temperature of the water. Figure B-1 is a schematic of the test apparatus.

The test section is several turns of stainless steel screen wrapped on a stainless steel rod. The screen and rod are force fit into a section of 1.0-inch stainless steel tubing. Pressure taps, to which a mercury manometer can be attached, are located 8 inches apart on the tube. Figure B-2 shows the test section and the dimensions used for testing the two stainless steel screens.

The supply of distilled water is contained in a 6-inch-diameter tank that has a nitrogen pressurization system. Also contained in the flow system are valves and a filter for the water.

The instrumentation consists of a mercury manometer, a thermocouple, a graduated cylinder, and a stop watch.

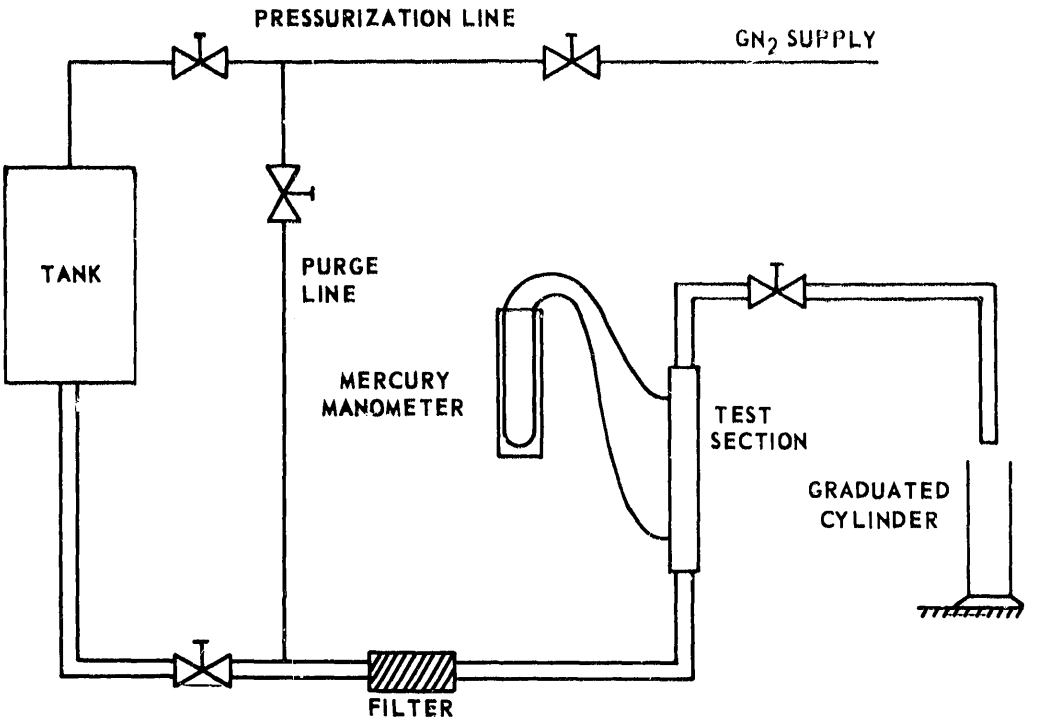

FIGURE B-1. TEST APPARATUS

One variable that is difficult to control is the tightness of the screen in the test section. The method used here is to calculate the length of screen required based on the thickness of the screen and the dimensions of the test section.

4. Description of Experiment

Major problems in measuring permeability are clogging of the porous media by foreign matter and air bubbles and ensuring that the test section is always full of water.

To prevent contamination by foreign matter, distilled water is used for the tests, and it is filtered before entering the test section.

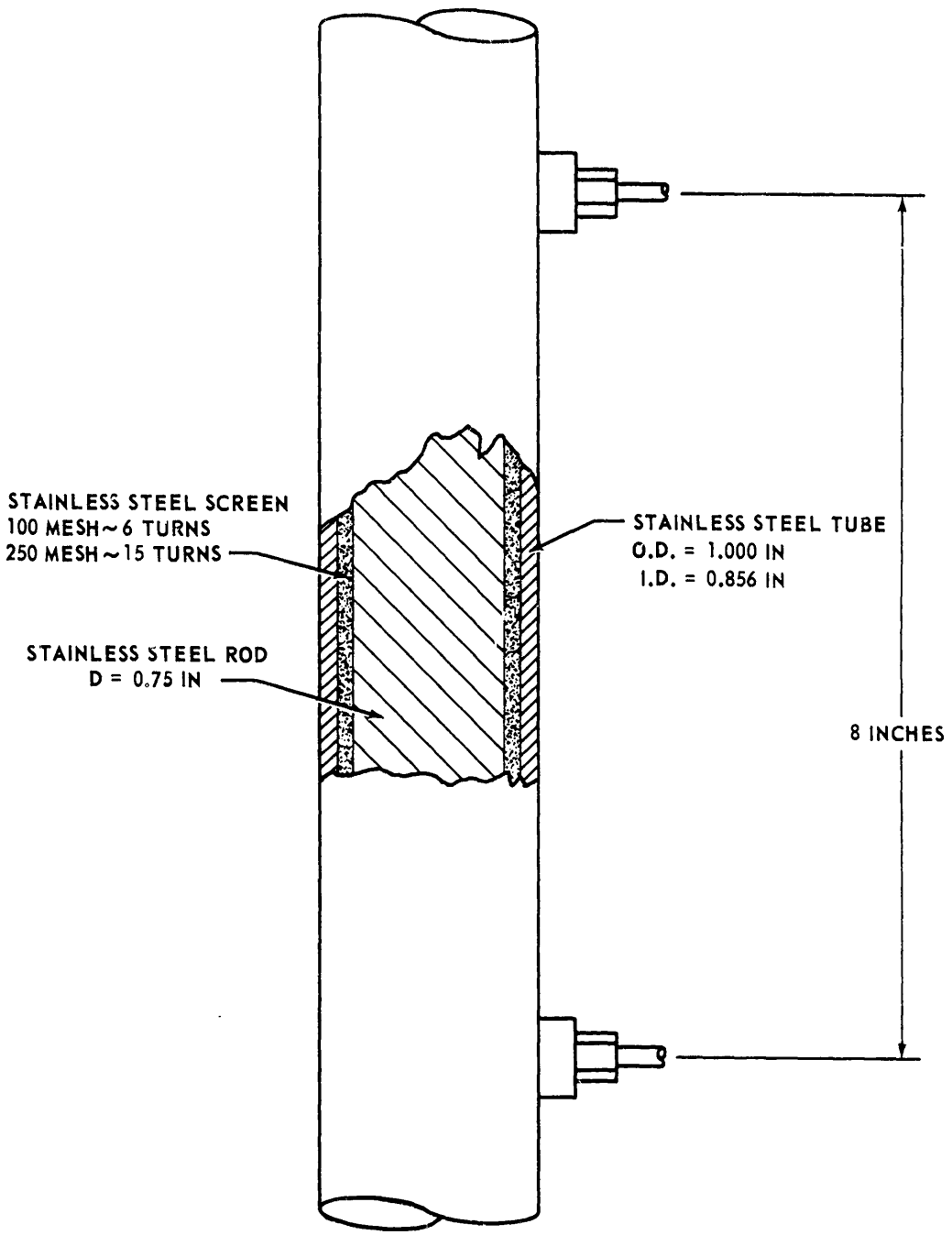

FIGURE B-2. TEST SECTION

To prevent air bubbles, the test section is baked at 300° F for 1 hour to force out water that is trapping the air bubbles. The actual test time is kept to a minimum to prevent clogging.

To ensure that it is filled with water during the test, the test section is mounted vertically in the system.

Observing the preceding precautions, the tank is filled with distilled water and pressurized. From the tank the water flows through a control valve, the filter, the test section, a control valve, and into the graduated cylinder.

Downstream of the test section, the temperature of the water is measured with a thermocouple, so that the viscosity, μ, can be obtained from existing data. The pressure drop across an 8-inch portion of the test section is measured with a mercury manometer to determine dP/dz. The water that flows into the graduated cylinder is measured, and the time for such an amount to flow is recorded by a stop watch (from this, the flow rate can be determined).

5. Results and Conclusions

Two different screens were subjected to tests to determine the permeability. The experimental data determined are presented in Figures B-3 and B-4, and average values of permeability are 2.67×10^{-9} ft^2 for the 100-mesh screen and 3.25×10^{-10} ft^2 for the 250-mesh screen.

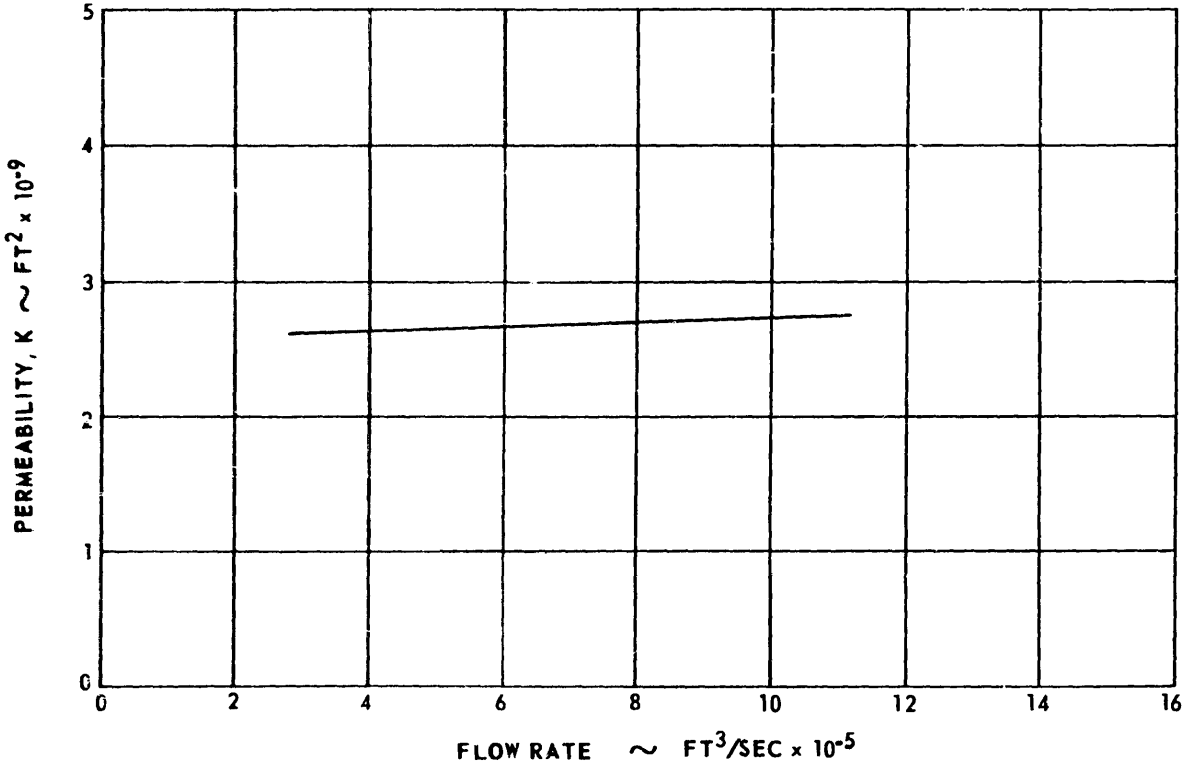

FIGURE B-3. PERMEABILITY VERSUS FLOW RATE FOR 100-MESH SCREEN

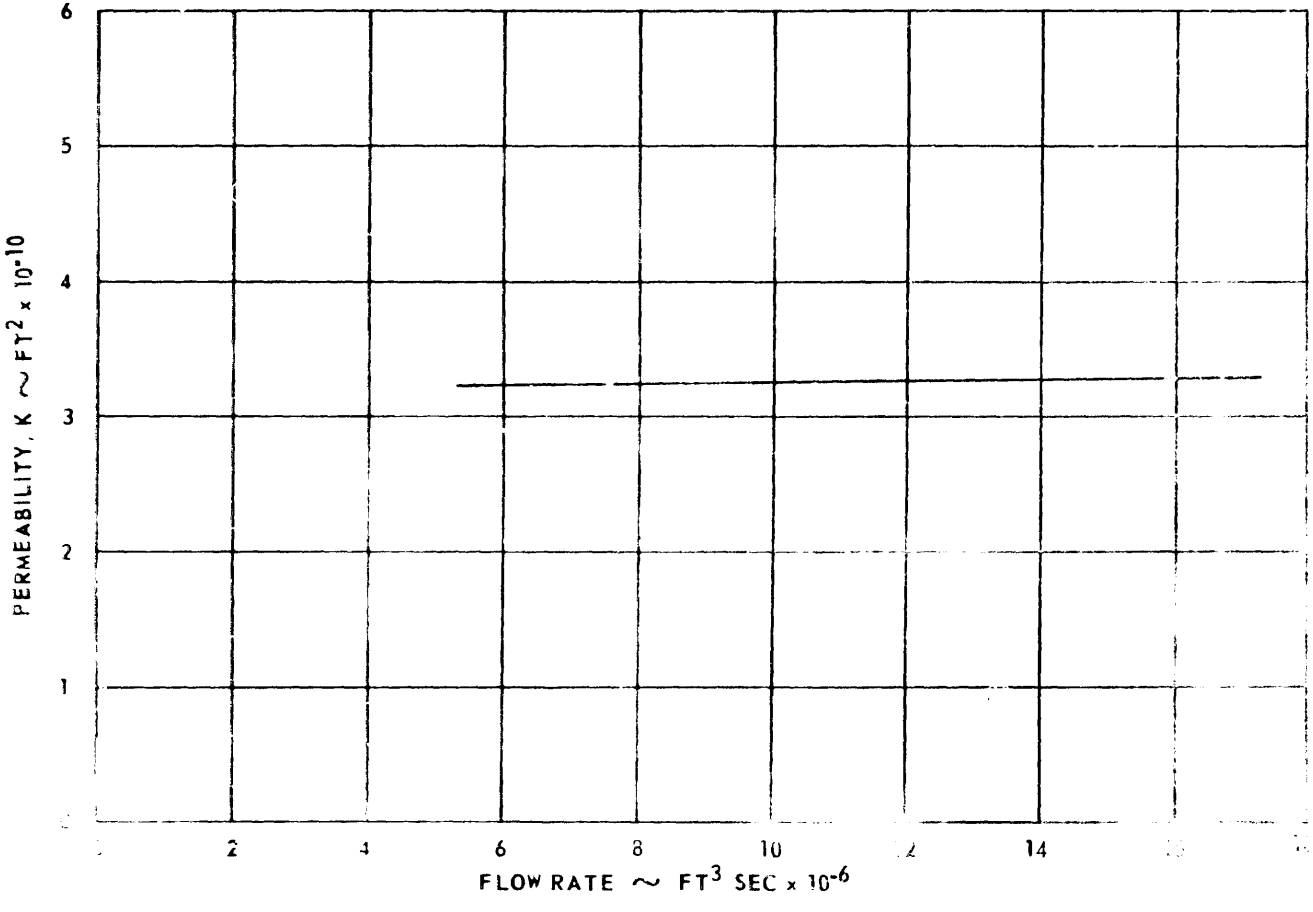

FIGURE B-1. PERMEABILITY VERSUS FLOW RATE FOR 250-MESH SCREEN

The consistency of the experimental data shows that if the procedure described herein is followed, the permeabilities determined are realistic. Also, compared to available data, the determined values for permeability are approximately correct.

APPENDIX C

ASSEMBLY PROCEDURE FOR HEAT PIPES

1. Steps for Assembling Heat Pipes as Radiating Fins

The procedure for assembling heat pipes that serve as radiating fins is as follows:

(1) Cut the stainless steel screen to the prescribed size and roll it until it is approximately the size of the opening in the cylindrical container.

(2) Place the rolled screen in the cylindrical container.

(3) Insert a spring inside the screen in the container.

(4) Silver solder the pressure transducer connection into the lower end cap.[1]

(5) Place the cylindrical container, screen, spring, caps, and other parts which protrude into vapor space in a sonic cleaner containing Freon 113 and clean for 30 minutes.

(6) Remove the assembly from sonic cleaner, screw end caps in, then silver solder around the end caps.

---

1. For heat pipes with an $r_o = 0.0208$ ft, silver solder a tube into a plug and screw the plug into lower end cap.

(7) Place the assembly into an oven at 550° F, and bake for a period of 16 hours.

(8) Remove the assembly from the oven and plug all openings.

(9) Wind the heater wire on the upper portion of the containing cylinder.

(10) Insulate and cover heater and connect to test fixture.

(11) Install all thermocouples that are on the outside of the heat pipe and heater.

(12) Remove the plug sealing the thermocouple outlet from the end cap.[2]

(13) Fill the inside of the heat pipe with a measured amount of distilled water.

(14) Wait approximately 15 minutes, drain and measure the excess distilled water.

(15) Add 2 to 3 cubic centimeters of distilled water to the heat pipe.

(16) Screw the thermocouple assembly into the end cap.[3]

(17) Connect the pressure transducer.

(18) Evacuate the heat pipe till a pressure of approximately 0.6 psia is obtained.

---

2. For heat pipes with an $r_o = 0.0208$ ft. remove plug containing the pressure transducer connection.

3. For heat pipes with an $r_o = 0.0208$ ft, screw in a plug containing the pressure transducer connection.

(19) Check for leaks with a leak detector.

(20) Stop the leaks by tightening fittings, etc.

(21) Evacuate the heat pipe to a pressure of approximately 0.6 psia.

(22) Paint the heat pipe and test fixture black to ensure an uniform emissivity.

(23) Place the test fixture and heat pipe in vacuum chamber and connect the power supplies, thermocouples leads, pressure transducer leads, etc.

The major parts to be assembled for a heat pipe as a radiating fin are shown in Figure C-1.

2. Steps for Assembling Heat Pipes with an Adiabatic Section

The procedure for assembling heat pipes with an adiabatic section is as follows:

(1 through 10) Steps 1 through 10 are the same as for a heat pipe serving as a radiating fin.

(11) Install all thermocouples that are on the outside of the heat pipe, heater, and the two on the condenser.

(12) Insulate the adiabatic section and the condenser.

(13 through 22) Steps 13 through 22 are the same as steps 12 through 21 for a heat pipe serving as a radiating fin.

(23) Connect the power supplies, water supply, thermocouple leads, pressure transducer leads, etc.

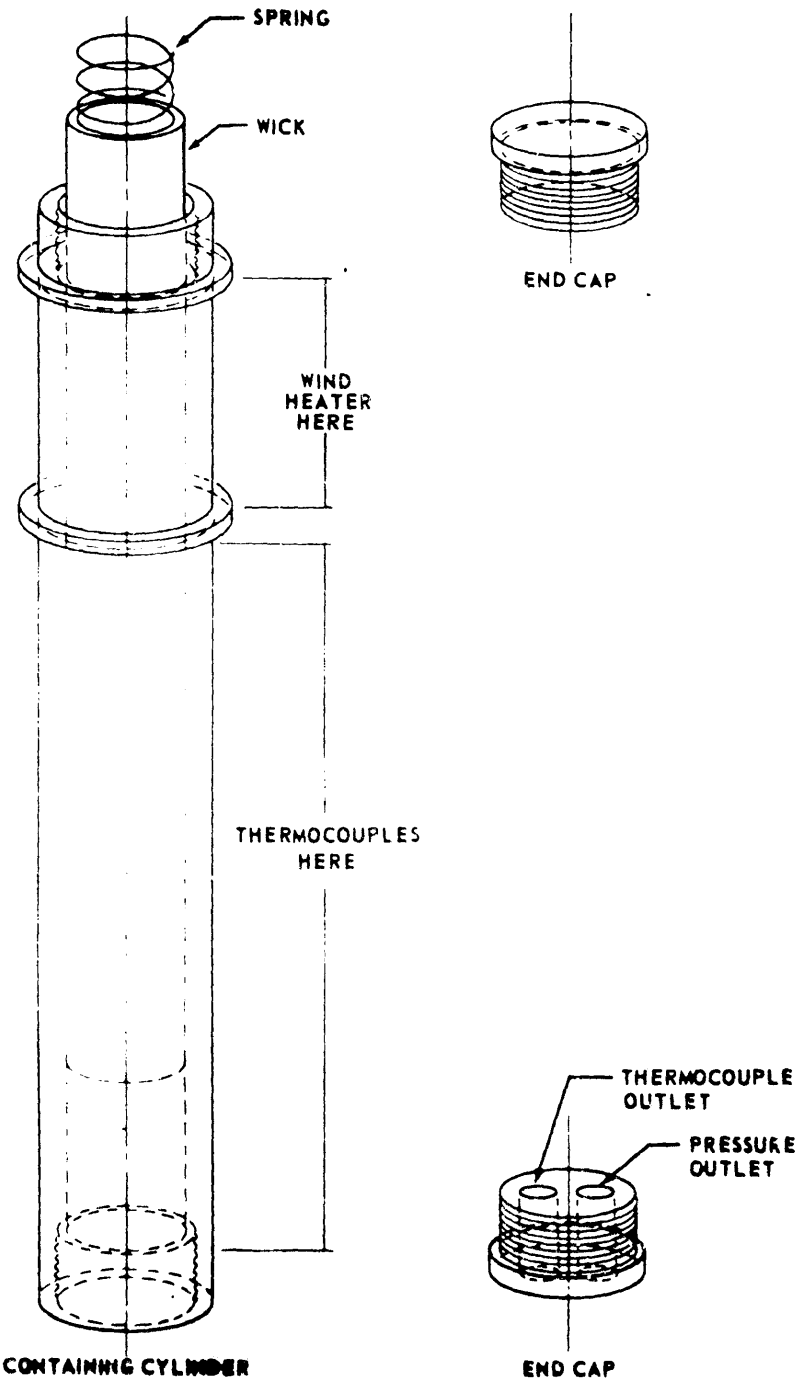

FIGURE C-1. HEAT PIPE PARTS (RADIATING FIN)

The major parts to be assembled for a heat pipe with an adiabatic section are shown in Figure C-2.

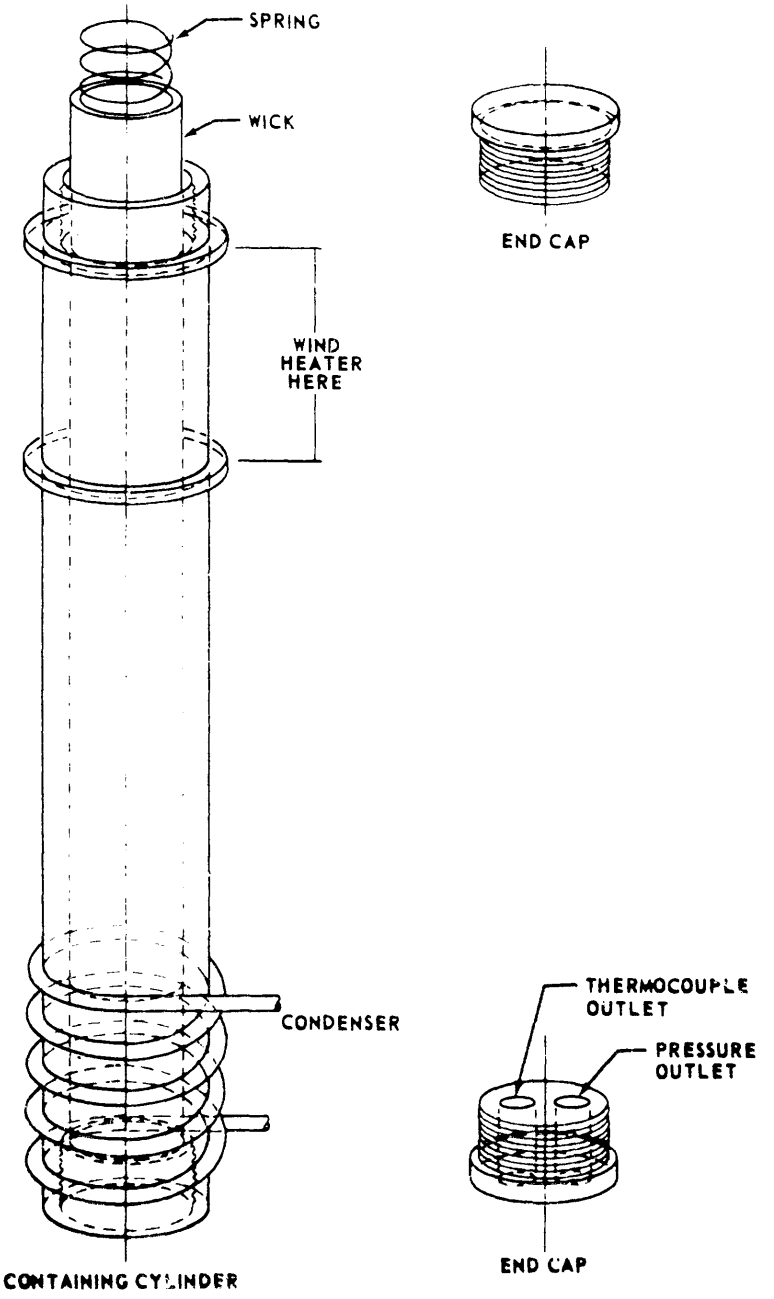

FIGURE C-2. HEAT PIPE PARTS (ADIABATIC SECTION)

APPENDIX D

EXPERIMENTAL EQUIPMENT FOR HEAT PIPES AS RADIATING FINS

The experimental equipment consisted of the high altitude simulation system and the data acquisition system. This equipment is government property maintained and operated by the Propulsion and Vehicle Engineering Laboratory of the George C. Marshall Space Flight Center.

1. High Altitude Simulation System

The high altitude simulation system, or vacuum system, consists of the following primary components: Vacuum chamber (diffusion pump, ejector pump, backing pump, and roughing pump), valves, pressure gauges, and liquid nitrogen sotrage trailer.

The vacuum chamber is a stainless steel cylinder approximately 8 feet long and 4 feet in diameter with a dished heat at each end. One of the dished heads is hinged for a door and the other is attached to the pumping system. The chamber encironment is controlled by a cooling jacket that permits a cooling liquid, such as liquid nitrogen, to be circulated through the cooling jacket and the chamber door. The door is of double wall construction connected to the jacket so that the cooling liquid circulates through both the

jacket and the door. The interior surfaces of the chamber viewed by the heat pipes are painted black to minimize radiant energy reflections.

The vacuum chamber wall is designed with three ports that can be used for viewing, instrumentation, or for power feedthrough. For these tests the ports were used for plugs to feedthrough 29 thermocouples, 2 pressure transducers, and 2 power supplies.

The pumping system consisted of four pumps that could produce a vacuum chamber minimum pressure of 5×10^{-7} mm Hg. The chamber vacuum was initiated by a roughing pump of large capacity. After a rough vacuum was obtained (150 mm Hg), the low vacuum was achieved and maintained by a fractionating oil diffusion pump, an oil ejector pump, and a rotary backing pump operating in series. The pumping system was designed and manufactured by the Consolidated Electrodynamics Corporation for NASA/MSFC. The following pumps were used in the system:

(1) Type MCF-15000 fractioning oil diffusion pump with 32-inch-diameter casing.

Operating range: 5×10^{-7} to 5×10^{-4} mm Hg

Maximum speed: 31 779 cfm at 3×10^{-4} mm Hg.

(2) Kinney Type KB-150 oil ejector pump

Operating range: 6×10^{-4} to 4×10^{-1} mm Hg

Maximum speed: 407 cfm at 3×10^{-2} mm Hg.

(3) Kinney Type KDH-130 rotary oil sealed backing pump.

Free air displacement: 131 cfm at 535 rpm

U'timate pressure: 1×10^{-2} mm Hg.

(4) Kinney Type KD-310 rotary oil sealed roughing pump.

Free air displacement: 311 cfm at 360 rpm

Ultimate pressure: 1×10^{-2} mm Hg.

The high altitude simulation system design incorporated the necessary valves and pressure gauges to control the system. All system valves were hand operated except the 32-inch valve between the vacuum chamber and the diffusion pump, which was motor driven. There were three types of pressure gauges used in the system: A cold cathode ionization type and a Pirani type were used to monitor the chamber vacuum; a Bourdon tube gauge was used to monitor the pressure in the liquid nitrogen storage trailer. Both the high and low vacuum gauges were products of the Consolidated Vacuum Corporation, Rochester Division, Rochester, New York, and were of the following specifications:

(1) Cold cathode ionization type

Discharge vacuum gauge

Type GPH-100A

Three range selections 25×10^{-3} to 1×10^{-8} mm Hg.

(2) Pirani Vacuum Gauge

Type 2203-04

Two range selection — 2000 - 50 microns.

The Pirani gauge was used to monitor the vacuum while the system was operating at a low vacuum, and the ionization gauge was used to monitor the vacuum when the system was operating at a high vacuum.

Liquid nitrogen was required for the vacuum pumping system cold trap and also for the vacuum chamber cooling jacket. The liquid nitrogen was supplied from a 9-ton-capacity liquid nitrogen storage trailer. The storage trailer was a self-pressurizing unit that was maintained at a pressure of 25 to 30 psig for the test runs. Flow was controlled to the vacuum system by a hand valve, and the storage trailer pressure was maintained by a hand vent valve and an automatic (spring-loaded) relief valve. For safety reasons, the storage trailer was located outside of the building that houses the vacuum system, and the liquid nitrogen was supplied by a 1-inch-diameter insulated pipe.

2. Data Acquisition System

The data acquisition system consisted of 29 thermocouples, 2 pressure transducers, a digital recording system, and a tape-controlled typewriter.

The thermocouples were standard 24-gauge copper and constantan thermocouple wiring. The thermocouples on the outside of the heat pipes and heaters were spot welded and brought out of the vacuum chamber through a standard vacuum-type feedthrough electrical connector. The thermocouples in the vapor spaces of the heat pipes followed the same exit path as the other thermocouples. A thermocouple cold junction (ice bath) was located

adjacent to the vacuum chamber, and the thermocouple outputs were carried by way of a floor conduit to the recording system approximately 50 feet away.

The pressure transducers were capable of monitoring pressures of 0 to 150 psia. The pressure transducers were connected to a tube that protruded from the end cap of the heat pipes. The leads from the pressure transducers were brought out of the vacuum chamber through a standard vacuum-type feedthrough electrical connector and carried by way of a floor conduit to the recording system.

The digital recording system was a Dymec system. This system could record up to 100 channels of data. A digital output was punched on paper tape along with the necessary signals to control a Frieden flexowriter. The tape was fed through the flexowriter control system for each recording, and the data outputs were typed in millivolts, newtons, volts, or amperes.

The data acquisition system accuracy was dependent upon the range selected. For this test series, a range of 0 to 10 millivolts was selected, and the system accuracy in converting the thermocouple output was ±0.01 millivolt (approximately 0.4° F).

APPENDIX E

SUMMARY OF EXPERIMENTAL AND CALCULATED DATA FOR HEAT PIPES AS RADIATING FINS

The temperature profiles, on the surface, that were obtained experimentally for the heat pipes are plotted in Figures E-1 through E-8. These temperatures were obtained by converting experimental readings from millivolts to ° F. To establish the profile, the temperatures were plotted at distances from the end of the heat pipe that corresponded to the location of thermocouples on the heat pipe. The temperature for the length, L_e, (see Figures E-1 through E-8) was the temperature in the vapor space since no thermocouples were located on the surface of the evaporator.

In Figures E-1, E-5, E-7, and E-8, peculiar temperature profiles exist that require additional explanation. Test 1a, shown in Figure E-1, depicts the temperature profile for a solid rod. Reduction of data reveals that for Test 1a the heat pipe did not function as a heat pipe and therefore it was a cylinder radiating heat. To obtain Figure E-5, data from Heat Pipe No. 5 were plotted. Since the wicking material (100-mesh screen) contained in Heat Pipe No. 5 did not possess sufficient capillary rise capability, no heat pipe existed and therefore explains the temperature profiles of Figure E-5. Tests 7f and 8f had larger temperature gradients on the surface of the

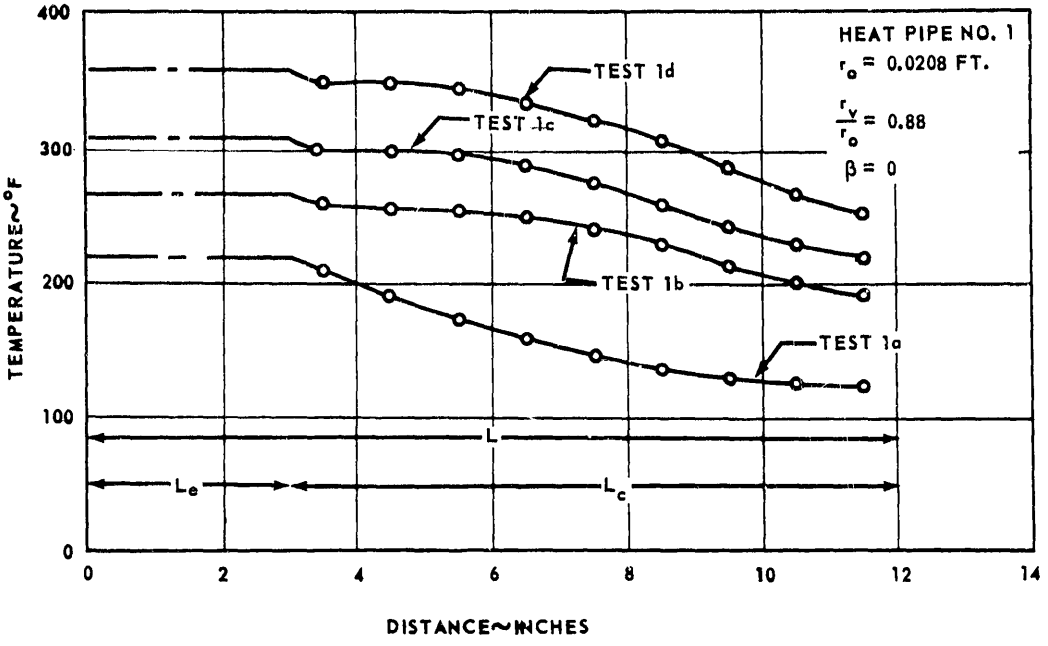

FIGURE E-1. SURFACE TEMPERATURE PROFILE (RADIATING FIN)

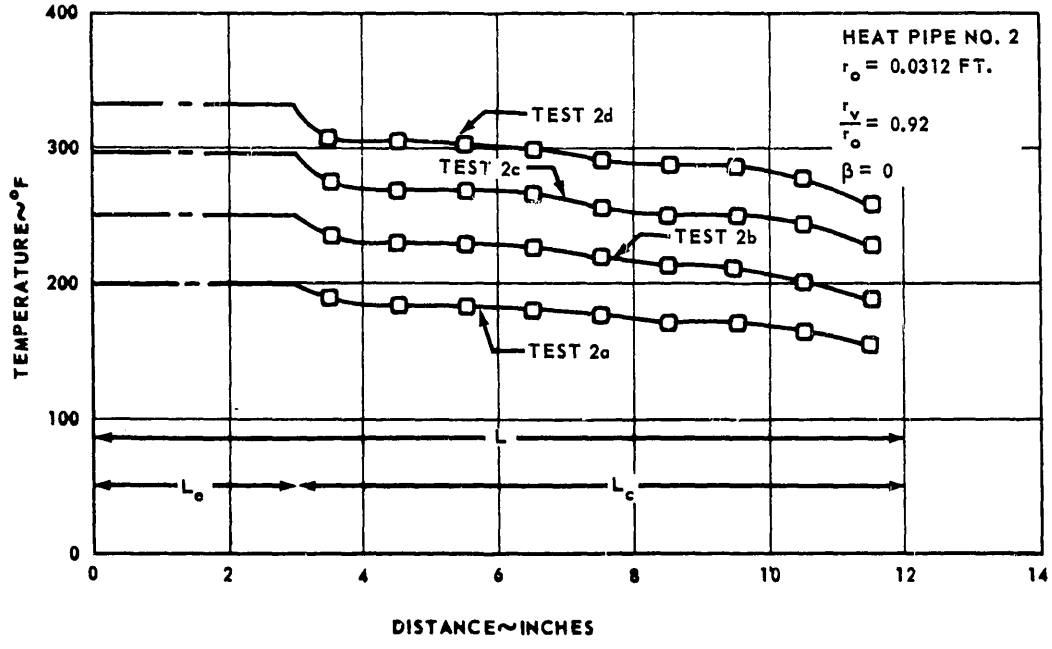

FIGURE E-2. SURFACE TEMPERATURE PROFILE (RADIATING FIN)

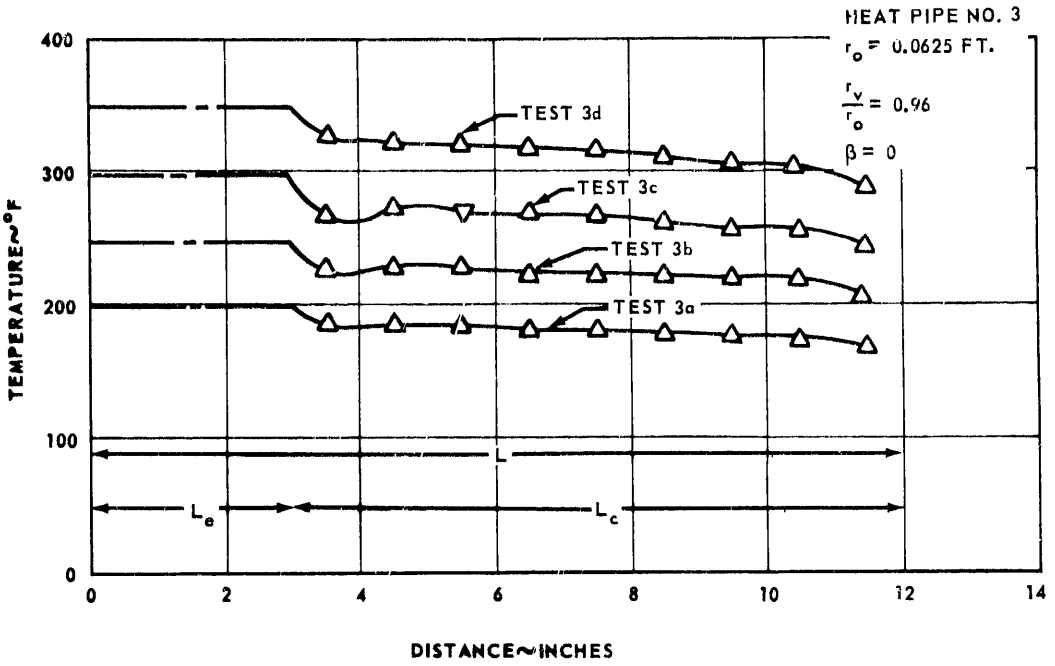

FIGURE E-3. SURFACE TEMPERATURE PROFILE (RADIATING FIN)

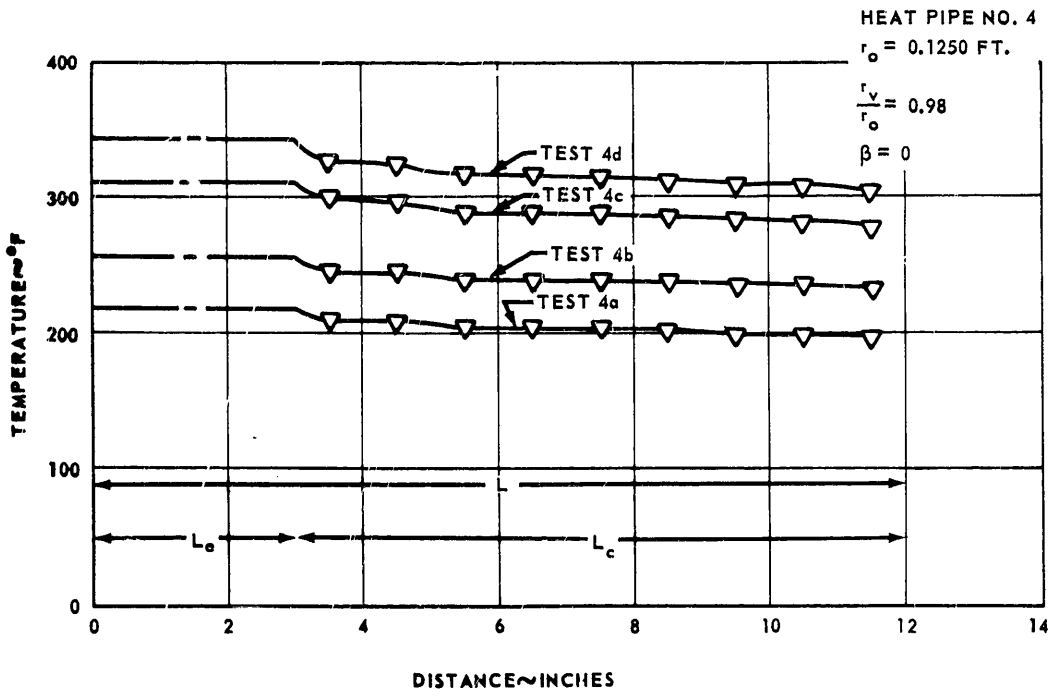

FIGURE E-4. SURFACE TEMPERATURE PROFILE (RADIATING FIN)

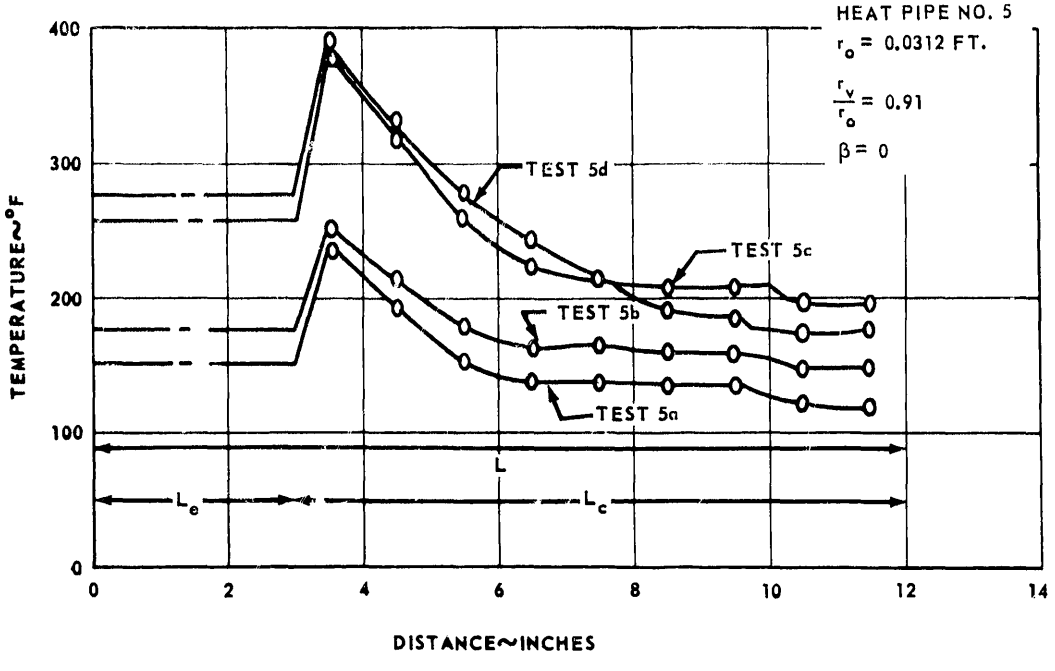

FIGURE E-5. SURFACE TEMPERATURE PROFILE (RADIATING FIN)

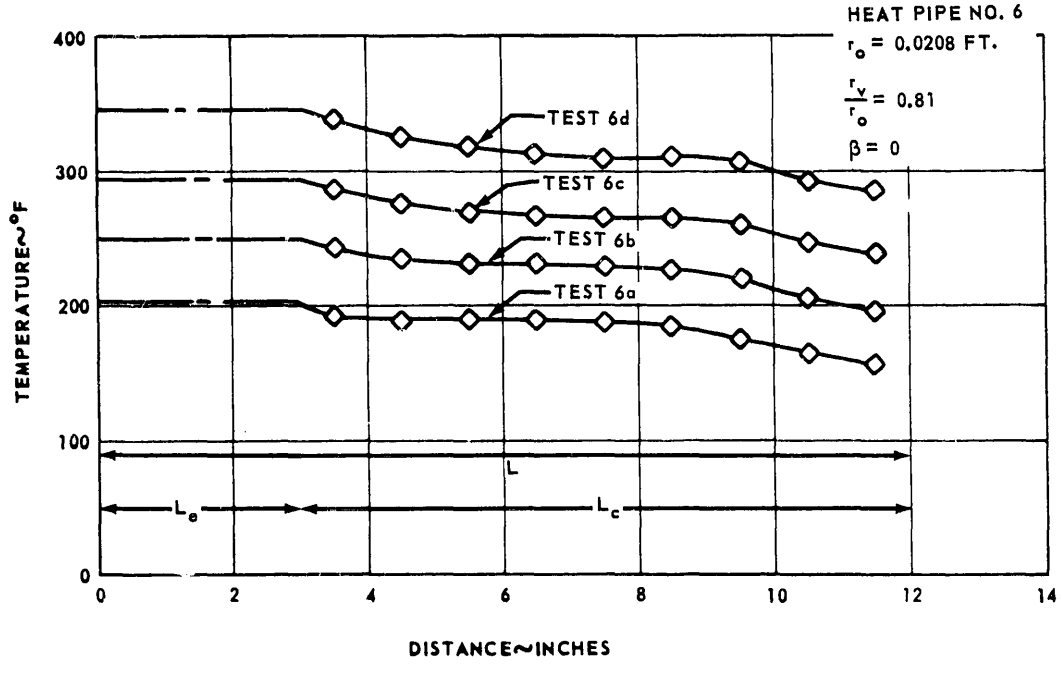

FIGURE E-6. SURFACE TEMPERATURE PROFILE (RADIATING FIN)

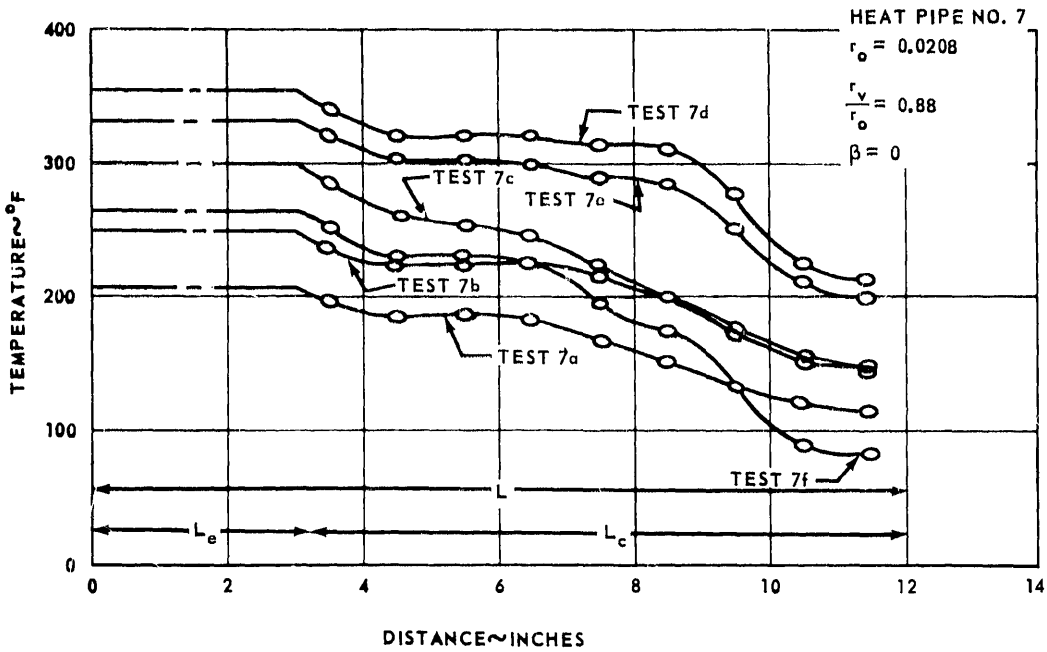

FIGURE E-7. SURFACE TEMPERATURE PROFILE (RADIATING FIN)

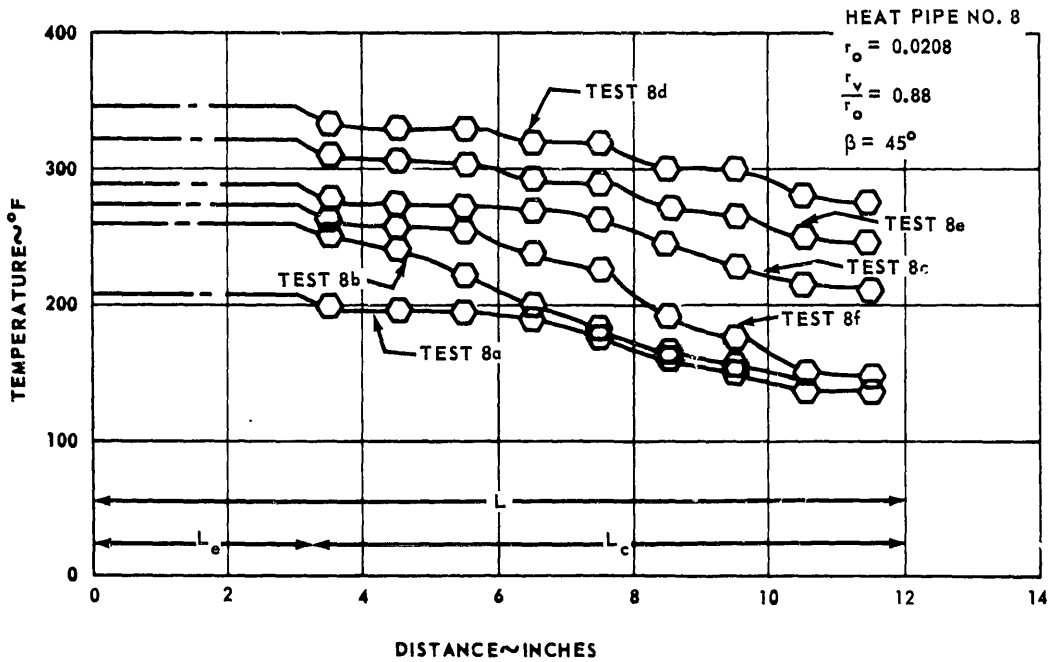

FIGURE E-8. SURFACE TEMPERATURE PROFILE (RADIATING FIN)

heat pipes than did the other tests of Figures E-7 and E-8. This larger temperature gradient was because for Tests 7f and 8f liquid nitrogen was circulated through the cooling jacket of the vacuum chamber.

Table E-I summarizes the heat inputs and losses for the eight heat pipes that were experimented. The temperature in the vapor space was recorded in millivolts by Thermocouple No. 13 or estimated from the readings on the surface of the heat pipes where r_o was equal to 0.0208 foot. The temperature, T_s was the temperature of the surroundings recorded by a thermocouple inside the vacuum chamber. The heat input to the system [Table E-I, Column (7)] was determined by the inputs to the heaters on the heat pipes. The amperage and voltage were recorded by the data acquisition system, and then by converting these readings, the heat input to the system was obtained.

The heat losses [Table E-I, Column (8)] were calculated by using the equation $q = A_s\ e\ \sigma_1\ (T^4 - T_s^4)$ and data recorded for thermocouples, 1, 2, and 3, that were fixed to the heater covers of the heat pipes. The data from these thermocouples were reduced to obtain temperatures, T, and with the other terms of the equation being defined as A_s = area of surface, ft^2, e = emissivity, 0.95, σ_1 = Stefan-Boltzmann constant, 0.1714×10^{-8} $Btu/ft^2\text{-}hr\text{-}^\circ R^4$, and T_s = surrounding temperature, the heat losses were calculated. The heat input [Table E-I, Column (9)] to the heat pipe was obtained by subtracting the heat loss from the heat input to the system.

TABLE E-I. SUMMARY OF EXPERIMENTAL HEAT INPUTS AND LOSSES (RADIATING FIN)

(1) Heat Pipe Number	(2) Test Number	(3) Date	(4) Time	(5) Temperature In The Vapor Space °F	(6) T_s °F	(7) Heat Input To System Btu/hr	(8) Heat Loss (Calculated) Btu/hr	(9) Heat Input To Heat Pipe Btu/hr	(10) Heat Input To Heat Pipe (Calculated) Btu/hr
1	1a	10/25/68	0900	220	82	52	27	25	25
1	1b	10/22/68	1030	267	97	98	43	55	58
1	1c	10/23/68	1045	309	100	137	60	77	79
1	1d	10/24/68	0930	358	103	209	94	115	111
2	2a	10/30/68	1440	199	86	65	24	41	39
2	2b	10/31/68	1300	252	93	111	47	64	61
2	2c	11/1/68	1400	298	100	176	84	92	87
2	2d	11/5/68	1430	333	105	293	71	122	113
3	3a	11/13/68	0730	201	90	109	48	61	61
3	3b	11/13/68	1330	249	92	171	72	99	99
3	3c	11/14/68	0900	297	105	245	106	139	137
3	3d	11/15/68	0730	351	127	352	164	188	188
4	4a	11/13/68	1330	220	92	207	65	142	136
4	4b	11/14/68	0900	258	105	269	81	188	184
4	4c	11/14/68	1530	313	111	419	142	277	275
4	4d	11/15/68	0730	345	127	522	193	329	324
5	5a	10/21/68	1055	152	68	144	98	46	28
5	5b	10/21/68	1530	176	76	145	112	33	35
5	5c	10/22/68	1030	258	97	306	214	92	68
5	5d	10/23/68	1045	276	100	288	189	99	67

TABLE E-I. SUMMARY OF EXPERIMENTAL HEAT INPUTS AND LOSSES (RADIATING FIN) (Concluded)

(1) Heat Pipe Number	(2) Test Number	(3) Date	(4) Time	(5) Temperature In The Vapor Space °F	(6) T_s °F	(7) Heat Input To System Btu/hr	(8) Heat Input (Calculated) Btu/hr	(9) Heat Input To Heat Pipe Btu/hr	(10) Heat Input To Heat Pipe (Calculated) Btu/hr
6	6a	10 30 68	1440	203	86	77	38	39	42
6	6b	10 31 68	1300	250	93	130	65	65	65
6	6c	11 1 68	1400	295	100	201	105	96	94
6	6d	11 5 68	0730	347	105	316	164	152	155
7	7a	11 21 68	1535	208	75	49	26	23	20
7	7b	11 26 68	0730	250	87	65	34	31	31
7	7c	11 22 68	1400	302	87	83	45	38	37
7	7d	11 26 68	1535	355	93	143	68	75	70
7	7e	11 27 68	0730	332	100	118	58	60	58
7	7f	11 27 68	1350	265	-188	120	67	53	51
8	8a	11 21 68	1535	209	75	83	50	33	33
8	8b	11 22 68	1400	260	87	118	80	38	39
8	8c	11 26 68	0730	290	87	162	92	70	72
8	8d	11 26 68	1535	348	93	248	128	120	112
8	8e	11 27 68	0750	323	100	204	116	88	89
8	8f	11 27 68	1350	275	-188	207	117	90	88

The heat input to the heat pipe obtained by the preceding was considered as the experimental heat input.

The heat input [Table E-1, Column (10)] to the heat pipe was calculated by using reduced data from Thermocouple Nos. 4 through 12 and the equation of the preceding paragraph. In these calculations, the reduced data from each thermocouple was considered as the surface temperature for a 1-inch section except for Thermocouple No. 12 which was for a 2-inch section. The heat radiated from each section was calculated and by summing the heat radiated from all sections the heat input was determined. The calculated heat inputs were used for comparison with heat inputs from the experiments.

Table E-II is a summary of data computed for heat pipes as radiating fins.

To obtain the heat input [Table E-II, Column (3)] through the stainless steel cylinder, the computer program of Reference 23 was used. The inputs to the computer program were as follows:

Area = Cross-sectional area of containing cylinder of the heat pipe

Perimeter = Perimeter of heat pipe

Length = Length of heat pipe exposed

Thermal Conductivity = Thermal conductivity of stainless steel or k = 10 Btu/hr-ft-°R

Base temperature = Temperature in the vapor space

Emissivity = 0.95.

TABLE E-II. SUMMARY OF CALCULATED DATA (RADIATING FIN)

(1) Test No.	(2) Heat Input To Heat Pipe Table E-1 Btu/hr	(3) Heat Input Thru S. S. Cylinder Btu/hr	(4) Heat Input Thru Vapor Space (Exp.) Btu/hr	(5) Heat Input Thru Vapor Space (Eq. 38) Btu/hr	(6) Temperature In Vapor Space °F	(7) Surrounding Temperature °F	(8) θ Fig. 25 degrees	(9) Heat Input To Solid Rod k=10 Btu/hr	(10) Heat Input To Solid Rod k=20 Btu/hr	(11) Heat Input To Solid Rod k=100 Btu/hr	(12) Heat Input To Solid Rod k=210 Btu/hr	(13) Heat Input For Fin Efficiency Btu/hr	(14) Fin Efficiency %
1a	25	24	1	5	220	82	40.5	27	33	49	52	56	45
1b	55	32	23	19	267	97	33.5	36	45	69	74	81	69
1c	77	41	36	24	309	100	26	45	57	92	101	112	69
1d	115	52	63	30	358	103	7	56	74	123	137	154	75
2a	41	24	17	15	199	86	41.5	28	34	48	50	53	77
2b	64	37	27	27	252	93	35.5	42	52	77	82	87	74
2c	92	46	46	38	298	100	28.5	53	70	106	115	123	75
2d	122	55	67	49	333	105	18.5	63	84	132	144	156	75
3a	61	37	24	28	201	90	41.5	48	58	76	75	80	76
3b	99	55	44	44	249	92	36.5	70	89	120	126	125	77
3c	139	72	67	79	297	105	28.5	91	119	167	175	181	77
3d	186	91	97	107	351	127	11	115	154	226	243	251	75
4a	142	75	67	46	220	92	40.5	111	134	165	168	161	88
4b	198	92	96	102	253	105	35	143	176	222	231	219	86
4c	277	136	141	182	313	111	25	204	255	334	349	333	83
4d	329	152	177	207	347	127	13.5	234	298	396	417	401	82
5a	45	12	34	-	152	68	-	15	18	24	24	26	177
5b	33	15	18	-	176	76	-	19	22	31	32	34	97
5c	92	25	67	-	258	97	-	33	41	62	66	71	130
5d	99	28	71	-	276	100	-	37	46	70	76	82	121
6a	39	25		45	203	86	41.5	29	36	50	52	56	70
6b	65	35	30	66	250	93	36.0	41	51	75	80	86	76
6c	96	46	50	83	295	100	29	53	68	104	113	121	79
6d	152	60	92	115	347	105	12.5	67	90	144	158	172	88
7a	23	11	12	8	208	75	41.0	15	19	30	32	36	64
7b	31	15	16	16	250	87	36.0	19	25	41	45	51	61
7c	38	22	16	26	302	87	27.5	26	35	59	66	77	49
7d	75	28	47	37	355	93	9	31	45	79	91	108	69
7e	60	25	35	32	332	100	19	30	40	69	80	88	68
7f	53	27	26	17	265	-189	34	32	42	67	74	84	63
8a	33	21	12	-	209	75	-	24	31	46	48	52	63
8b	38	31	7	-	260	87	-	33	44	67	73	80	48
8c	70	37	33	-	290	87	-	41	54	84	92	100	70
8d	120	51	69	-	348	93	-	54	73	119	132	147	82
8e	88	44	44	-	323	100	-	48	62	101	111	122	72
8f	90	52	39	-	275	-188	-	55	72	108	117	127	71

The heat input [Table E-II, Column (4)] (the heat which is transported through the interportion of the heat pipe) was determined by subtracting. The heat input [Table E-II, Column (5)] was calculated by using equation (38), the dimensions of the heat pipe considered, and the angle, θ, as shown in Table E-II. The heat input to the solid rod [Table E-II, Columns (9 - 12)] was calculated by the computer program of Reference 23 using the dimensions of the corresponding heat pipe and for four different thermal conductivities as shown in the table. The lengths of the corresponding exposed heat pipes were considered for the solid rods.

The heat input for fin efficiency [Table E-II, Column (13)] was calculated by using the equation $q = A_s \, e \, \sigma_1 \, (T^4 - T_s^4)$. These calculations used a constant temperature at the surface, with this temperature being the temperature of the vapor space for the case under consideration. The other terms of the equation were as previously defined. The fin efficiency [Table E-II, Column (14)] was obtained by dividing the total heat input to the heat pipe by the heat input for fin efficiency.

Table E-III is an example of the input and output from the computer program of Reference 23. The case shown is for a solid rod having the same dimensions of Heat Pipe No. 4 and the same temperatures obtained in Test 4b.

Table E-IV defines the temperature difference at the ends away from the source for heat pipes and solid rods of comparable material.

TABLE E-III. COMPUTER INPUT AND OUTPUT FOR A SOLID ROD (RADIATING FIN)

Output			
x ft	q Btu/hr	T °R	T °F
0.833	143	717	257
0.750	123	703	243
0.667	105	691	231
0.583	89	680	220
0.500	75	671	211
0.417	62	664	204
0.333	50	658	198
0.250	39	653	193
0.167	29	650	190
0.083	21	647	187
0.164×10^{-10}	9	645	185

Input		
Cross-section area	=	0.07712 ft^2
Length	=	0.83333 ft
Perimeter	=	0.98457 ft
Surrounding temperature	=	565 °R
Base temperature	=	718 °R
Emissivity	=	0.95
Heat transfer coeff.	=	0.0
Thermal conductivity	=	10 Btu/hr-ft-°R

TABLE E-IV. TEMPERATURE DIFFERENCES AT THE END OF HEAT PIPES AND SOLID RODS (RADIATING FIN)

Heat Pipe No.	a Test $\Delta T \sim {}^\circ F$	b Test $\Delta T \sim {}^\circ F$	c Test $\Delta T \sim {}^\circ F$	d Test $\Delta T \sim {}^\circ F$
1	-6	43	60	82
2	25	38	61	83
3	30	49	62	79
4	35	45	65	73
6	27	47	84	105
7	6	10	18	75
8	18	5	63	115

NOTE: Minus (-) indicates end of heat pipe below temperature of end of solid rod.

TABLE E-V. HEAT INPUTS THROUGH THE VAPOR SPACE OF FOUR HEAT PIPES (RADIATING FIN)

Heat Pipe No.	L inches	D inches	$\frac{L}{D}$	q for T=200° F Btu/hr	q for T=250° F Btu/hr	q for T=300° F Btu/hr	q for T=350° F Btu/hr
1	12	$\frac{1}{2}$	24	12	20	33	58
2	12	$\frac{3}{4}$	16	17	27	47	77
3	12	$1\frac{1}{2}$	8	24	44	69	97
4	12	3	4	52	90	129	183

Table E-V defines the heat inputs through the vapor space of Heat Pipe Nos. 1 through 4 if the heat input through the stainless steel cylinder was not included. These heat inputs were taken from Table E-II and presented in Table E-V when comparing L/D ratios. Interpolation was used since the exact temperature does not appear in Table E-II.

Figure E-9 depicts the geometry for the heat pipes and solid rods for determining heat input per pound. The solid rods are shorter in comparison to the heat pipes because longer heat pipes are needed to provide an area for the heater.

Table E-VI summarizes the data required to determine the heat input per pound for two heat pipes and three solid rods. The heat inputs through the stainless steel cylinders (k = 10), stainless steel rods (k = 10), and copper rod (k = 210) were calculated by using the computer program of Reference 22. The volume of stainless steel or copper was computed using the geometry shown in Figure E-9. The weight was computed from the volume with the density of stainless steel = 490 lb/ft^3 and the density of copper = 559 lb/ft^3.

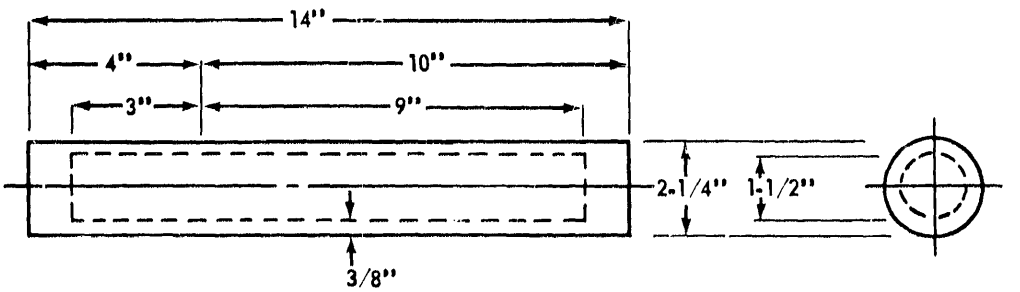

HEAT PIPE NO. 3

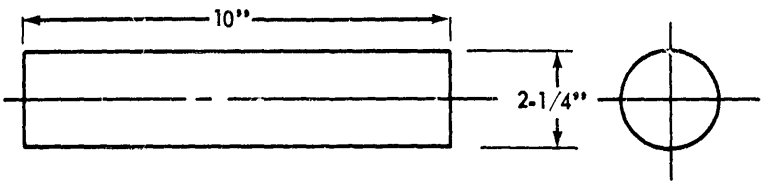

STAINLESS STEEL ROD NO. 1

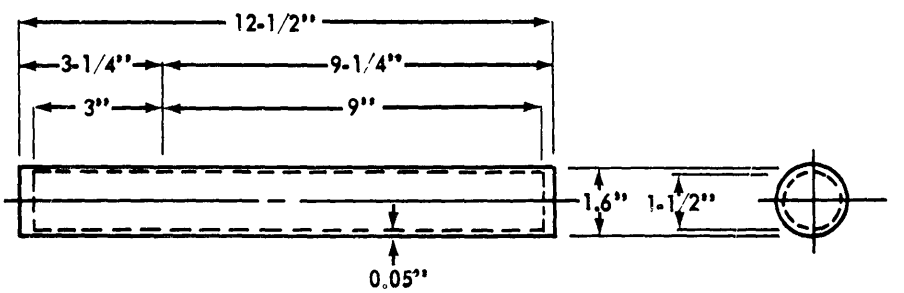

MODEL HEAT PIPE

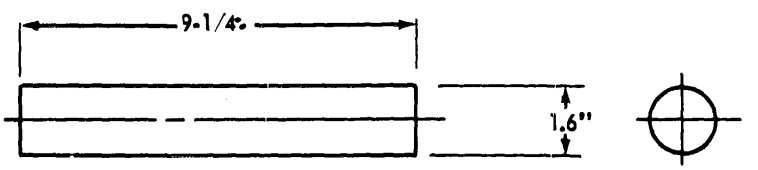

STAINLESS STEEL ROD NO. 2 OR COPPER ROD NO. 1

FIGURE E-9. GEOMETRY OF HEAT PIPES AND SOLID RODS (RADIATING FIN)

TABLE E-VI. HEAT INPUT PER POUND (RADIATING FIN)

Test No.	Base Temperature °F	Surrounding Temperature °F	Heat Input Thru S.S. Cylinder or Solid Rod k = 10 Btu/hr	Heat Input Thru Vapor Space Table E-II Btu/hr	Total Heat Input Btu/hr	Volume of S. Steel in.^{3}	Weight 250-Mesh Screen lb	Weight Cylinder or Rod lb	Total Weight lb	Heat Input Per Pound Btu/hr-lb
H.P.3a	201	90	37	24	61	34.4	0.1	9.8	9.9	6.2
H.P.3b	249	92	55	44	99	34.4	0.1	9.8	9.9	10
H.P.3c	297	105	72	67	139	34.4	0.1	9.8	9.9	14
H.P.3d	351	127	91	97	188	34.4	0.1	9.8	9.9	19
S.S.R.1a	201	90	48	-	48	39.4	-	11.2	11.2	4.4
S.S.R.1b	249	92	70	-	70	39.4	-	11.2	11.2	6.3
S.S.R.1c	297	105	91	-	91	39.4	-	11.2	11.2	8.1
S.S.R.1d	351	127	115	-	115	39.4	-	11.2	11.2	10.3
M.H.P.3a	201	90	9	24	33	4.0	0.1	1.1	1.2	27.5
M.H.P.3b	249	92	14	44	58	4.0	0.1	1.1	1.2	47.3
M.H.P.3c	297	105	20	67	87	4.0	0.1	1.1	1.2	72.5
M.H.P.3d	351	127	25	97	122	4.0	0.1	1.1	1.2	102
S.S.R.2a	201	90	33	-	33	18.6	-	5.3	5.3	6.2
S.S.R.2b	249	92	43	-	43	18.6	-	5.3	5.3	8.1
S.S.R.2c	297	105	56	-	56	18.6	-	5.3	5.3	10.6
S.S.R.2d	351	127	71	-	71	18.6	-	5.3	5.3	13.5
C.R.1a	201	90	*59	-	59	*18.6	-	6.1	6.1	9.8
C.R.1b	249	92	*86	-	86	*18.6	-	6.1	6.1	14.9
C.R.1c	297	105	*112	-	112	*18.6	-	6.1	6.1	20.2
C.R.1d	351	127	*162	-	162	*18.6	-	6.1	6.1	26.8

*Heat input through copper rod (k = 210) and volume of copper

NOTE: H.P. denotes Heat Pipe; S.S.R. denotes Stainless Steel Rod; M.H.P. denotes Model Heat Pipe; C.R. denotes Copper Rod

APPENDIX F

SUMMARY OF EXPERIMENTAL AND CALCULATED DATA FOR HEAT PIPES HAVING AN ADIABATIC SECTION

The temperature profiles, on the steel surface of the heat pipes, that were obtained experimentally are plotted in Figures F-1 through F-8. The temperature for the length, L_e, was the temperature obtained in the vapor space since thermocouples were not present on the surface of the evaporator. These temperature profiles were obtained by converting an experimental reading from millivolts to °F and then plotting these temperatures at distances from the end of the heat pipe that corresponded to the location of the thermocouples on the surface of the heat pipe. Note the change in the temperature profiles with the change in condenser length. For Heat Pipe Nos. 9, 10, and 11, the total condenser length was approximately 4 inches, whereas for Heat Pipe Nos. 12, 13, 14, 15, and 16, the total condenser length was approximately 1 1/2 inches.

In Figures F-1, F-2, F-3, and F-5, peculiar temperature profiles occur. In Figure F-1, the temperature profile for Test 9c has a large decrease in temperature and intersects the temperature profiles from Tests 9a and 9b. This large decrease in temperature was due to a leak developing in the heat pipe during the test. In Figure F-2, the circumstances that existed

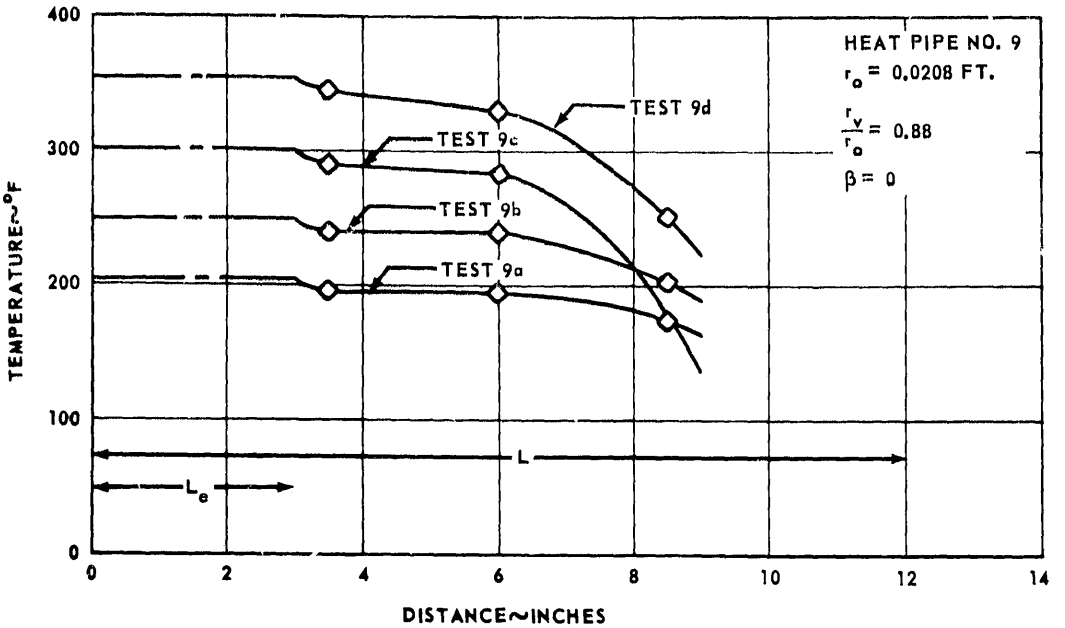

FIGURE F-1. SURFACE TEMPERATURE PROFILE (ADIABATIC SECTION)

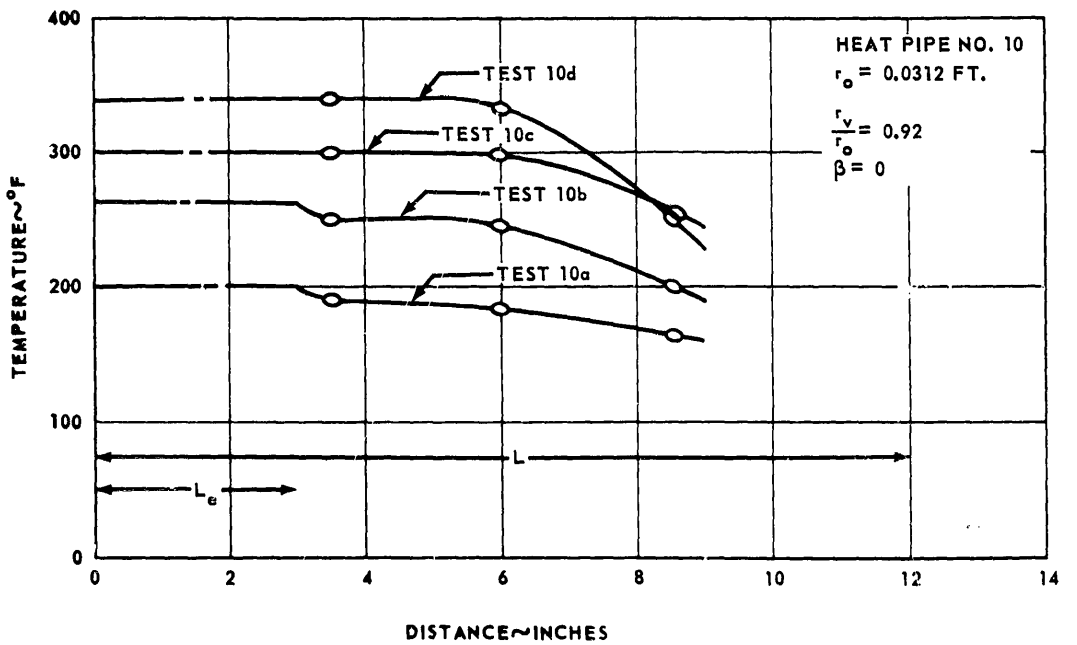

FIGURE F-2. SURFACE TEMPERATURE PROFILE (ADIABATIC SECTION)

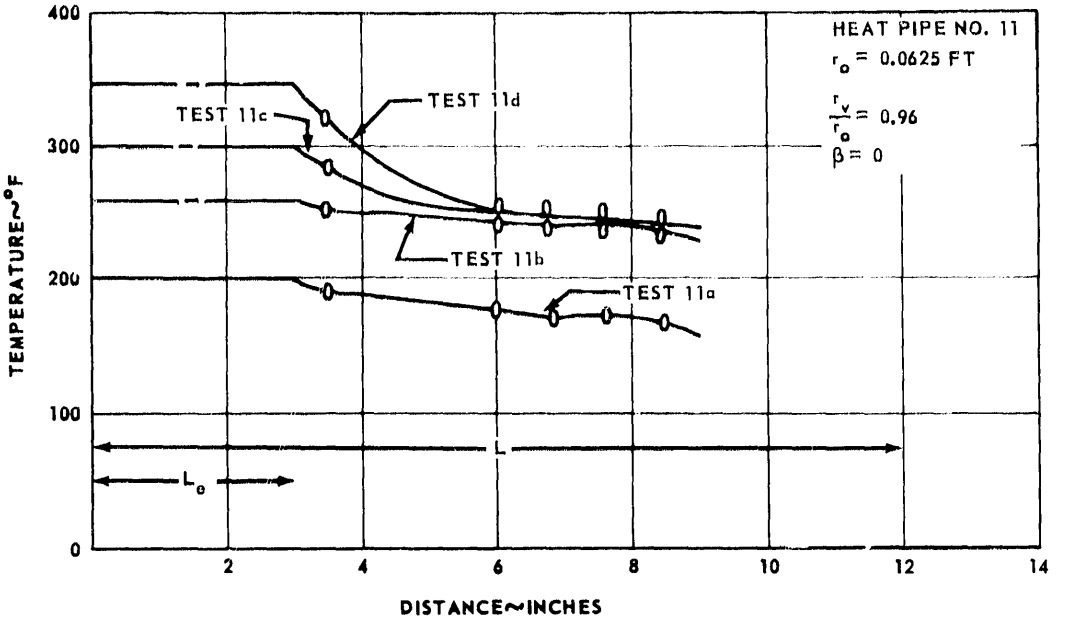

FIGURE F-3. SURFACE TEMPERATURE PROFILE (ADIABATIC SECTION)

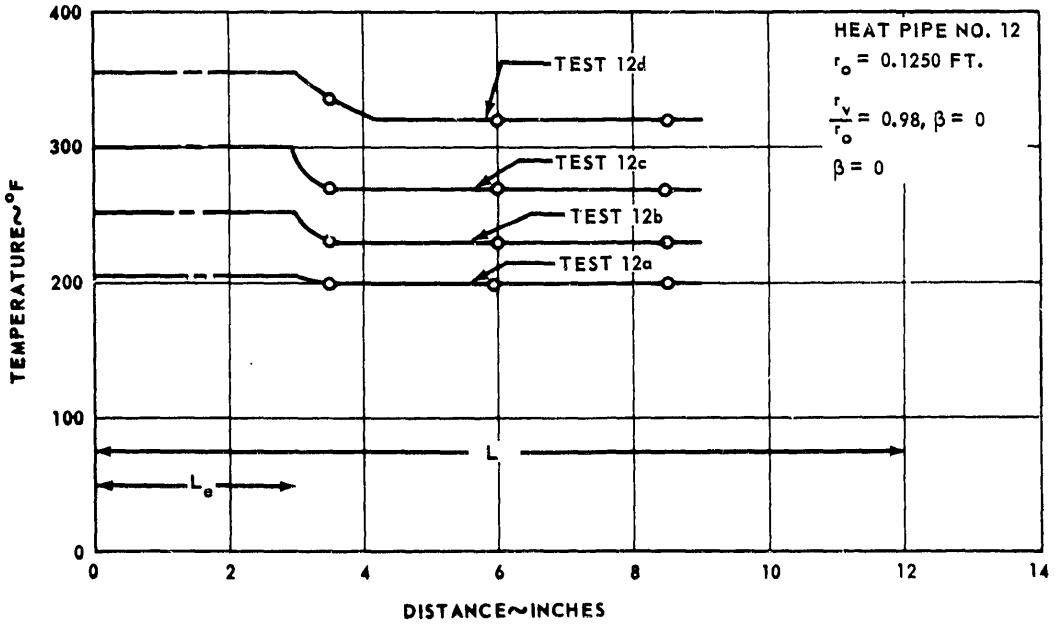

FIGURE F-4. SURFACE TEMPERATURE PROFILE (ADIABATIC SECTION)

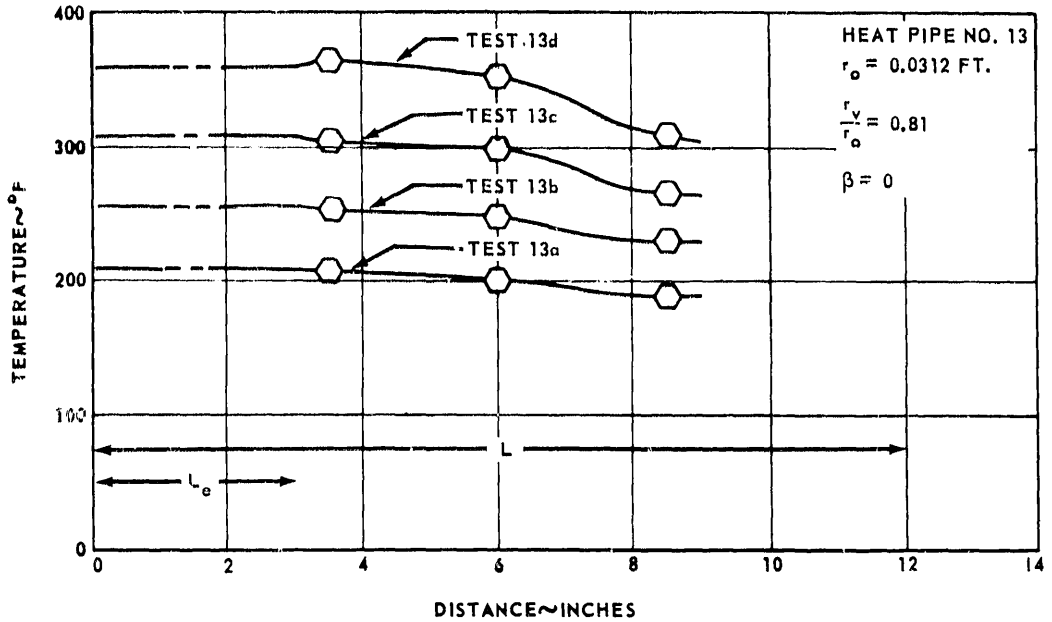

FIGURE F-5. SURFACE TEMPERATURE PROFILE (ADIABATIC SECTION)

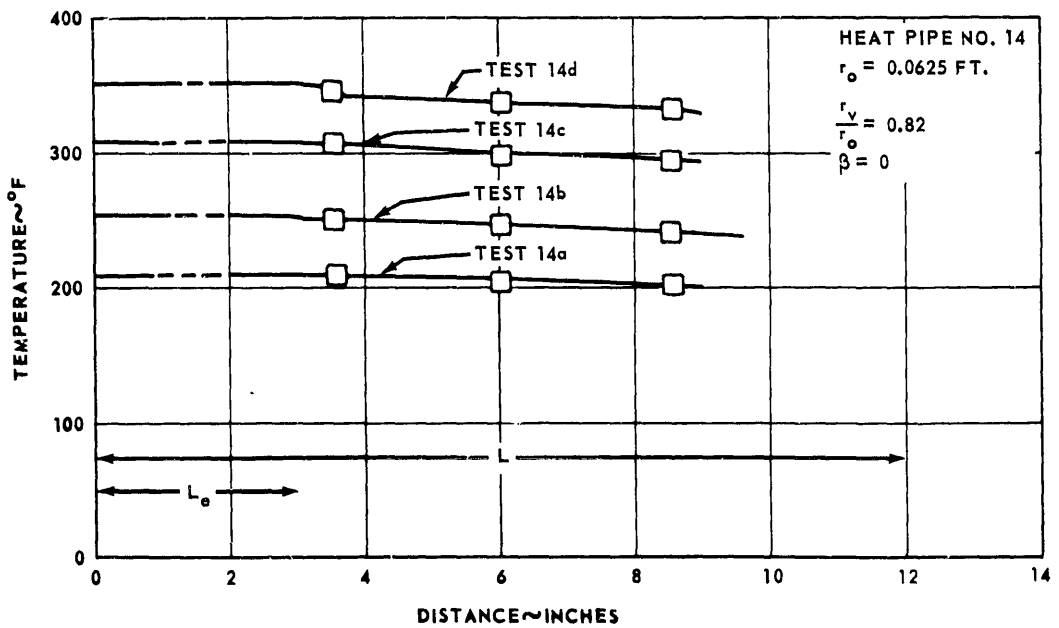

FIGURE F-6. SURFACE TEMPERATURE PROFILE (ADIABATIC SECTION)

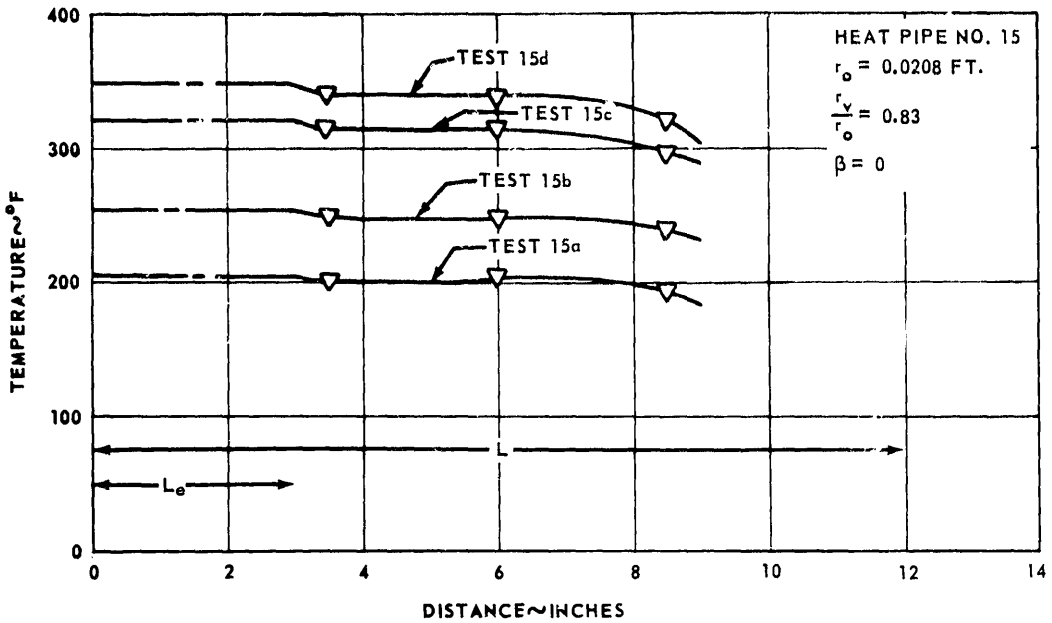

FIGURE F-7. SURFACE TEMPERATURE PROFILE (ADIABATIC SECTION)

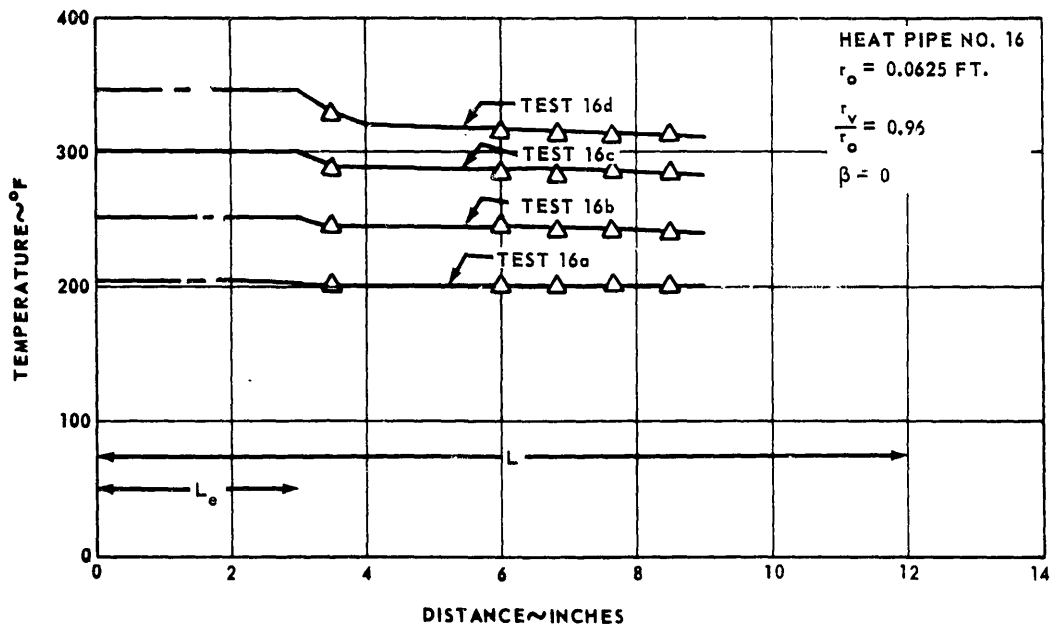

FIGURE F-8. SURFACE TEMPERATURE PROFILE (ADIABATIC SECTION)

for Test 10d were similar to those of Test 9c except the leak was less severe. No cause for the temperature profiles for Tests 11c and 11d was found. A logical conclusion for these two temperature profiles of Figure F-3 was that a leak developed during the tests. In Figure F-5, the temperature profile for Test 13d is high near the evaporator but no cause for the high temperature was found.

Table F-I summarizes the heat inputs and losses for the eight heat pipes used in the experiments. The temperature in the vapor space was recorded in millivolts by Thermocouple No. 6 or estimated from the readings on the surface of the heat pipe where r_o was equal to 0.0208 foot. The temperature, T_s, was the temperature of the surroundings recorded by a thermocouple located in the room where the experiments were run. The heat input to the system [Table F-I, Column (7)] was determined by the inputs to the heaters on the heat pipes. The amperage and voltage were recorded by the data acquisition system, and then by converting these readings, the heat input to the system was obtained.

The heat losses by radiation [Table F-I, Column (8)] were calculated by using the equation $q = A_s \, e \, \sigma_1 \, (T^4 - T_s^4)$, data recorded by Thermocouple Nos. 1 and 2 that were fixed to the heater cover, and data from the thermocouple in the room. The data from the three thermocouples were reduced to yield T and T_s, and with $e = 0.95$, the heat losses due to radiation were calculated by using the above equation.

TABLE F-I. SUMMARY OF EXPERIMENTAL HEAT INPUTS AND LOSSES (ADIABATIC SECTION)

(1) Heat Pipe Number	(2) Test Number	(3) Date	(4) Time	(5) Temperature in Vapor Space °F	(6) T_s °F	(7) Heat Input to System Btu/hr	(8) Heat Loss by Radiation (Calculated) Btu/hr	(9) Heat Loss by Convection (Calculated) Btu/hr	(10) Heat Input To Heat Pipe Btu/hr
9	9a	12/9/68	1430	206	75	235	59	51	125
9	9b	12/10/68	1240	249	75	365	97	80	188
9	9c	12/12/68	1400	302	74	245	87	75	83
9	9d	12/11/68	1400	355	75	443	151	124	168
10	10a	12/9/68	1430	201	75	503	122	102	279
10	10b	12/10/68	1240	263	75	510	149	122	239
10	10c	12/23/68	1315	300	80	398	93	70	235
10	10d	12/26/68	1130	349	81	517	115	82	319
11	11a	12/19/68	1430	201	75	906	223	175	508
11	11b	12/20/68	1400	259	76	468	176	141	151
11	11c	12/23/68	1315	298	80	827	245	186	396
11	11d	12/26/68	1130	347	81	927	297	217	413
12	12a	1/3/69	1500	205	79	391	61	44	286
12	12b	1/6/69	1300	252	78	706	86	61	559
12	12c	1/7/69	1045	299	78	907	117	87	703
12	12d	1/7/69	1345	354	79	919	144	107	668
13	13a	1/14/69	1330	209	79	62	24	17	21
13	13b	1/15/69	1415	257	79	141	30	22	141
13	13c	1/16/69	1330	308	79	208	41	30	137
13	13d	1/17/69	1330	359	79	309	57	43	209
14	14a	1/14/69	1330	210	79	112	33	25	54
14	14b	1/15/69	1415	253	79	206	48	37	121
14	14c	1/16/69	1330	308	79	249	59	47	143
14	14d	1/17/69	1330	352	79	454	69	53	333
15	15a	1/22/69	1500	205	71	83	29	24	30
15	15b	1/22/69	1230	254	70	142	43	35	64
15	15c	1/21/69	1415	320	70	204	52	50	102
15	15d	1/23/69	1345	348	73	222	63	53	106
16	16a	1/3/69	1500	203	79	209	49	37	123
16	16b	1/6/69	1300	252	78	410	93	84	233
16	16c	1/7/69	1045	300	79	586	141	113	332
16	16d	1/7/69	1345	346	79	796	229	176	391

The heat losses by convection [Table F-I, Column (9)] were calculated by using the equation $q = A_s\ h\ (T - T_s)$ and data recorded by the three preceding thermocouples. The data from the thermocouples were reduced to yield T and T_s and with the other terms of the equation defined as A_s = area of surface, (ft^2) and h = film coefficient, ($Btu/ft^2\text{-}hr\text{-}^\circ R$) the heat losses due to convection were calculated by using the above equation. The film coefficient, h, was calculated by using the method shown in Reference 25, pages 333 through 340.

The heat input [Table F-I, Column (10)] was found by subtracting losses due to radiation and convection from the heat input to the system.

Table F-II summarizes the data computed for heat pipe having an adiabatic section. To obtain the heat input through the stainless steel cylinder [Table F-II, Column (3)] the equation $q = A\ k \frac{\Delta T}{\Delta z}$ was used. The heat input to the solid rods [Table F-II, Column (8-10)] was calculated by using the preceding equation. The terms of the equation are defined as follows: A = cross-sectional area, ft^2, k = thermal conductivity, $Btu/hr\text{-}ft\text{-}^\circ R$, ΔT = difference in temperature, $^\circ R$, and Δz = length where ΔT occurs, ft. The heat input through the vapor space [Table F-II, Column (4)] was determined by subtracting and is the heat transported through the interportion of the heat pipe.

The heat inputs [Table F-II, Columns (5-7)] from the equations were calculated by the computer program defined in Chapter II. The apparent contact angle (θ) used in these calculations was zero degrees.

TABLE F-II. SUMMARY OF CALCULATED DATA (ADIABATIC SECTION)

(1) Test Number	(2) Heat Input To Heat Pipe Table F-I Btu/hr	(3) Heat Through S. S. Cyl. k=10 Btu/hr	(4) Heat Input Thru Vapor Space (Exp.) Btu/hr	(5) Heat Input Thru Vapor Space Eq. 42 L_a = 6 inches Btu/hr	(6) Heat Input Thru Vapor Space Eq. 42 L_a = 0 Btu/hr	(7) Heat Input Thru Vapor Space Marcus' Eq. Btu/hr	(8) Heat Input To Solid Rod k=10 Btu/hr	(9) Heat Input To Solid Rod k=100 Btu/hr	(10) Heat Input To Solid Rod k=210 Btu/hr	(11) Approximate Thermal Conductivity For Heat Pipe Btu/hr-ft-°F
9a	125	29	96	96	144	193	10	102	216	124
9b	188	34	154	90	136	159	15	147	308	128
9c	83	34	49	68	105	124	25	251	528	33
9d	168	43	125	26	41	86	32	317	665	53
10a	279	34	245	148	222	295	16	163	343	173
10b	239	51	188	130	195	230	24	235	494	101
10c	235	26	209	108	162	190	25	246	516	95
10d	310	44	266	60	90	147	42	425	892	74
11a	508	84	424	302	454	430	37	368	773	139
11b	151	75	76	273	405	412	31	312	621	50
11c	396	64	332	223	328	389	39	388	515	101
11d	413	89	324	105	160	279	53	534	1122	77
12a	286	39	247	608	915	1200	10	102	214	283
12b	559	153	406	569	852	1000	28	278	583	201
12c	703	206	497	445	668	790	36	361	758	195
12d	668	123	545	177	265	550	42	416	875	160
13a	21	11	10	329	491	270	5	49	102	43
13b	141	14	127	300	452	222	6	60	127	233
13c	137	21	116	220	331	170	9	93	196	273
13d	209	52	157	80	124	120	16	164	343	128
14a	54	6	48	1250	1876	450	6	56	119	96
14b	121	20	101	1175	1768	380	9	86	182	140
14c	143	11	132	840	1260	345	9	93	196	153
14d	333	57	276	390	570	263	16	156	329	212
15a	30	25	5	132	199	185	10	101	212	30
15b	64	48	16	122	183	152	15	146	306	51
15c	102	65	37	77	112	110	19	192	404	53
15d	106	56	50	45	66	90	22	220	462	48
16a	123	11	112	301	453	460	5	46	98	263
16b	233	33	200	282	422	430	9	93	195	251
16c	332	44	288	221	332	389	13	126	265	263
16d	391	64	327	108	160	285	19	186	390	210

The approximate thermal conductivity [Table F-II, Column (11)] was obtained by comparing the heat inputs [Table F-II, Column (2)] with the heat inputs to the solid rods.

Table F-III defines the heat inputs through the vapor space of Heat Pipe Nos. 9, 10, 12, and 16 if the heat input through the stainless steel cylinder was not considered. These heat inputs were taken from Table F-II and presented in Table F-III for comparing L/D ratios. Interpolation was used since the exact temperature does not appear in Table F-II.

TABLE F-III. HEAT INPUTS THROUGH THE VAPOR SPACE OF FOUR HEAT PIPES (ADIABATIC SECTION)

Heat Pipe No.	inches	D inches	$\frac{L}{D}$	q for T=200° F Btu/hr	q for T=250° F Btu/hr	q for T=300° F Btu/hr	q for T=350° F Btu/hr
9	12	$\frac{1}{2}$	24	92	155		
10	12	$\frac{3}{4}$	16		180	209	280
16	12	$1\frac{1}{2}$	8	112	200	288	330
12	12	3	4	230	399	498	541

Figure F-9 depicts the geometry for the heat pipes and solid rods for determining heat inputs per pound. The solid rods are shorter in comparison to the heat pipes because larger heat pipes are needed to provide an area for the heater.

Table F-IV summarizes the data required to determine the heat input per pound for two heat pipes and two solid rods. The heat inputs through the stainless steel cylinder (k = 10) and copper rods (k = 210) were taken from

Table F-II. The volume of stainless steel or copper was calculated using the geometry shown in Figure F-9. The weight was computed by using the volume with the density of stainless steel = 490 lb/ft^3 and the density of copper = 559 lb/ft^3.

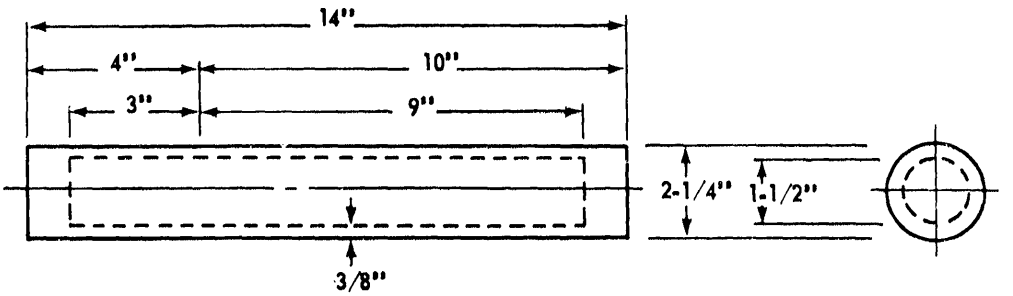

HEAT PIPE NO. 16

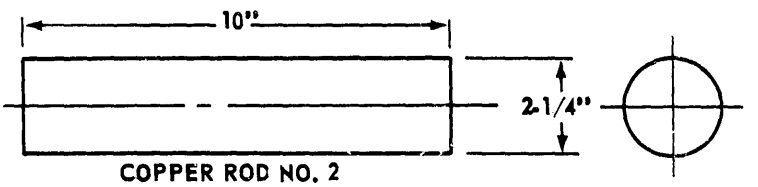

COPPER ROD NO. 2

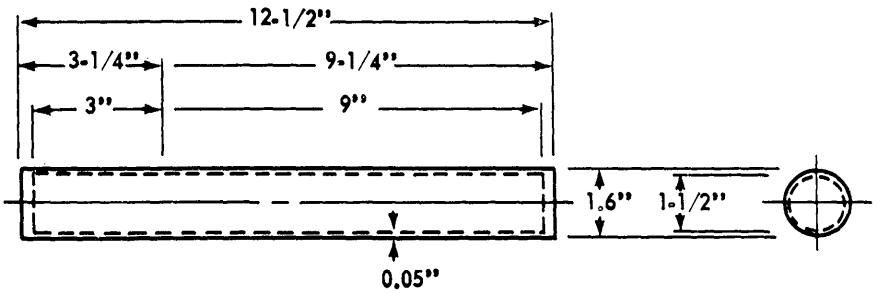

MODEL HEAT PIPE

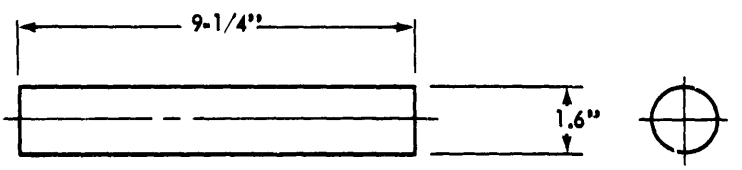

COPPER ROD NO. 3

FIGURE F-9. GEOMETRY OF HEAT PIPES AND SOLID RODS (ADIABATIC SECTION)

TABLE F-IV. HEAT INPUT PER POUND (ADIABATIC SECTION)

Test Number	Base Temperature °F	Temperature Drop °F	Heat Input Thru S.S. Cylinder or Solid Rod k=10 Btu/hr	Heat Input Thru Vapor Space Table F-II Btu/hr	Total Heat Input Btu/hr	Volume of Stainless Steel in.^{3}	Weight 250-Mesh Screen lb	Weight Cylinder or Rod lb	Total Weight lb	Heat Input Per Pound Btu/hr-lb
H.P.16a	203	14	11	112	123	34.4	0.1	9.8	9.9	11.3
H.P.16b	252	28	33	200	233	34.4	0.1	9.8	9.9	23.5
H.P.16c	300	38	44	288	332	34.4	0.1	9.8	9.9	33.5
H.P.16d	346	56	64	327	391	34.4	0.1	9.8	9.9	39.5
C.R.3a	203	14	98	-	98	*39.4	-	12.7	12.7	7.7
C.R.3b	252	28	195	-	195	*39.4	-	12.7	12.7	15.3
C.R.3c	300	38	265	-	265	*39.4	-	12.7	12.7	20.8
C.R.3d	346	56	390	-	390	*39.4	-	12.7	12.7	30.7
M.H.P.16a	203	14	1	112	113	4.0	0.1	1.1	1.2	94
M.H.P.16b	252	26	4	200	204	4.0	0.1	1.1	1.2	170
M.H.P.16c	300	35	5	288	293	4.0	0.1	1.1	1.2	244
M.H.P.16d	346	52	7	327	334	4.0	0.1	1.1	1.2	278
C.R.3a	203	14	*63	-	63	*18.6	-	6.1	6.1	10.3
C.R.3b	252	26	105	-	105	*18.6	-	6.1	6.1	17.2
C.R.3c	300	35	147	-	147	18.6	-	6.1	6.1	24.1
C.R.3d	346	52	*210	-	210	*18.6	-	6.1	6.1	34.5

Heat input through copper rod (k = 210) and volume of copper

NOTE: H.P. denotes Heat Pipe; M.H.P. denotes Model Heat Pipe; C.R. denotes Copper Rod

REFERENCES

1. Gaugler, R.: Heat Transfer Device. U.S. Patent 2,350,348, June 6, 1944.

2. Gifford, W. E.: The Thermal Check Valve - A Cryogenic Tool. Advances in Cryogenic Engineering, Vol. 7, Plenum Press, New York, 1962, pp. 551-555.

3. Grover, G. M., Cotter, T. P., and Erickson, G. F.: Structures of Very High Thermal Conductance. Journal of Applied Physics, Vol. 35, No. 6, June 1964, pp. 1990-1991.

4. Cotter, T. P.: Theory of Heat Pipes. Los Alamos Scientific Laboratory Report No. LA-3246-MS, March 1965.

5. Yuan, S. W., and Finkestein, A. B.: Laminar Pipe Flow with Injection and Suction Through a Porous Wall. Transactions of the ASME, May 1956, pp. 719-724.

6. Knight, B. K., and McInteer, B. B.: Laminar Incompressible Flow in Channels with Porous Walls. Los Alamos Scientific Laboratory Report No. LADC-5309.

7. Wageman, W. E., and Guevara, F. A.: Fluid Flow Through a Porous Channel. Physics of Fluids, Vol. 3, 1960, pp. 878-881.

8. Marcus, B. D.: On the Operation of Heat Pipes. TRW Space Technology Laboratories Report No. 99900-6114-R000, May 1965.

9. Deverall, J. E., and Kemme, J. E.: Satellite Heat Pipe. Los Alamos Scientific Laboratory Report No. LA-3278-MS, April 1965.

10. Ranken, W. A., and Kemme, J. E.: Survey of Los Alamos and Euratom Heat Pipe Investigations. Los Alamos Scientific Laboratory Report No. LA-7555-MS, December 1965.

REFERENCES (Continued)

11. Clayton, J. L.: Heat Pipe. TRW Space Technology Laboratories Report No. 9871-6001-R0000, December 1965.

12. Kemme, J. E.: Heat Pipe Capability Experiments. Los Alamos Scientific Laboratory Report No. LA-3585-MS, October 1966.

13. Kemme, J. E.: Heat Pipe Capability Experiments. Los Alamos Scientific Laboratory Report No. LA-3938-MS, January 1967.

14. Feldman, K. T.: Workshop on Heat Pipe Design and Analysis. The University of New Mexico, April 1968.

15. Frank, S., Smith, J. T., and Taylor, K. M.: Heat Pipe Design Manual. Martin Marietta Report No. MND-3288, February 1967.

16. Kunz, H. R., Langston, L. S., Hilton, B. H., Wyde, S. S., and Nashick, G. H.: Vapor-Chamber Fin Studies. National Aeronautics and Space Administration Report No. CR-812, June 1967.

17. Katzoff, S.: Heat Pipes and Vapor Chambers for Thermal Control of Spacecraft. AIAA Thermophysics Specialist Conference, New Orleans, La., April 17-20, 1967, Paper No. 67-310, April 1967.

18. Deverall, J. E., Salmi, E. W., and Knapp, R. J.: Orbital Heat Pipe Experiment. Los Alamos Scientific Laboratory Report No. LA-3714-MS, June 1967.

19. Haskin, W. L.: Cryogenic Heat Pipe. Air Force Flight Dynamics Laboratory Technical Report AFFDL-TR-66-228, June 1967.

20. Anand, D. K., and Hester, R. B.: Heat Pipe Application for Spacecraft Thermal Control. The John Hopkins University Report No. TG-922, August 1967.

REFERENCES (Concluded)

21. Neal, L. G.: An Analytical and Experimental Study of Heat Pipes. TRW Space Technology Laboratories Report No. 99900-6114-R000, January 1967.

22. Thurman, J. L., and Mei, S.: Application of Heat Pipes to Spacecraft Thermal Control Problems. Technical Note AST-275, Brown Engineering Company, Inc., Huntsville, Alabama, July 1968.

23. Price, J. W.: A Computer Program for Finding the Nonlinear Heat Transfer and Temperature Distribution Through a Constant Cross-Sectional Area Fin. Report No. IN-P&VE-P-68-9, MSFC, Huntsville, Ala., September 1968.

24. Jakob, M., and Hawkins, G. A.: Elements of Heat Transfer. John Wiley and Sons, Inc., New York, 1957.

25. Kreith, F.: Principles of Heat Transfer. International Textbook Company, Scranton, Pa., 1965.

BIBLIOGRAPHY

Bird, B. R., Stewart, W. E., and Lightfoot, E. N.: Transport Phenomena. John Wiley and Sons, Inc., New York, 1960.

Eckert, E. R. G., and Drake, R. M., Jr.: Heat and Mass Transfer. McGraw-Hill Book Company, Inc., New York, 1959.

Green, D. W., and Perry, R. H.: Heat Transfer with a Flowing Fluid Through Porous Media. Chemical Engineering Progress Symposium Series, Vol. 47, No. 32, pp. 61-68, Heat Transfer, Buffalo, New York, 1961.

Kaplan, W.: Advanced Calculus. Addison-Wesley Publishing Company, Inc., Reading, Massachusetts, July 1959.

Scheidegger, A. E.: The Physics of Flow Through Porous Media. The Macmillan Company, New York, 1960.

Van Wylen, G. J.: Thermodynamics. John Wiley and Sons, Inc., New York, 1959.

June 6, 1969 APPROVAL NASA TM X-53849

AN EXPERIMENTAL AND ANALYTICAL STUDY OF WATER HEAT PIPES FOR MODERATE TEMPERATURE RANGES

By

Billy Grant McKinney

The information in this report has been reviewed for security classification. Review of any information concerning Department of Defense or Atomic Energy Commision programs has been made by the MSFC Security Classification Officer. This report, in its entirety, has been determined to be unclassified.

This document has also been reviewed and approved for technical accuracy.

C. G. Fritz
Chief, Research Analysis Section

R. R. Head
Chief, Applied Research Branch

H. G. Paul
Chief, Propulsion and Thermodynamics Division

K. L. Heimburg
Director, Astronautics Laboratory